学位(博士)論文

Positioning accuracy improvement of multi-tasking machine tool having a swivel spindle by compensating influence of the identified inherent geometric deviations

2022 年 2 月

東京農工大学大学院
工学府　機械システム工学専攻

姚　雁

Contents

Chapter 1 Introduction

1.1 Background

1.1.1 History of machine tool

There are all kinds of indispensable industrial products in our modern lives, such as, mobile phones, personal computers, automobiles, aircraft, etc. However, the progress of machine tools is not well known, which is closely related to the background of such rich industrial products around us.

A machine tool is defined in JIS [1] as a machine involving cutting, grinding, using electricity or other energy to remove unnecessary parts from the original shape and get a required shape. Almost all of the machining products in the manufacturing industry and the traffic industry are made with the machine tool. In addition, plastic parts of a mobile phone or a personal computer and molds for forged parts are also machined by the machine tool. Because the machine tool is used to make other machines directly related to our daily lives, it is called “mother machine”.

As the mother machine, the machine tool was further developed in the 19th century in the United States. With the development of the weapons industry needed by the Revolutionary War and the Civil War, machine tool for mass production was available, such as milling machines (Eli Whitney, 1827), grinding machines (Brown & Sharp, 1868), turret lathes (Ramson), and automatic lathes (Spencer).

After World War II, the machine tool has achieved rapid growth with the emergence of Numerical Control (NC). The first NC milling machine was developed by the Massachusetts Institute of Technology in 1952. The design idea is to control each axis of the machine tool with a pulse and generate a control pulse on each axis to cut to the desired contour. The relative position between the tool and the workpiece, which is conventionally controlled with turning the handle by the operator, can be automatically performed by incorporating a servo system. Therefore, it is possible to process various complex curved surfaces by controlling multiple axes at the same time. Furthermore, it also becomes possible to repeatedly produce the same product multiple times by using the same NC program.

With the advancement of computer technology, the NC machine tool has been further developed and the computerized NC (CNC) machine tool becomes mainstream at present. There are various types of CNC machine tools, and a machining center is a typical one of them. A machining center is defined in JIS [1] as a CNC machine tool that has an automatic tool change function and performs various processes without replacing the workpiece. Therefore, it is no longer necessary to move the workpiece for each process with the emergence of a machining center. The delivery time is shortened. Moreover, the machining accuracy is improved since there is no misalignment of the workpiece among various processes.

With the increasing demand for automation, a multi-axis machining center is popular in machining parts with complex geometric structures and sculptured surfaces in recent years. A multi-axis machining center is a numerically controlled machine tool that has a swivel axis in addition to a straight axis and controls not only the relative position but also the relative angle of the tool and the workpiece. Among multi-axis machining centers, the five-axis machining center with tilt rotary axes added to a three-axis machining center that has three straight axes (X, Y, Z) has been widely used in many production factories.

The five-axis machining center has various structural forms based on the location of the swivel axis [2]. The structural configuration can be divided into three types shown in Fig. 1.1, which are tilting rotary table type with two rotary axes in the workpiece side (Fig. 1.1 (a)), universal head type with two rotary axes in the spindle head (Fig. 1.1 (b)), swivel head and rotary table type with one swivel axis in the spindle head and one rotary axis in the workpiece side (Fig. 1.1 (c)). They are applied differently depending on the products manufactured.

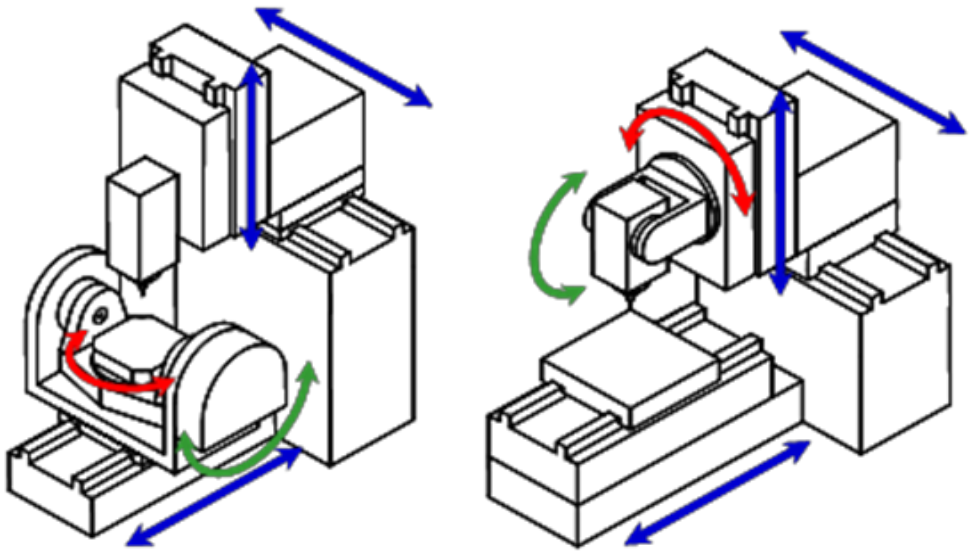

(a) Tilting rotary table type (b) Universal head type

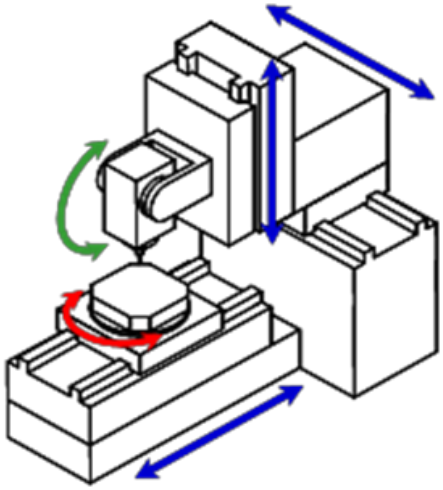

(c) Swivel head and rotary table type

Figure 1.1 Typical three types of five-axis machining center

The tilting rotary table type, a miniaturized structure of five-axis machining center, is suitable for machining relatively small parts such as mold, etc. The universal head type is large itself, and it is used to process aircraft parts. The middle-size parts are usually machined by the swivel head and rotary table type.

1.1.2 Development of multi-tasking machine tool

Today's consumers not only demand diversified products but also expect that the manufacturing life cycles will become shorter. As the final product becomes more and more complex, the key is to develop a machine tool that can handle the great complexity of various processes during manufacturing the products. A multi-tasking machine tool is paid more attention to for coping with this situation.

In order to perform various processes with one machine tool, the multi-tasking machine is an extremely high-performance machine tool that fuses together the technologies of a lathe and a machining center, and it has not only the turning function by a rotary table but also the milling, drilling, boring, etc. functions by using a swivel spindle.

A practical multi-tasking machine tool that combines lathe and machining center technologies was born in 1983 at Yamazaki Mazak Corporation in Japan. A turret lathe was adopted to proceed with the development of a turret mill method, which combined the turret lathe with a milling tool to achieve the turning and milling functions. The "Slant Turn 40N Mill Center" [3] was developed in 1981, shown in Fig. 1.2. The mill was driven by a DC motor with large output, and a tool was incorporated in the holder to implement 4-inch surface milling. Therefore, this machine tool was a lathe capable to perform surface

milling. However, interference between the lathe and the mill occurred sometimes, and the number of tools was limited to ten.

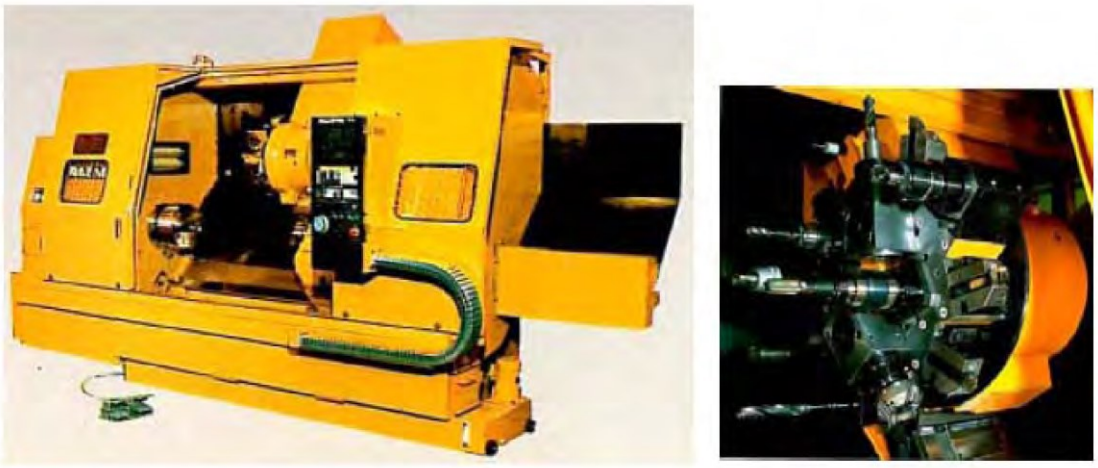

Figure 1.2 Slant Turn 40N Mill Center [3]

In order to perform full-scale machining such as milling and end mill machining by the multi-tasking machine tool, the design route was changed from the turret mill method to the ATC method. The “Slant Turn 25ATC Mill Center” was developed by the ATC method.

The “Integrex 50, 70” developed in 1994 has realized the improvement of milling capacity and an increase in the number of tools. This machine tool has become a mature multi-tasking machine tool beyond the definition of a turning center.

The “Integrex 200SY” developed in 1997 has realized the addition of B axis. By adding the rotary B axis, it has become a five-axis controlled multi-tasking machine tool. It is possible to efficiently process three-dimensional complex shapes, such as turbine blades for the aircraft industry. Furthermore, a second spindle has been added, which makes continuously machining by moving the workpiece from the main spindle to the second spindle. It can also complete the entire machining process of a long workpiece. The multi-tasking machine tool is put into mass production every year and used in various industries around the world.

1.1.3 Issue of multi-tasking machine tool

The multi-tasking machine tool is defined in JIS [1] as a numerically controlled machine tool that can perform multiple processing such as turning, drilling, thread cutting, and pendulum, which is equipped with a rotary spindle, a workpiece table capable of

continuous indexing, and a tool magazine with the automatic tool change function. Figure 1.3 shows an example of the multi-tasking machine tool.

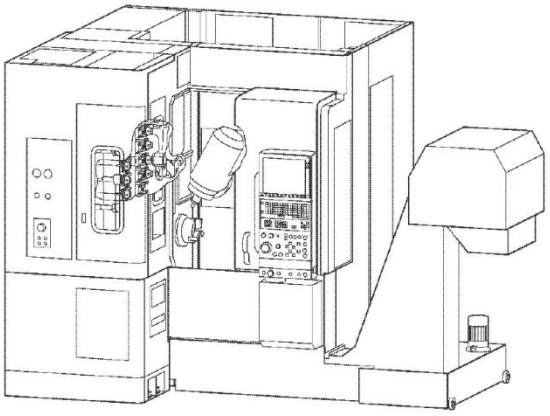

Figure 1.3 Example of multi-tasking machine tool [1]

In order to allow the tool to tilt relative to the workpiece at various angles, B axis is added to the multi-tasking machine tool. Through adjusting the orientation of the cutting tool with respect to the workpiece, more possible cutter paths can be provided without any special jigs or special tools. The multi-tasking machine tool offers notable benefits in producing twisted ruled surfaces such as an impeller and a turbine blade because of the additional rotary degrees of freedom.

However, the motion accuracy of the tool center point is inevitably hard to be guaranteed since the movement of the multi-tasking machine tool is complicated. Compared to the conventional three-axis machine tool, the multi-tasking machine tool with two additional rotary axes has a large number of axes. Thus, it will inevitably bring more additional errors to influence the accuracy of the machine tool. In general, it is said that the mechanical elements causing a rotation, such as a rotary table and a trunnion mechanism, are inferior to a linear motion mechanism in terms of the accuracy and the motion performance [4]. It has also been clarified that since the worm gears and direct drive motors are used in the rotating shafts of the multi-tasking machine tool, the gear engagement and the motor cogging cause the vibration in the rotary direction. In addition, it is necessary to consider the synchronization error between the translational axis and the rotary axis when the machining is controlled by multiple axes at the same time.

The geometric errors exist inevitably between each axis during the process of the manufacturing and assembling of the machine tool. Since two rotary axes are added to three translational axes to compose the multi-tasking machine tool, many geometric errors related to the rotary axis will affect the accuracy of the machine tool. Therefore, the geometric errors to be considered not only refer to the straightness and perpendicularity of

three translational axes, but also include the perpendicularity and parallelism between the translational axis and the rotary center of the swivel axis, the perpendicularity and positional error between two centerlines of swivel axes.

Until now, there is not a unified standard to measure and evaluate motion accuracy after assembling the multi-tasking machine tool. In order to improve the accuracy of multi-tasking machine tool, an evaluation method for the geometric error is required to be studied. The straightness and perpendicularity of each translational axis in the three-axis machine tool are evaluated based on the measurement results of static geometric accuracy [5], positioning accuracy [6], and circular motion tests [7]. However, as mentioned above, the evaluation method for the geometric errors related to the rotary axis are still in the research stage. The machine tool manufactures can only inspect the shape accuracy for each component of the machine tool. They think if the shape accuracy of each component is guaranteed, the position error of tool center point will not be very large after assembling the whole machine tool. They measure and correct the geometric errors related to the rotary axis according to the experience of the operator by the method of each manufacturer. Some manufacturers refer to ISO 13041-5: 2015, Annex A to measure and evaluate the motion accuracy, which is a kinematic test for numerically controlled horizontal turning center, because they regard the multi-tasking machine tool as a turning center with milling spindle, considering the milling spindle as a turret. But they can't measure the milling spindle, only measure the rotary table. Some makers refer to ISO 10791-6: 2014, Annex C, which is a kinematic test for a five-axis machining center with a swivel head and/or a rotary table. They think that the multi-tasking machine tool is similar with a five-axis machining center that has one rotary axis on the workpiece side and one swivel axis on the tool side. However, the total measurement about the geometric deviations of the rotary table and the swivel milling spindle is not specified. At present, there is no uniform standard to evaluate all of geometric errors existing in the multi-tasking machine tool. Therefore, it is necessary to study and establish an effective measuring procedure to fully compensate the geometric deviations of the rotary table and the swivel spindle on the positioning accuracy of tool center point for the multi-tasking machine tool.

1.2 Error sources affecting the accuracy

1.2.1 Error sources in multi-tasking machine tool

There is a vast number of error sources which will affect the accuracy of the multi-tasking machine tool. These error sources can cause a geometric deformation of the

components present in the structural loop of the machine tool. In a multi-tasking machine tool, many components constitute the structural loop, which are the spindle, bearings and spindle housing, the machine head stock, the machine slideways and frame, the fixtures for holding the tool, and workpiece [5]. If there is any change in geometry of these components, the actual position and orientation of the tool relative to the workpiece differs from the required position and orientation. Thus, the accuracy of the machine tool is influenced greatly.

The major error sources can be categorized into quasi-static errors and dynamic errors, shown in Table 1.1.

The quasi-static errors refer to those between the tool and the workpiece which are related to the structure of the multi-tasking machine tool and varying with time slowly [9]. These sources include the geometric and kinematic errors, errors because of the dead weight of the machine tool's components, and those caused by thermally induced strains in the machine tool structure. On the other hand, the dynamic errors refer to those caused by spindle error motion, vibrations of the machine structure, controller errors etc. These sources are almost dependent on the particular operating conditions of the machine tool. Quasi-static errors account for approximately 70% of the total error budgeting of a machine tool [8]. Therefore, they are the major contributors to the inaccuracy of the multi-tasking machine tool.

Table 1.1 Error proportions of a multi-tasking machine tool [8]

Characteristic	Type	Emerging stage	Proportion (%)	Total proportion (%)
Quasi-static errors	Geometric error	Machine itself	20-30	45-65
	Thermal deformation error		25-35	
Dynamic errors	Tool error	During the cutting process	10-15	25-40
	Fixture error		6-10	
	Cutting force deformation error on workpiece and tool		3-5	
	Others (Servo tracking error, etc.)		6-10	
-	Fixture error of measurement device	During the detecting process	8-10	10-15
	others		2-5	

Geometric error is formed during the manufacturing and assembling, since the imperfections of the geometries and dimensions of machine tool components and axis misalignments or flaws in the machine tool measuring system are inevitable. About 75% of the initial errors of a new multi-tasking machine tool are due to deficiencies in the manufacture or assembly. The machine tool structures yield geometric deformations are caused by different factors including the weight of the workpiece and moving slides because of the limited structural stiffness [10]. There are various components in the geometric error, such as linear displacement error (positioning accuracy), straightness and flatness of movement of the axis, spindle inclination angle, squareness error, backlash error etc. [11]. They will cause the defect and inaccuracy during manufacturing and assembling processes. The geometric error is regarded as constant over short-term time intervals although it can be subject to change because of wear and a limited long-term stability of the machine tool components. Therefore, the geometric error is considered to constants during measuring and calibration of the machine tool.

Thermal deformation of the machine tool components is another major error which will affect the accuracy of the multi-tasking machine tool. The reference temperature of operating the multi-tasking machine tool is defined as 20℃ in the ISO standard [12]. However, the temperature distribution of the machine tool's structural loop differs from the reference temperature since the internal and external heat sources exist in the multi-tasking machine tool. Such heat sources are usually generated by friction in spindle bearings, gear boxes, joints, drives, the machining process, electronic and hydraulic systems, the operator, and environment temperature [10,13]. Therefore, the relative position and orientation between the tool and the workpiece change due to the significant expand of the materials used in the multi-tasking machine tool with the temperature. Because the thermal deformation changes slowly without high frequency, the requirement of real-time performance can be lowered in CNC compensation [8].

The dynamic errors also have a direct impact on the geometric accuracy of the machined production surfaces besides the quasi-static errors, shown in Table 1.1. Dynamic errors vary relatively fast in time and are caused by a number of reasons including vibrations of the machine and its environment, faulty motion control, axes accelerations/decelerations and jerk [14]. Cutting force is the major factor to generate internal vibration and affect the surface finish of the machined product. During the cutting process, a light cut is generally more accurate than a heavy cut due to the influence of the dynamic stiffness of the structure on the finishing quality. Therefore, dynamic simulation and analysis are necessary for the machine tool design stage to ensure that the natural

frequency and damping factors of the machine tool should avoid the resonance frequency range of most cutting processes.

Viewing from Table 1.1, geometric error and thermal deformation error takes a high proportion (about 70%) in the total machining error, although there are some other slight errors affecting the accuracy [15,16]. In this thesis, the objective is to establish an identification and compensation method for describing the geometrical induced errors of the multi-tasking machine tool, while the other errors are ignored.

1.2.2 Definition of geometric errors

A rigid body has six degrees of freedom in a three-dimensional space based on the rigid body kinematics [17,18]. These six degrees of freedom refer to three translational degrees and three rotational degrees, which can determine the position and orientation of a rigid body in the three-dimensional space. Correspondingly, there is a component error for each degree of freedom, shown in Fig. 1.4. In this figure, the angular error around the X, Y, and Z axes is represented by α, β, and γ, and the positional error in the X, Y, and Z axes is represented by δx, δy, and δz.

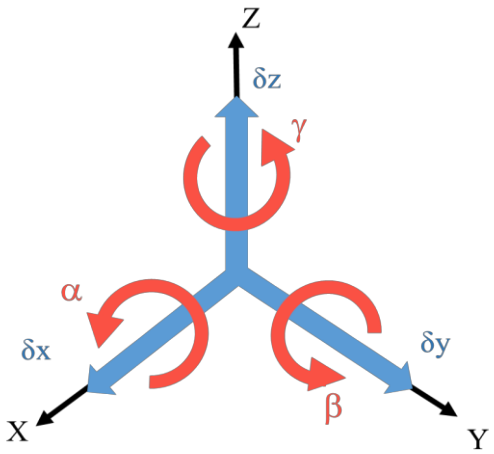

Figure 1.4 Six degrees of freedom

A classification has been proposed to distinguish the geometric error according to different defects, which are the position-dependent geometric errors (PDGEs) and position-independent geometric errors (PIGEs). As the name implies, the value of position-dependent geometric error (PDGE) is dependent on the different positions. Regarding the rigid body behavior, it is assumed that the PDGE relies on the position of the moving object with respect to a predefined reference and the PDGE is only a function of its nominal movement [19]. The PDGEs are caused by the manufacturing defects between the moving couples. Thus, the accuracy of the movement is decreased due to the exist of the

PDGEs.

The PDGEs cannot be considered as constants since they change from position to position. On the contrary, position-independent geometric errors (PIGEs), appearing during assembling process, are modelled as constants no matter where they occur because they can cause constant deviations of the position and orientation of the axis. In this thesis, the PIGEs of a multi-taking machine tool are focused on. The PIGEs compositions for translational and rotary axes are explained as follows.

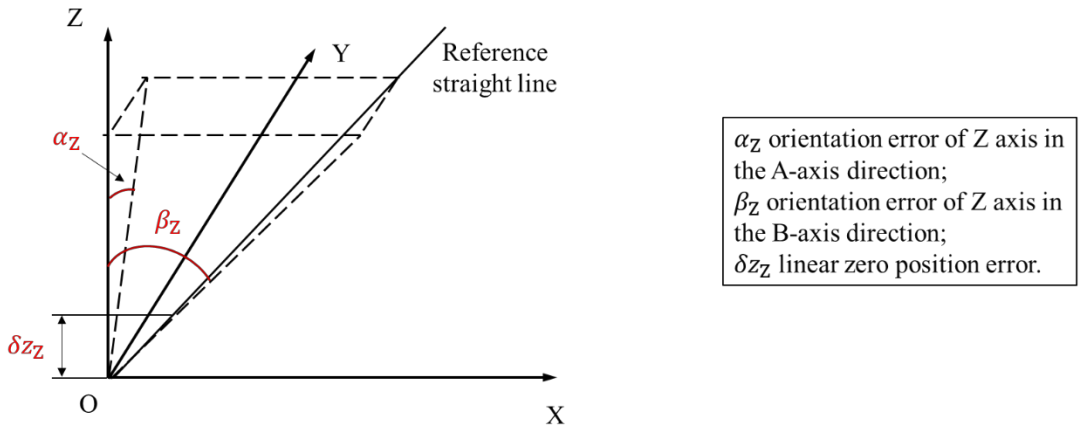

Figure 1.5 PIGEs of a linear axis (Z axis) [5]

Figure 1.5 shows a prismatic joint which is moving along Z axis. A straight line fitting the measured points is considered as the reference straight line [5]. The reference straight line represents the actual condition of the axis, which is calculated by least squares method. The position and orientation errors can be determined by the reference straight line with respect to the nominal coordinate system. α_Z and β_Z are squareness errors, which are angles between Z axis and the projections of the reference straight line on the YZ and XZ planes, respectively. δz_Z is a linear zero positioning error of the axis. Since it exists along the axis nominal moving direction, δz_Z can be compensated by adjusting the numerical parameters in a numerical controlled machine tool.

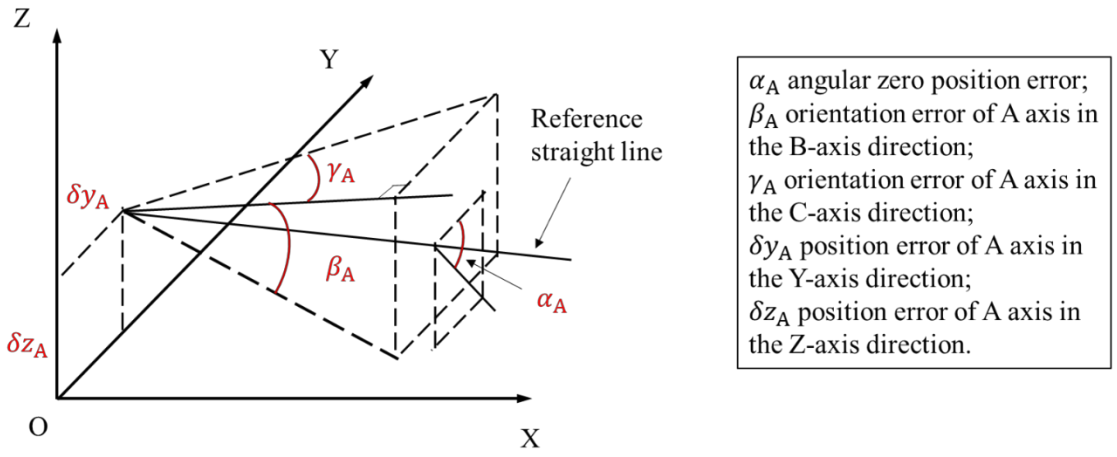

Figure 1.6 PIGEs of a rotary axis (A-axis) [5]

Figure 1.6 shows the composition for the geometric error of A axis. There are five PIGEs for each rotary axis, which are two position errors, two orientation errors, and one angular zero positioning error. Similar with the above analysis of linear axis, the angular zero positioning error can be compensated in the encoder or the numerical controller. Therefore, in terms of rotary axis, four PIGEs should be taken into consideration.

1.3 Previous research on geometric errors of five-axis machining center

Identifying the geometric error by using a measurement instrument is the first step to improve the accuracy of the machine tool. To identify the geometric error, there are two kinds of error models to simulate the error influence: one is developed from the trigonometric relationship for geometric modelling, which is effective for three-axis machine tool. And the other one is based on the rigid body kinematics theory from the robotics, which is suitable for a five-axis machining center or a multi-tasking machine tool. The multi-tasking machine tool is constituted of several moving linkages and the machine tool errors are caused by the linkage errors and motion errors. In order to express the geometric error conventionally and model the structure of machine tool simply, the homogeneous transformation matrices (HTMs) related to the rigid body kinematic theory are adopted widely to express the geometric errors in translational and rotary axes [20,21]. Thus, the position and orientation of the tool with respect to the workpiece can be obtained by a sequential multiplication of the HTMs containing geometric errors according to the order of the kinematic chain of the targeted machine tool.

After identifying the geometric error, it is necessary to use certain measuring

techniques to determine them. Until now, the ball bar, R-test, a touch-trigger probe or a tracking interferometer [22,23] has been proposed and widely used by many researchers to measure the geometric error of a five-axis machining center.

Mayer et al. [24] proposed five tests by the ball bar with a single setup to assess the axis motion errors of a trunnion-type A-axis. And an error model containing cubic polynomial functions and modified qualitative variables, for hysteresis modeling, was also proposed to identify geometric and hysteretic errors of the three nominally orthogonal linear axes machine [25]. In the literature [26], Mayer et al. also estimated all axis to axis location errors and some axis component errors of a five-axis horizontal machining center by probing a scale enriched reconfigurable uncalibrated master balls artefact.

Lei et al. [27,28] presented a new method by using the ball bar to inspect motion errors of the rotary axes of a five-axis machine tool. It was concluded that the servo mismatch of the rotary axes was successfully detected by a particularly circular test path which only caused the two rotary axes to move simultaneously and kept the other three linear axes stationary.

Lee et al. [29] used the ball bar to measure the position-independent geometric errors (PIGE) of a five-axis machining center and verify them through numerical compensation. And the setup errors of ball bar were modeled to increase the estimation accuracy [30]. Besides that, parallelism errors between the spindle axis and the linear axis of machine tool were also measured [31].

Tsutsumi et al. [32] proposed an algorithm for identifying particular deviations relating to rotary axes in five-axis machining centers. In the literature [33], Tsutsumi et al. applied the ball bar to diagnose the motion accuracy of simultaneous four-axis control movements for identifying the eight deviations inherent to five-axis machining centers. Tsutsumi et al. [34] also investigated the kinematic accuracy of five-axis machining centers with a tilting rotary table by two different settings of the ball bar in simultaneous three axis motion. They corrected the squareness deviations of three translational axes for identifying the geometric deviations inherent to five-axis machining centers with an inclined A-axis [35]. In the literature [36], they also proposed an additional method for identifying the geometric deviations inherent to five-axis machining centers with a universal spindle head.

Zhang et al. [37] proposed a novel ball bar measuring method, in which only the C axis rotated. But unfortunately, it could only evaluate five position-dependent geometric errors (PDGE) of the C axis. Khan et al. [38] developed a ball bar methodology that was capable of evaluating five errors out of the six error components in rotary axes. Xiang et al. [39] proposed three measuring patterns by using the ball bar for identifying eight PIGEs on

the rotary axes of a five-axis machine tool, in which the translational axes were kept stationary and only two rotary axes moved to obtain a circular trajectory. Chen et al. [40] presented an identification model of geometric errors based on the homogeneous matrix and verified the method by measuring geometric errors of a four-axis machining center by a double ball bar.

Ibaraki et al. [41,42] identified the kinematic errors of five-axis machining centers by developing a simulator and a set of machining tests. The simulator graphically presented the influence of rotary axis geometric errors on the geometry of a finished workpiece measured by R-test [43–47]. Ibaraki et al. [48] also applied a touch-trigger probe to calibrate the error map of the rotary axes for five-axis machining centers by means of on-the-machine measuring of test pieces. Li et al. [49] used static R-test to identify the geometric error components for the five-axis machining centers with a swiveling head.

After the geometric error has been identified and determined, an effective compensation is necessary to enhance the accuracy of the machine tool. There are two ways for the compensation, which are the feedback interruption compensation and the origin shift compensation [9,50]. The feedback interruption compensation is applicable to most CNC machine tools, in which the phase signal should be inserted into the feedback loop of the servo system. Thus, the signal is easy to interfere with the machine feedback signal. The origin shift compensation works by sending the compensation signal to the CNC unit and then controlling the program logic control (PLC) unit to shift the zero position of each axis under inspection [51–53]. Since this compensation method does not modify the hardware, it is necessary to modify NC code or design a new software to compensate the geometric error.

1.4 Purpose of this research

The multi-tasking machine tool has a structure in which a milling spindle is attached to a CNC lathe. Thus, some researchers [54] think it can be classified into the swivel head and rotary table type of five-axis machining centers. However, the development of multi-tasking machine tool is not only an easy functional addition, but also the pursuit of synergistic effects through multiplication [3]. Therefore, to improve the accuracy, the previous research about the geometric errors for five-axis machining centers cannot be directly and simply applied to a multi-tasking machine tool. In addition, although the ball bar measurement method of simultaneous X-, Y- and C-axes motion is described in ISO 13041-5:2015 [55], the measurement method of simultaneous X-, Z-, and B-axes motion has not been discussed. Furthermore, the identification method of geometric deviations

related to the swivel spindle (B axis) and the rotary table (C axis) has not been explored according to the above measurement method. The accuracy measurement method for these two rotary axes has not clarified and standardized. There is not enough research about the geometric errors for a multi-tasking machine tool. The study in this thesis is the first time to identify and compensate geometric deviations related to a swivel spindle based on the topological structure of the multi-tasking machine tool. Therefore, the objective of this research is to establish an effective method to identify the geometric deviations correctly at first, which are geometric errors of relationship between each adjacent axis. Then, a measuring procedure is designed to compensate the influence of the identified geometric deviations about a swivel spindle and a rotary table on the positioning accuracy of the tool center point in order to improve the accuracy of a multi-tasking machine tool. The purpose focuses on the following aspects:

1. Establish a mathematical model to simulate the simultaneous three axis motions for exploring the relationship between the measured eccentricities and the geometric deviations existing in the target machine tool.

2. Put forward to a measurement procedure by ball bar to identify the geometric deviations based on the analysis of factors affecting the measured trajectory.

3. Put forward to a method by simply modifying the NC code to compensate the influence of the geometric deviations on tool center point to reduce its position error.

4. Verify the identified geometric deviations by using a touch-trigger probe.

1.5 Structure of this thesis

This thesis is arranged as the following 6 chapters.

In Chapter 1, the development of the multi-tasking machine tool is introduced. Then, the errors which will influence the accuracy of the machine tool are analyzed. At last, the objective of this study, which is the development of identification and compensation methods for the geometric deviations of multi-tasking machine tool, is described.

In Chapter 2, according to the theory of form-shaping system, the geometric deviations existing in the multi-tasking machine tool with a swivel spindle head in a horizontal position are defined. Then, a mathematical model to simulate the simultaneous three-axis motions is proposed. And the simulation both in the cylindrical coordinate system and in the Cartesian coordinate system is carried out. From the simulation results, it is confirmed that to eliminate the influence of the mounting errors of workpiece side ball on the measured results, measurements for the B axis should be performed in Cartesian coordinate system and those for the C axis should be performed in cylindrical coordinate

system. The relationship between the geometric deviations and the eccentricities of the measured trajectories is established. It is found that the circular trajectories of the B axis X direction, B axis Y direction, C axis radial direction and C axis axial direction are adequate to identify the geometric deviations by designing an appropriate measuring procedure.

In Chapter 3, current compensation methods for the rotary axis of five-axis machining center are discussed firstly. Then, based on the idea of screw theory, the flowchart of the compensation algorithm is determined and the formulae to generate the modified NC code are derived according to the special topological structure of the targeted machine tool by using the homogenous transformation matrix.

In Chapter 4, at first, the circular trajectories of four measuring patterns are analyzed in three views of the space, respectively. Then, a measuring procedure by using ball bar is designed based on the analysis of the influence factors on each circular trajectory. After that, the measuring procedure is applied in a multi-tasking machine tool, which has a swivel spindle head in the horizontal position, and the geometric deviations are identified by using the eccentricities of trajectories. Finally, according to the proposed compensation method in Chapter 3, the NC code is modified to measure the trajectories of four measuring patterns again. By comparing with the trajectories before and after compensation, it is confirmed that the position error of TCP is reduced significantly after the compensation. It is found that the geometric deviations about two rotary axes can be compensated effectively. However, the geometric deviations of the spindle cannot be compensated by this method.

In Chapter 5, at first, a measuring procedure using a touch-trigger probe is devised to identify the geometric deviations. Then, the formulae to calculate the geometric deviations are derived by analyzing the influence of the geometric deviations on the measurements for the respective rotations of B and C axes. Finally, the measuring procedure and the calculation method are applied in INTEGREX i-200, which is the same multi-tasking machine tool used in the ball bar measurement of Chapter 4. By comparing the identified values obtained from these two measurement instruments, the effectiveness of the identification and compensation methods by a ball bar is verified which can be used to correctly identify the angular deviations related to two rotary axes of the multi-tasking machine tool.

In Chapter 6, the main achievements in this study are summarized to the conclusions.

Chapter 2 Identification method based on simultaneous three-axis motions

2.1 Preface

A multi-tasking machine tool with a swivel spindle head in a horizontal position is considered as the target. Referring to CK1 and CK2 of ISO 10791-6 [12], the deviations of the tool center point (TCP) trajectory can be checked during the simultaneous three-axis motions (STM) of two linear axes and a rotary axis. In order to design a reasonable measuring procedure for identifying the geometric deviations of the targeted machine tool, the simulation about the trajectories of the STM is conducted both in the cylindrical coordinate system and in the Cartesian coordinate system, respectively.

In this chapter, the geometric deviations existing in the multi-tasking machine tool with a swivel spindle head in a horizontal position are defined in Section 2.2. Then, in Section 2.3, the STM are explained both in the cylindrical coordinate system and in the Cartesian coordinate system. A mathematical model to simulate the STM is proposed in Section 2.4. After the simulation, the influences of mounting errors of ball bar and the squareness of translational axes on the eccentricities of the trajectories are analyzed in Section 2.5. And the geometric deviations related to the eccentricities of the trajectories are determined according to the simulation results.

2.2 Geometric deviations of multi-tasking machine tool

2.2.1 Configuration of the multi-tasking machine tool with a swivel spindle head in a horizontal position

Figure 2.1 illustrates the configuration of a multi-tasking machine tool with a swivel spindle head in a horizontal position. The machine tool consists of 5 axes: C axis as a turning spindle, B axis as a milling spindle, and 3 translational X, Y, and Z axes. The structural configuration can be described as w-C'bZYXB (C1)-t by connecting the motion axes from the workpiece side to the tool side. In this description, the workpiece side and the tool side are distinguished by naming the workpiece by "w", the tool by "t", and the bed by "b"; (C1) stands for the spindle axis without numerical control for angular

positioning.

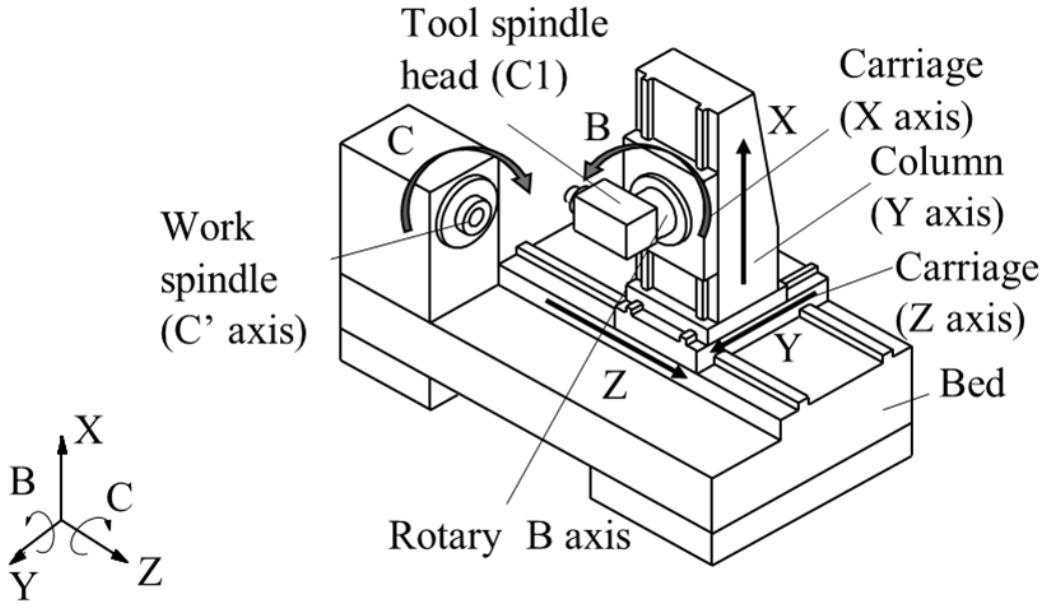

Figure 2.1 Configuration of a multi-tasking machine tool with a swivel spindle head in a horizontal position.

2.2.2 Definition of geometric deviations

Figure 2.2 explains the geometric deviations and the relationship of each axis for the considered machine tool. In Fig. 2.2, δx, δy, and δz correspondingly indicate the positional deviations in X, Y, and Z axes. The letters of α, β, and γ correspondingly indicate the angular deviations around X, Y and Z axes. The large suffixes indicate two neighboring axes. For example, δx_{CZ} means the positional deviation in X direction of C axis origin with respect to machine coordinate origin. The variable α_{CZ} means the parallelism error of C axis of rotation with respect to Z axis about X axis.

According to the theory of form-shaping system for machine tools [2], I delete the negligible deviations of each axis from the possible deviations in order from ① to ⑤ shown in Fig. 2.2. As a result, there are totally thirteen geometric deviations left, which will significantly affect the motion accuracy of the machine tool. Among them, ten geometric deviations are related with two rotary axes—B and C axes, and three geometric deviations are related with three translational axes—X, Y, and Z axes, which are my research objective in this study.

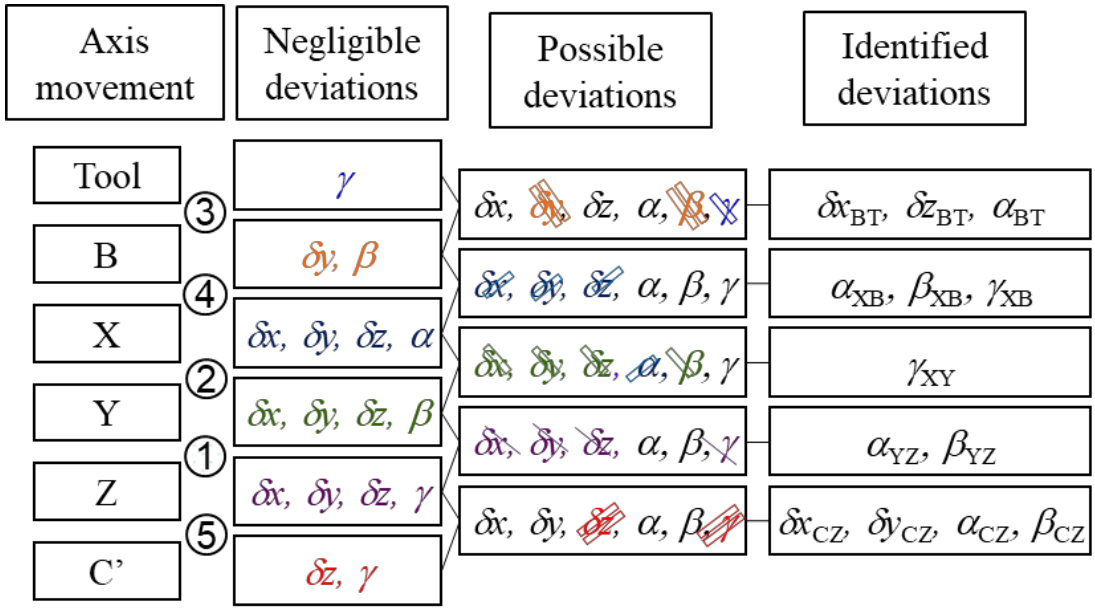

Figure 2.2 Geometric deviations according to the structural configuration of the machine tool

Table 2.1 Definitions of geometric deviations

Symbol	Description
δx_{BT}	X direction offset of spindle rotation with respect to B axis origin
δz_{BT}	Z direction offset of spindle rotation with respect to B axis origin
α_{BT}	Squareness error of B axis with respect to spindle rotation about X axis
α_{XB}	Squareness error of B axis of rotation with respect to Z axis motion
β_{XB}	Initial angular position error of B axis of rotation with respect to X (Z) axis motion
γ_{XB}	Squareness error of B axis of rotation with respect to X axis motion
γ_{XY}	Squareness error between X axis motion and Y axis motion
α_{YZ}	Squareness error between Y axis motion and Z axis motion
β_{YZ}	Squareness error between Z axis motion and X axis motion
δx_{CZ}	X direction offset of C axis origin with respect to machine coordinate origin
δy_{CZ}	Y direction offset of C axis origin with respect to machine coordinate origin
α_{CZ}	Parallelism error of C axis of rotation with respect to Z axis about X axis
β_{CZ}	Parallelism error of C axis of rotation with respect to Z axis about Y axis

Table 2.1 interprets the definitions of thirteen geometric deviations and Fig. 2.3 illustrated them in XZ, YZ, and XY planes. There are four coordinate systems, which are machine coordinate system (O_M-XYZ), B axis coordinate system (O_B-$X_BY_BZ_B$), C axis coordinate system (O_C-$X_CY_CZ_C$) and spindle coordinate system (O_T-$X_TY_TZ_T$). The machine coordinate system is regarded as the reference system, whose origin is the intersection position of the rotary centerlines of B and C axes when there are no geometric deviations and all axes move to zero position. However, since B and C axes are

not directly connected in the multi-tasking machine tool, the origin of the machine coordinate system can't be easily determined by the above definition. In this paper, it is set on the upper surface of the C axis worktable for research convenience.

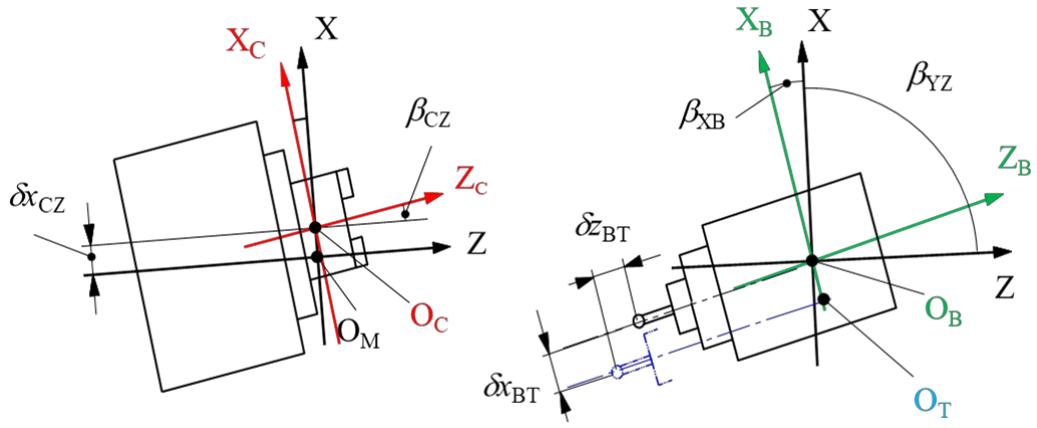

XZ plane

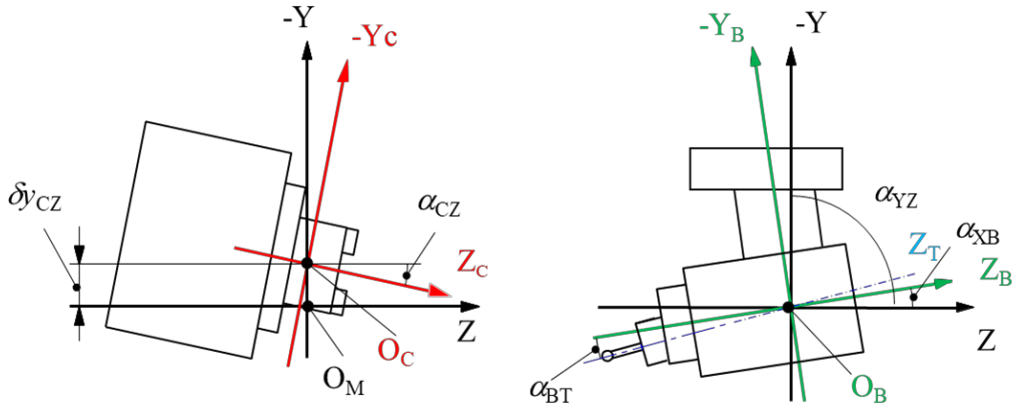

YZ plane

O_MXYZ
Machine coordinate system
$O_CX_CY_CZ_C$
C-axis coordinate system
$O_BX_BY_BZ_B$
B-axis coordinate system
$O_TX_TY_TZ_T$
Tool spindle coordinate system

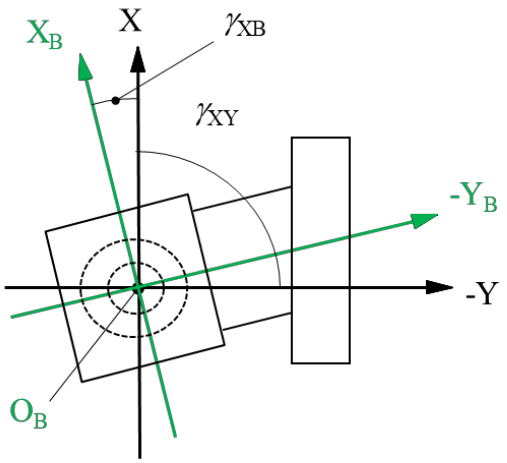

XY plane

Figure 2.3 Illustration of coordinate systems and geometric deviations

2.3 Simultaneous three-axis motions

Simultaneous three-axis motions (STM) mean that the relative motion between the workpiece and the spindle is controlled simultaneously by two orthogonal linear axes to make a circular motion which is synchronized with the rotation of one swivel axis. For example, the motion shown in Fig. 2.4(d) is a STM of XYC axes. The sphere on the spindle side moves in a circle which is interpolated in XY plane, and the sphere on the table rotates synchronously in 360 degrees which is controlled by C axis.

In this study, to identify and compensate the geometric deviations existing in the multi-tasking machine tool, the trajectories of the STM are studied and measured by means of a measuring instrument of a ball bar both in the cylindrical coordinate system and in the Cartesian coordinate system.

2.3.1 Measurement in cylindrical coordinate system

The cylindrical coordinate system consists of the radial, tangential, and axial directions of a circle. Since the ball bar is a one-dimensional measuring instrument, three directions should be measured one by one. The sensitive direction of the ball bar is always kept consistent with respect to the radial, tangential, and axial directions of the rotational motion. Therefore, they are named as radial, tangential, and axial direction measurements in the cylindrical coordinate system, illustrated in Fig. 2.4.

When B axis is rotated, X and Z axes are simultaneously controlled in the XZ plane to perform an arc interpolation motion of 1/4 circle, synchronized with the rotation of B axis. In this case, there are three measurements in the cylindrical coordinate system: B axis radial measurement shown in Fig. 2.4 (a), B axis tangential measurement shown in Fig. 2.4 (b), and B axis axial measurement shown in Fig. 2.4 (c).

When C axis is rotated, X and Y axes are simultaneously controlled in the XY plane to perform a circular interpolation motion, synchronized with the rotation of C axis. In this case, there are three measurements in the cylindrical coordinate system: C axis radial measurement shown in Fig. 2.4 (d), C axis tangential measurement shown in Fig. 2.4 (e), and C axis axial measurement shown in Fig. 2.4 (f).

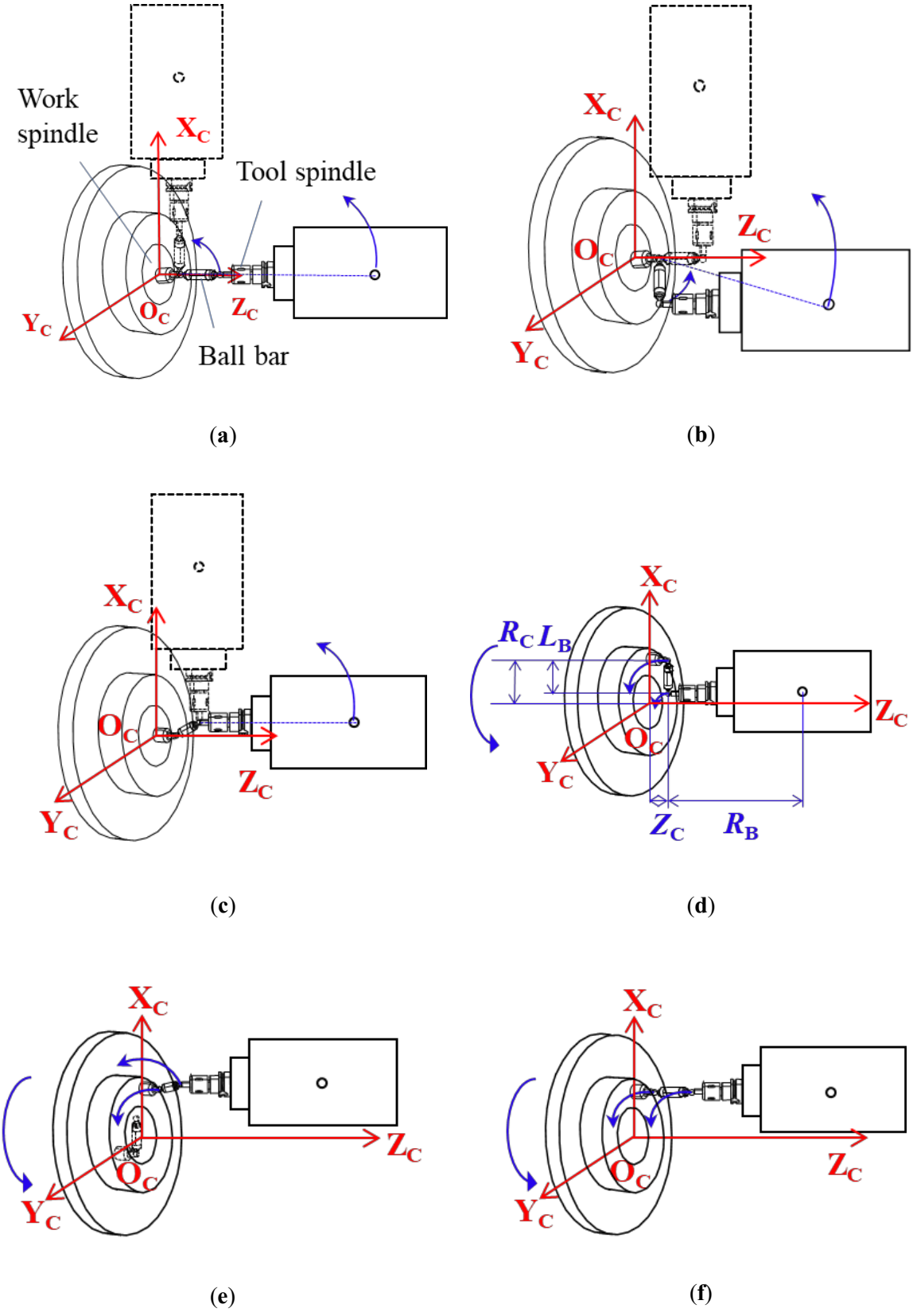

Figure 2.4 (**a**) B axis radial measurement; (**b**) B axis tangential measurement; (**c**) B axis axial measurement; (**d**) C axis radial measurement; (**e**) C axis tangential measurement; (**f**) C axis axial measurement.

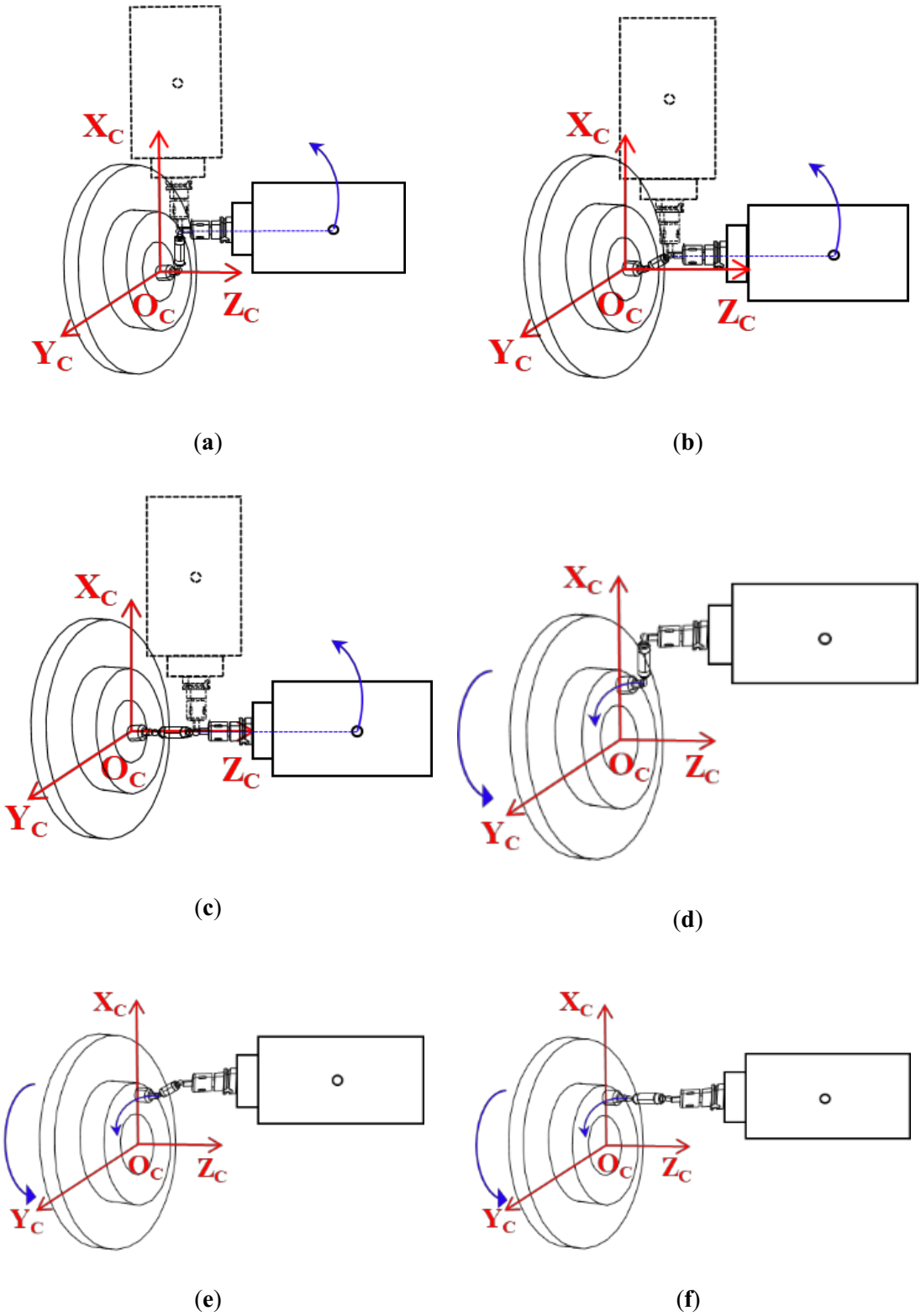

Figure 2.5 B axis X direction measurement; (**b**) B axis Y direction measurement; (**c**) B axis Z direction measurement; (**d**) C axis X direction measurement; (**e**) C axis Y direction measurement; (**f**) C axis Z direction measurement.

2.3.2 Measurement in Cartesian coordinate system

The Cartesian coordinate system consists of X axis, Y axis, and Z axis of the machine coordinate system. During the measurement of the STM, the sensitive direction of the ball bar is always kept consistent with respect to X axis, Y axis, and Z axis directions. Therefore, they are named as X, Y, and Z direction measurements in the Cartesian coordinate system, illustrated in Fig. 2.5.

When B axis is rotated, X and Z axes are simultaneously controlled in the XZ plane to perform an arc interpolation motion of 1/4 circle, synchronized with the rotation of B axis. In this case, there are three measurements in Cartesian coordinate system: B axis X direction measurement shown in Fig. 2.5 (a), B axis Y direction measurement shown in Fig. 2.5 (b), and B axis Z direction measurement shown in Fig. 2.5 (c). In fact, the motion in B axis Y direction measurement is exactly same as the motion in B axis axial measurement shown in Fig. 2.4 (c).

When C axis is rotated, X and Y axes are simultaneously controlled in the XY plane to perform a circular interpolation motion, synchronized with the rotation of C axis. In this case, there are three measurements in Cartesian coordinate system: C axis X direction measurement shown in Fig. 2.5 (d), C axis Y direction measurement shown in Fig. 2.5 (e), and C axis Z direction measurement shown in Fig. 2.5 (f). In fact, the motion in C axis Z direction measurement is exactly same as the motion in C axis axial measurement shown in Fig. 2.4 (f).

2.4 Mathematical model

In the mathematical model, the geometric deviations are introduced as additional geometric parameters in each elemental homogeneous transformation matrices, resulting in the real homogeneous transformation matrix for the multi-tasking machine tool [56]. Since the angular deviations are generally less than 1°, it is reasonable to assume them as the small angles and neglect second order errors during devising the mathematical model. Therefore, the small angle approximation theory ($\sin\theta \approx \theta$, $\cos\theta \approx 1$, if the angle $\theta < 0.1$ (5.7°), the relative error does not exceed 1%) is applied in this study.

Moreover, as an infinitesimal rotation, it is possible to interchange the order of rotation matrices, add or subtract another infinitesimal rotation matrix. Therefore, according to the above infinitesimal rotation approximation theory, it is reasonable to simplify the homogeneous transformation matrix (HTM) in the mathematical model to express the center coordinates of both the spindle side ball (T-side ball) and the work spindle side ball (W-side ball) viewed from the machine coordinate system.

The symbols used in the following mathematical model are explained firstly.

$T\ (x_t, y_t, z_t)$ represents the center coordinate of the T-side ball viewed from the machine coordinate system, and $W\ (x_w, y_w, z_w)$ represents the center coordinate of the W-side ball viewed from the machine coordinate system. The rotation angle of B axis is expressed by $\emptyset$, and the rotation angle of C axis is expressed by θ. The coordinate transformation by geometric deviation is represented by M, and the coordinate transformation by command value is represented by E.

2.4.1 Determination of center coordinate *T* of the T-side ball viewed from the machine coordinate system

The center coordinate T_{T} of the T-side ball in the spindle coordinate system is expressed by Equation (2.1). In there, the parameter R_{B} is the distance from the rotational center of B axis to the center of the T-side ball.

$$T_{\mathrm{T}} = [0 \quad 0 \quad -R_{\mathrm{B}} \quad 1]^{\mathrm{T}} \tag{2.1}$$

Based on the theory of form-shaping system [2], considering angular deviation α_{BT} and positional deviations δx_{BT}, δz_{BT} from the spindle coordinate system to the B axis coordinate system, the homogeneous transformation matrix M_{BT} is expressed by Equation (2.2).

$$M_{\mathrm{BT}} = \begin{bmatrix} 1 & 0 & 0 & \delta x_{\mathrm{BT}} \\ 0 & 1 & -\alpha_{\mathrm{BT}} & 0 \\ 0 & \alpha_{\mathrm{BT}} & 1 & \delta z_{\mathrm{BT}} \\ 0 & 0 & 0 & 1 \end{bmatrix} \tag{2.2}$$

Similarly, from B axis to X axis, the homogeneous transformation matrix M_{XB} is defined as Equation (2.3) since there are angular deviations α_{XB}, β_{XB} and γ_{XB} between them.

$$M_{\mathrm{XB}} = \begin{bmatrix} 1 & -\gamma_{\mathrm{XB}} & \beta_{\mathrm{XB}} & 0 \\ \gamma_{\mathrm{XB}} & 1 & -\alpha_{\mathrm{XB}} & 0 \\ -\beta_{\mathrm{XB}} & \alpha_{\mathrm{XB}} & 1 & 0 \\ 0 & 0 & 0 & 1 \end{bmatrix} \tag{2.3}$$

Because the T-side ball circularly moves around B axis with the radius R_{B}, the transformation matrix E_{B} by the rotation angle value $\emptyset$ to express the circular motion of the T-side ball is shown in Equation (2.4).

$$E_{\mathrm{B}} = \begin{bmatrix} \cos\emptyset & 0 & \sin\emptyset & 0 \\ 0 & 1 & 0 & 0 \\ -\sin\emptyset & 0 & \cos\emptyset & 0 \\ 0 & 0 & 0 & 1 \end{bmatrix} \tag{2.4}$$

The homogeneous transformation matrix M_{YZ} and M_{XY} to reflect the squareness of

the X, Y and Z translational axes can be expressed by Equations (2.5) and (2.6). The transformation matrices E_{X}, E_{Y} and E_{Z} express translational motions controlled by the command values of X, Y and Z axes respectively, shown in Equations (2.7) to (2.9).

$$M_{\mathrm{YZ}} = \begin{bmatrix} 1 & 0 & \beta_{\mathrm{YZ}} & 0 \\ 0 & 1 & -\alpha_{\mathrm{YZ}} & 0 \\ -\beta_{\mathrm{YZ}} & \alpha_{\mathrm{YZ}} & 1 & 0 \\ 0 & 0 & 0 & 1 \end{bmatrix} \tag{2.5}$$

$$M_{\mathrm{XY}} = \begin{bmatrix} 1 & -\gamma_{\mathrm{XY}} & 0 & 0 \\ \gamma_{\mathrm{XY}} & 1 & 0 & 0 \\ 0 & 0 & 1 & 0 \\ 0 & 0 & 0 & 1 \end{bmatrix} \tag{2.6}$$

$$E_{\mathrm{X}} = \begin{bmatrix} 1 & 0 & 0 & \mathrm{X} \\ 0 & 1 & 0 & 0 \\ 0 & 0 & 1 & 0 \\ 0 & 0 & 0 & 1 \end{bmatrix} \tag{2.7}$$

$$E_{\mathrm{Y}} = \begin{bmatrix} 1 & 0 & 0 & 0 \\ 0 & 1 & 0 & \mathrm{Y} \\ 0 & 0 & 1 & 0 \\ 0 & 0 & 0 & 1 \end{bmatrix} \tag{2.8}$$

$$E_{\mathrm{Z}} = \begin{bmatrix} 1 & 0 & 0 & 0 \\ 0 & 1 & 0 & 0 \\ 0 & 0 & 1 & \mathrm{Z} \\ 0 & 0 & 0 & 1 \end{bmatrix} \tag{2.9}$$

As a result, the center coordinate T of the T-side ball viewed from the machine coordinate system is denoted in Equation (2.10).

$$T = E_{\mathrm{Z}} M_{\mathrm{YZ}} E_{\mathrm{Y}} M_{\mathrm{XY}} E_{\mathrm{X}} M_{\mathrm{XB}} E_{\mathrm{B}} M_{\mathrm{BT}} T_{\mathrm{T}} \tag{2.10}$$

2.4.2 Determination of center coordinate *W* of the W-side ball viewed from the machine coordinate system

As there are angular deviations α_{CZ}, β_{CZ} and positional deviations δx_{CZ}, δy_{CZ} between C axis and Z axis as shown in Fig. 2.2, the homogeneous transformation matrix M_{CZ} is expressed by Equation (2.11).

$$M_{\mathrm{CZ}} = \begin{bmatrix} 1 & 0 & \beta_{\mathrm{CZ}} & \delta x_{\mathrm{CZ}} \\ 0 & 1 & -\alpha_{\mathrm{CZ}} & \delta y_{\mathrm{CZ}} \\ -\beta_{\mathrm{CZ}} & \alpha_{\mathrm{CZ}} & 1 & 0 \\ 0 & 0 & 0 & 1 \end{bmatrix} \tag{2.11}$$

The rotation of C axis around Z axis is expressed by the transformation matrix E_{C} where θ is the rotation angle of C axis, shown in Equation (2.12).

$$E_{\mathrm{C}} = \begin{bmatrix} \cos\theta & -\sin\theta & 0 & 0 \\ \sin\theta & \cos\theta & 0 & 0 \\ 0 & 0 & 1 & 0 \\ 0 & 0 & 0 & 1 \end{bmatrix} \tag{2.12}$$

As a result, the center coordinate W of the W-side ball viewed from the machine coordinate system is denoted as Equation (2.13). In there, W_{C} $(x_{w\mathrm{C}}, y_{w\mathrm{C}}, z_{w\mathrm{C}})$ is the initial position of the center coordinate of the W-side ball in the C axis coordinate system.

$$W = M_{\mathrm{CZ}} E_{\mathrm{C}} W_{\mathrm{C}} \tag{2.13}$$

2.4.3 Determination of the initial position W_{C} for center coordinate of the W-side ball

Since the W-side ball is positioned based on the center coordinate of the T-side ball, the influence of geometric deviations needs to be considered to determine the initial position of the W-side ball.

The position W'_{C} of the W-side ball in the machine coordinate system is mounted according to the center coordinate T of the T-side ball in the machine coordinate system by using a dummy sphere. In addition, the initial position of the W-side ball is decided only by the command values of the translational axes without the B axis rotation. Thus, the position W'_{C} of the W-side ball can be calculated by removing E_{B} from the Equation (2.10). It is correspondingly expressed as the following Equations (2.14) and (2.15) for different setup of the B and C axes measurements.

When W-side ball is set for the B axis measurement,

$$W'_{\mathrm{C}} = \begin{bmatrix} 1 & 0 & 0 & 0 \\ 0 & 1 & 0 & 0 \\ 0 & 0 & 1 & Z_{\mathrm{C}} + R_{\mathrm{B}} \\ 0 & 0 & 0 & 1 \end{bmatrix} \begin{bmatrix} 1 & -\gamma_{XY} & \beta_{YZ} & 0 \\ \gamma_{XY} & 1 & -\alpha_{YZ} & 0 \\ -\beta_{YZ} & \alpha_{YZ} & 1 & 0 \\ 0 & 0 & 0 & 1 \end{bmatrix} \begin{bmatrix} 1 & 0 & 0 & 0 \\ 0 & 1 & 0 & 0 \\ 0 & 0 & 1 & 0 \\ 0 & 0 & 0 & 1 \end{bmatrix} \begin{bmatrix} 1 & -\gamma_{\mathrm{XB}} & \beta_{\mathrm{XB}} & \delta x_{\mathrm{BT}} \\ \gamma_{\mathrm{XB}} & 1 & -\alpha_{\mathrm{XB}} - \alpha_{\mathrm{BT}} & 0 \\ -\beta_{\mathrm{XB}} & \alpha_{\mathrm{XB}} + \alpha_{\mathrm{BT}} & 1 & \delta z_{\mathrm{BT}} \\ 0 & 0 & 0 & 1 \end{bmatrix} \begin{bmatrix} 0 \\ 0 \\ -R_{\mathrm{B}} \\ 1 \end{bmatrix} \tag{2.14}$$

When W-side ball is set for the C axis measurement,

$$W'_{\mathrm{C}} = \begin{bmatrix} 1 & 0 & 0 & 0 \\ 0 & 1 & 0 & 0 \\ 0 & 0 & 1 & Z_{\mathrm{C}} + R_{\mathrm{B}} \\ 0 & 0 & 0 & 1 \end{bmatrix} \begin{bmatrix} 1 & -\gamma_{XY} & \beta_{YZ} & 0 \\ \gamma_{XY} & 1 & -\alpha_{YZ} & 0 \\ -\beta_{YZ} & \alpha_{YZ} & 1 & 0 \\ 0 & 0 & 0 & 1 \end{bmatrix} \begin{bmatrix} 1 & 0 & 0 & R_{\mathrm{C}} \\ 0 & 1 & 0 & 0 \\ 0 & 0 & 1 & 0 \\ 0 & 0 & 0 & 1 \end{bmatrix} \begin{bmatrix} 1 & -\gamma_{\mathrm{XB}} & \beta_{\mathrm{XB}} & \delta x_{\mathrm{BT}} \\ \gamma_{\mathrm{XB}} & 1 & -\alpha_{\mathrm{XB}} - \alpha_{\mathrm{BT}} & 0 \\ -\beta_{\mathrm{XB}} & \alpha_{\mathrm{XB}} + \alpha_{\mathrm{BT}} & 1 & \delta z_{\mathrm{BT}} \\ 0 & 0 & 0 & 1 \end{bmatrix} \begin{bmatrix} 0 \\ 0 \\ -R_{\mathrm{B}} \\ 1 \end{bmatrix} \tag{2.15}$$

The transformation matrix from the machine coordinate system to the C axis coordinate system is performed by the inverse transformation of Equation (2.11). In addition, the W-side ball is mounted at the condition of 0° of C axis, so the transformation matrix E_{C} for C axis rotation is removed from the Equation (2.13). Thus, the conversion from W'_{C} to W_{C} is expressed by Equation (2.16).

$$W_{\mathrm{C}} = \begin{bmatrix} 1 & 0 & -\beta_{\mathrm{CZ}} & -\delta x_{\mathrm{CZ}} \\ 0 & 1 & \alpha_{\mathrm{CZ}} & -\delta y_{\mathrm{CZ}} \\ \beta_{\mathrm{CZ}} & -\alpha_{\mathrm{CZ}} & 1 & 0 \\ 0 & 0 & 0 & 1 \end{bmatrix} W'_{\mathrm{C}} \tag{2.16}$$

2.4.4 Calculation of the difference ΔL between reference length and measured length of ball bar

In conclusion, the actual relative distance L between the T-side ball and the W-side ball can be calculated by the center coordinates T (x_t, y_t, z_t) and W (x_w, y_w, z_w). The actual relative distance L is strongly affected by the geometric deviations in the multi-tasking machine tool. Thus, the ball bar length change amount ΔL can be calculated from the actual relative distance L by subtracting the ball bar reference length L_B as shown in Equation (2.17).

$$\Delta L = \sqrt{(x_t - x_w)^2 + (y_t - y_w)^2 + (z_t - z_w)^2} - L_B \tag{2.17}$$

2.5 Simulation

2.5.1 Simulation results

The influence of each deviation on the eccentricity is investigated by using the above mathematical model. The simulation is conducted by MATLAB not only in a cylindrical coordinate system but also in a Cartesian coordinate system.

As shown in Fig. 2.4(d), Z_C is the distance of the W-side ball center from the C axis surface, R_C is the distance of the W-side ball center from the C axis centerline, and R_B is the distance of the T-side ball center from the center of the B axis. L_B is the reference length of the ball bar.

The commands given to each axis for the B axis measurements both in the cylindrical coordinate system and in the Cartesian coordinate system are shown in Table 2.2. The commands given to each axis for the C axis measurements both in the cylindrical coordinate system and in the Cartesian coordinate system are shown in Table 2.3.

The parameters R_{BT} and R_{CT} in the above table are calculated by Equations (2.18) and (2.19).

$$R_{\mathrm{BT}} = \sqrt{R_{\mathrm{B}}^2 + L_{\mathrm{B}}^2} \tag{2.18}$$

$$R_{\mathrm{CT}} = \sqrt{R_{\mathrm{C}}^2 + L_{\mathrm{B}}^2} \tag{2.19}$$

The simulation of the simultaneous three-axis motions is carried out under the condition of L_B = 100 mm, Z_C = 100 mm, R_B = 200 mm, R_C = 50 mm. ±0.005 degrees and ±20 μm is correspondingly given to angular deviations and positional deviations. The effect of each deviation on the eccentricity is investigated as follows.

Table 2.2 Commands given to each axis for B axis measurements

Cylindrical	**Radial**	**Tangential**	**Axial**
Command X	$(L_B + R_B) \sin \varphi$	$R_{BT} \sin (\varphi + \tan^{-1} L_B/R_B)$	$R_B \sin \varphi$
Command Y	0	0	L_B
Command Z	$Z_C + (L_B + R_B) \cos \varphi$	$Z_C + R_{BT} \cos(\varphi + \tan^{-1} L_B/R_B)$	$Z_C + R_B \cos \varphi$
Command B	φ	φ	φ
Command C	0	0	0
Cartesian	**X direction**	**Y direction**	**Z direction**
Command X	$L_B + R_B \sin \varphi$	$R_B \sin \varphi$	$R_B \sin \varphi$
Command Y	0	L_B	0
Command Z	$Z_C + R_B \cos \varphi$	$Z_C + R_B \cos \varphi$	$L_B + Z_C + R_B \cos \varphi$
Command B	φ	φ	φ
Command C	0	0	0

Table 2.3 Commands given to each axis for C axis measurements

Cylindrical	**Radial**	**Tangential**	**Axial**
Command X	$(R_C - L_B) \cos \theta$	$R_{CT} \cos (\theta + \tan^{-1} L_B/R_C)$	$R_C \cos \theta$
Command Y	$(R_C - L_B) \sin \theta$	$R_{CT} \sin (\theta + \tan^{-1} L_B/R_C)$	$R_C \sin \theta$
Command Z	$Z_C + R_B$	$Z_C + R_B$	$Z_C + L_B + R_B$
Command B	0	0	0
Command C	θ	θ	θ
Cartesian	**X direction**	**Y direction**	**Z direction**
Command X	$L_B + R_C \cos \theta$	$R_C \cos \theta$	$R_C \cos \theta$
Command Y	$R_C \sin \theta$	$L_B + R_C \sin \theta$	$R_C \sin \theta$
Command Z	$Z_C + R_B$	$Z_C + R_B$	$L_B + Z_C + R_B$
Command B	0	0	0
Command C	θ	θ	θ

The simulation results for a multi-tasking machine tool with a swivel head in a horizontal position are obtained. The effect of geometric deviations on the eccentricities of circular trajectories for B axis measurements and for C axis measurements are shown respectively in Tables 2.4 and 2.5. The dotted circle indicates theoretical trajectory when there is no geometric deviation. The red and blue lines indicate changed trajectory affecting by negative and positive values of geometric deviations respectively.

Table 2.4 Effect of geometric deviations on the eccentricities of circular trajectories for B axis measurements

	δx_{BT}	δz_{BT}	α_{XB}	β_{XB}	γ_{XB}	α_{BT}	δx_{CZ}	δy_{CZ}	α_{CZ}	β_{CZ}	α_{YZ}	β_{YZ}	γ_{XY}
B axis Radial	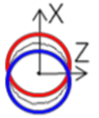	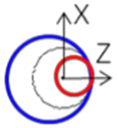		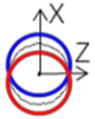								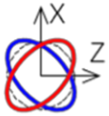	
B axis Tangential	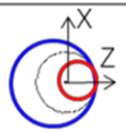	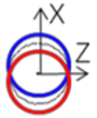		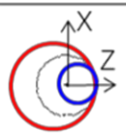								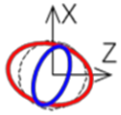	
B axis Axial			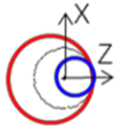		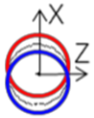						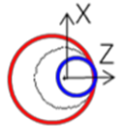		
B axis X direction	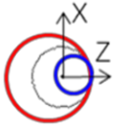	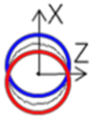		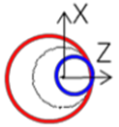								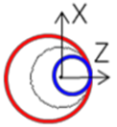	
B axis Y direction			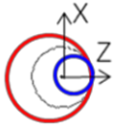		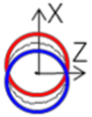						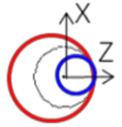		
B axis Z direction	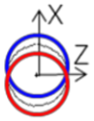	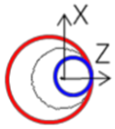		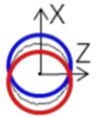									

Table 2.5 Effect of geometric deviations on the eccentricities of circular trajectories for C axis measurements

	δx_{BT}	δz_{BT}	α_{XB}	β_{XB}	γ_{XB}	α_{BT}	δx_{CZ}	δy_{CZ}	α_{CZ}	β_{CZ}	α_{YZ}	β_{YZ}	γ_{XY}
C axis Radial	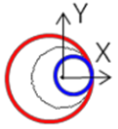		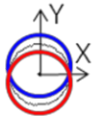	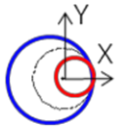	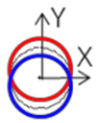	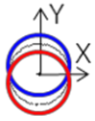	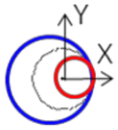	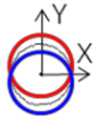	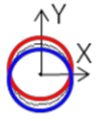	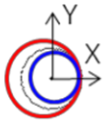	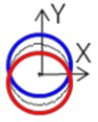	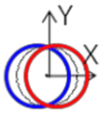	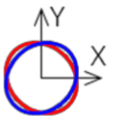
C axis Tangential	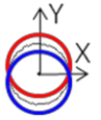		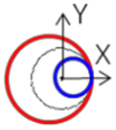	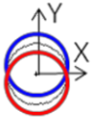	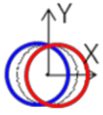	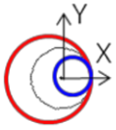	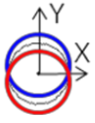	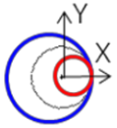	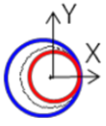	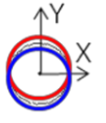	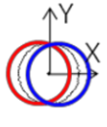	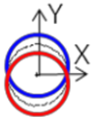	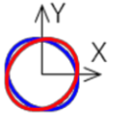
C axis Axial									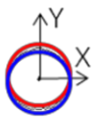	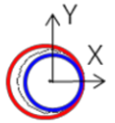	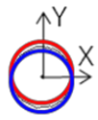	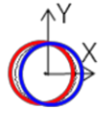	
C axis X direction	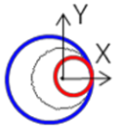		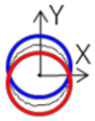	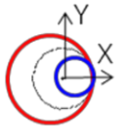	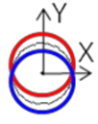	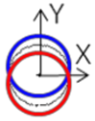	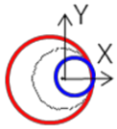	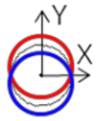	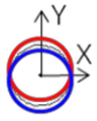	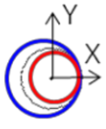	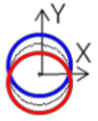	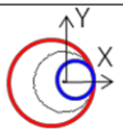	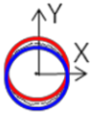
C axis Y direction													
C axis Z direction													

The figures show that if only one of the thirteen geometric deviations exist, the effect of the given deviation on the eccentricity will be reflected by the red or blue circular trajectory. For example, when a value of +20 μm is given to δx_{CZ} for C axis radial direction measurement while other twelve geometric deviations are all zero, eccentricity of trajectory occurs in -X axis direction. On the contrary, when a value of −20 μm is given to δx_{CZ}, eccentricity of trajectory occurs in +X axis direction.

The blank part in Tables 2.4 and 2.5 shows that the trajectory obtained from simulation is same as the reference circle. Therefore, there is no influence of the geometric deviation on the trajectory. For example, for the radial, tangential and axial measurements of B axis in the cylindrical coordinate system, α_{XB} only affects the trajectory of the axial measurement and does not affect those of the radial and tangential measurements.

As a result, the trajectory has changed in the following three aspects.

1. Only the position of trajectory center is changed, and the shape of trajectory is not changed. For example, the effect of α_{XB} on eccentricity in case of the C axis radial measurement.
2. The size of trajectory radius and the position of trajectory center are changed. For example, the effect of δx_{BT} on eccentricity in case of the C axis radial measurement.
3. The shape of trajectory is changed, and the position of trajectory center is not changed. For example, the effect of γ_{XY} on eccentricity in case of the C axis radial measurement.

2.5.2 Influence of mounting errors of ball bar on circular trajectories

The mounting errors are inevitable for measurement no matter which measuring instrument is used. Therefore, it is necessary to investigate the influence of the mounting errors of the T-side ball and the W-side ball on the eccentricity of the measured circular trajectory. For example, when a ball bar is used to measure the trajectory, the W-side ball is positioned by the magnet of the table side socket. The position of the W-side ball is determined as follows. Firstly, attach the dummy sphere to the socket on the spindle side and place the cup of the table side ball on the table. Secondly, make the dummy sphere close to the cup of the table side ball by moving the spindle, and adjust the position of the cup of the table side ball to attach the magnetic socket to the dummy sphere. In this state, the table side ball is mounted at the ideal position. Finally, flip down the lever of the

socket on the table side to fix the magnetic cup.

When the socket is fixed on the table, the position of the W-side ball will shift slightly. This is the main source of the mounting error of the W-side ball. It has been confirmed that the amount of the mounting error of the W-side ball shifts by 10 to 60 μm in a random direction when it is fixed for each time. Therefore, it is necessary to consider the mounting errors during identifying the geometric deviations from the eccentricity of the trajectory.

The actual center coordinate of the T-side ball in the spindle coordinate system, expressed as Equation (2.20), is derived by adding the center offset of the T-side ball (x_T, y_T, z_T) to the ideal center coordinate. Similarly, adding the center offset of the W-side ball (x_W, y_W, z_W) to the ideal center coordinate, the actual center coordinate of the W-side ball is expressed as the following Equation (2.21).

$$T_{\mathrm{T}} = \begin{bmatrix} x_T \\ y_T \\ z_T \\ 0 \end{bmatrix} + \begin{bmatrix} 0 \\ 0 \\ -R_{\mathrm{B}} \\ 1 \end{bmatrix} \tag{2.20}$$

$$W_{\mathrm{C}} = \begin{bmatrix} x_W \\ y_W \\ z_W \\ 0 \end{bmatrix} + \begin{bmatrix} 1 & 0 & -\beta_{\mathrm{CZ}} & -\delta x_{\mathrm{CZ}} \\ 0 & 1 & \alpha_{\mathrm{CZ}} & -\delta y_{\mathrm{CZ}} \\ \beta_{\mathrm{CZ}} & -\alpha_{\mathrm{CZ}} & 1 & 0 \\ 0 & 0 & 0 & 1 \end{bmatrix} W'_{\mathrm{C}} \tag{2.21}$$

A simulation is performed in cylindrical coordinate system and in Cartesian coordinate system to research the effect of the mounting errors on each measured circular trajectory. In the simulation, the geometric deviations are all zero and the mounting errors are individually set to 20 μm. The results are shown in Table 2.6.

In Table 2.6, a dotted circle indicates theoretical trajectory without any mounting errors of ball bar and the red circle indicates changed trajectory affecting by only one mounting error. The blank means the trajectory has not changed although the mounting error exists.

It is found that the mounting errors of the T-side ball will strongly influence the eccentricity of circular trajectories in these two coordinate systems. Therefore, to achieve correct results, it is crucial to perfectly coincide the center of the T-side ball to the spindle before conducting measurements.

However, the mounting errors of W-side ball do not influence the eccentricity in Cartesian coordinate system for the B axis measurements, and in cylindrical coordinate system for the C axis measurements. When B axis is measured in X, Y, Z direction or C axis is measured in radial, tangential, or axial direction, the sensitive direction of the ball bar is always kept constant viewed from the tableside. As a result, the mounting errors of

the W-side ball do not need to be considered in these measurements. However, the eccentricities from the measurements of B axis radial, tangential, axial direction, or C axis X, Y, Z direction are strongly affected by the mounting errors because the sensitive direction of the ball bar changes with respect to the table at all times. For example, in case of B axis radial direction measurement, B axis was rotated around the W-side ball and the ball bar would be rotated at the same time. Therefore, the measurement results were affected by the mounting error of the W-side ball.

Table 2.4 Influence of mounting errors of ball bar on the eccentricity of circular trajectories.

		x_W	y_W	z_W	x_T	y_T	z_T
Cylindrical coordinate system	B axis Radial						
	B axis Tangential	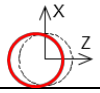					
	B axis Axial		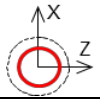				
Cartesian coordinate system	B axis X direction	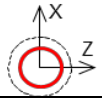					
	B axis Y direction		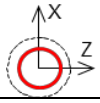				
	B axis Z direction			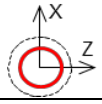	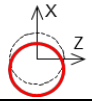		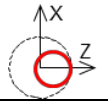
Cylindrical coordinate system	C axis Radial					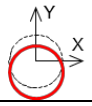	
	C axis Tangential		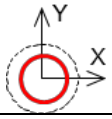		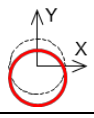	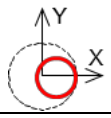	
	C axis Axial			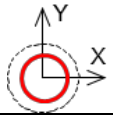			
Cartesian coordinate system	C axis X direction	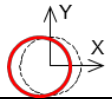	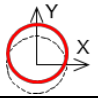		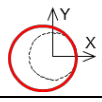	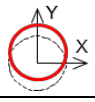	
	C axis Y direction	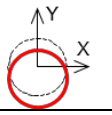			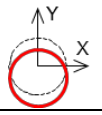		
	C axis Z direction			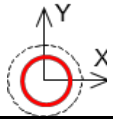			

Figure 2.6 intuitively explains that the mounting errors of W-side ball do not affect the eccentricity of trajectory measured in C axis radial direction measurement. The red circle represents the ideal path of the spindle side ball, and its radius is $(R_C + L)$. The black circle represents the ideal path of the workpiece side ball, and its radius is R_C. In Fig. 2.6 (a), the ideal condition is described when there is no mounting error. In Fig. 2.6 (b), if there is mounting error y_W in the +Y direction, the real path of the workpiece side ball will express as the blue circle, and its radius is $(R_C + y_W)$. Compared with these two figures, it is concluded that if there is a mounting error on the workpiece side ball, the diameter of the trajectory changes, but the eccentricity does not occur. That is consistent with the result obtained from the simulation.

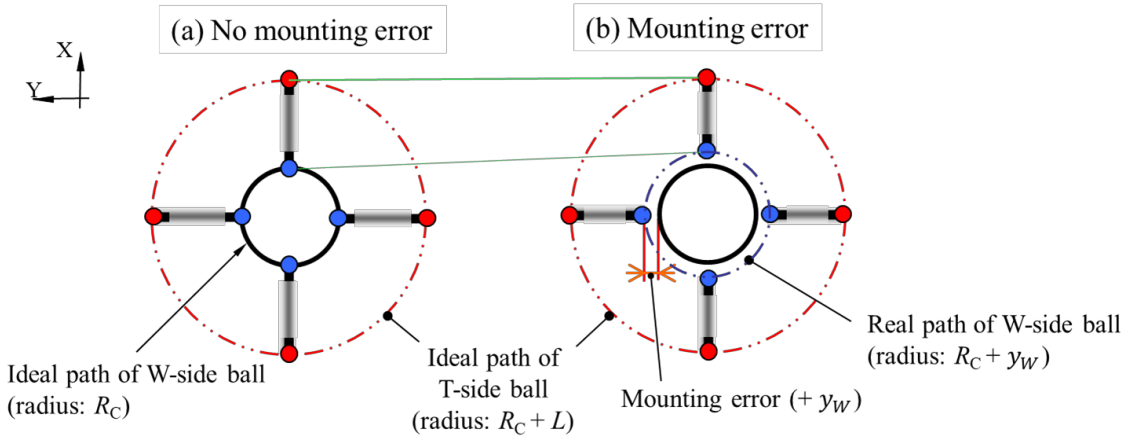

Figure 2.6 Influence of the mounting error of W-side ball on the trajectory

In conclusion, the B axis measurements in Cartesian coordinate system and C axis measurements in cylindrical coordinate system are proposed to identify the geometric deviations of multi-tasking machine tools to avoid the influence of mounting errors.

2.5.3 Influence of squareness between translational axes on circular trajectories

The influence of squareness deviations of translational axes, α_{YZ}, β_{YZ}, and γ_{XY}, on the eccentricity of circular trajectories are also achieved by the simulation, shown in Table 2.7. It is observed that the squareness deviation γ_{XY} only influence the eccentricity of circular trajectory in case of the C axis X direction measurement. Therefore, it is indispensable to conduct C axis X direction measurement to identify the squareness deviations γ_{XY}. However, the mounting errors of W-side ball and T-side ball will strongly affect the measurement accuracy of eccentricity under the C axis X direction

measurement, shown in Table 2.6. Thus, it can't be measured correctly. Moreover, the squareness deviations α_{YZ} and β_{YZ}, can't be separated from α_{XB} and β_{XB}. Additionally, in theory, the squareness deviations are very smaller than the geometric deviations of the rotary axes. Therefore, the identification for squareness deviations of translational axes will not be researched in this study.

Table 2.5 Influence of squareness deviations of translational axes

		α_{YZ}	β_{YZ}	γ_{XY}
Cylindrical coordinate system	B axis Radial		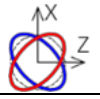	
	B axis Tangential		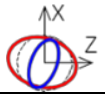	
	B axis Axial	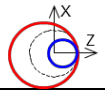		
Cartesian coordinate system	B axis X direction		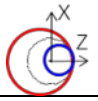	
	B axis Y direction	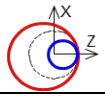		
	B axis Z direction			
Cylindrical coordinate system	C axis Radial	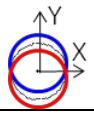		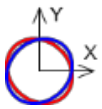
	C axis Tangential			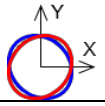
	C axis Axial	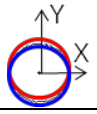	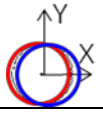	
Cartesian coordinate system	C axis X direction			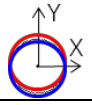
	C axis Y direction			
	C axis Z direction	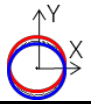	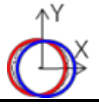	

2.5.4 Relationship between geometric deviations and eccentricities

Based on the simulation result shown in Tables 2.4 and 2.5, the relationship between each geometric deviation and the eccentricity of circular trajectory obtained

from each measurement is derived as follows. To simplify the calculation, the positional deviation appears as eccentricity is, while the angular deviation, multiplied by a coefficient, such as Z_C, R_B, R_C, Z_T or X_T, appears in eccentricity. The sign of the deviation can be judged by the consistency with the positive direction of each geometric deviation. If the positive direction of the eccentricity occurs in the condition of blue lines in Tables 2.4 and 2.5, the deviation is positive. On the contrary, if the negative direction of the eccentricity occurs in the condition of blue lines in Tables 2.4 and 2.5, the deviation is negative. In there, the blue line means the simulation result under the positive value of geometric deviation.

The relationship for B axis trajectory measured in the Cartesian coordinate system and C axis trajectory measured in the cylindrical coordinate system are summarized in Table 2.8, where *ex*, *ey* and *ez* represent the components of eccentricities in X, Y and Z axes directions, respectively. The subscripts indicate the type of measurements, for example, BX and CR represent measurements of the B axis X direction and C axis radial direction, respectively.

As an example, the mathematical expression for the radial direction measurement of C axis in Table 2.8 is derived as follows. According to the simulation result in Table 2.5, it is found that the eccentricity of trajectory is influenced by 12 geometric deviations, which are δx_{BT}, α_{XB}, β_{XB}, γ_{XB}, α_{BT}, δx_{CZ}, δy_{CZ}, α_{CZ}, β_{CZ}, α_{YZ}, β_{YZ}, and γ_{XY}. Among these geometric deviations, 5 geometric deviations of δx_{BT}, β_{XB}, δx_{CZ}, β_{CZ}, and β_{YZ} affect the eccentricity in the X direction. Through analysis, it is confirmed that the angular deviations of β_{XB} and β_{YZ}, which exist in the spindle side according to the structure of the targeted machine, are multiplied by the coefficient Z_T in the mathematical expression. And the angular deviation of β_{CZ}, which exists in the workpiece side according to the structure of the targeted machine, is multiplied by the coefficient Z_C in the mathematical expression. The coefficients Z_T and Z_C respect Z-axis coordinate of the tool-holding spindle head in machine coordinate system and Z-axis coordinate of the center position of the workpiece side ball in table coordinate system, respectively. These 2 positional deviations of δx_{BT}, and δx_{CZ} appear as δx_{BT}, and δx_{CZ} in the mathematical expression, respectively. To judge the sign of the eccentricity due to the positive values of the geometric deviations (indicated by the blue line in Table 2.5), it can be found that δx_{BT} and β_{CZ} are positive, and β_{XB}, δx_{CZ}, and β_{YZ} are negative. From the above, the amount and the sign of the eccentricity due to each geometric deviation are all understood, and therefore, the eccentricity ex_{CR} in the X direction can be summarized by $\delta x_{BT} - Z_T\beta_{XB} - \delta x_{CZ} + Z_C\beta_{CZ} - Z_T\beta_{YZ}$. The squareness deviations of translational axes are not researched

in this study, so it is simplified as $\delta x_{BT} - Z_T\beta_{XB} - \delta x_{CZ} + Z_C\beta_{CZ}$.

Table 2.6 Relationship between eccentricity and geometric deviations

	ex	***ey***	***ez***
B axis X direction	δz_{BT}	—	$\delta x_{BT}+R_B\beta_{XB}$
B axis Y direction	$-R_B\gamma_{XB}$	—	$R_B\alpha_{XB}$
B axis Z direction	$\delta x_{BT}+R_B\beta_{XB}$		δz_{BT}
C axis Radial	$\delta x_{BT} - Z_T\beta_{XB} - \delta x_{CZ} + Z_C\beta_{CZ}$	$Z_T\alpha_{XB} - X_T\gamma_{XB} + Z_T\alpha_{BT} - \delta y_{CZ} - Z_C\alpha_{CZ}$	—
C axis Tangential	$Z_T\alpha_{XB} - X_T\gamma_{XB} + Z_T\alpha_{BT} - \delta y_{CZ} - Z_C\alpha_{CZ}$	$-(\delta x_{BT} - Z_T\beta_{XB} - \delta x_{CZ} + Z_C\beta_{CZ})$	
C axis Axial	$R_C\beta_{CZ}$	$-R_C\alpha_{CZ}$	—

It is discovered that the expression of the B axis X direction measurement is similar with that of the B axis Z direction measurement. Thus, only one of them is adopted in the following chapter to design the measuring procedure. The expression of the C axis tangential measurement is found to have only opposite arithmetic signs comparing to that of the C axis radial measurement. Furthermore, it has been known that a pitch error of the worm gear affects the eccentricity of circular trajectory measured in the tangential direction. Thus, the C axis tangential measurement is not discussed to identify geometric deviations in this study.

In summary, the geometric deviations inherent to a multi-tasking machine tool can be identified by measuring the circular trajectories of the B axis X direction, B axis Y direction, C axis radial direction and C axis axial direction.

2.6 Conclusion

In this chapter, to identify the geometric deviations which exist in a multi-tasking machine tool, the trajectories of simultaneous three-axis motions are investigated. The mathematical model is established, and the simulation is conducted both in the cylindrical coordinate system and in the Cartesian coordinate system, respectively. Conclusions are summarized as follows.

1. According to the structural configuration of a multi-tasking machine tool with a swivel spindle head in a horizontal position, the geometric deviations which will cause the position error of tool center point are clarified.

2. The simulation both in the cylindrical coordinate system and in the Cartesian coordinate system is conducted based on the established mathematical model to the targeted machine tool.
3. From the simulation results, it is confirmed that in order to eliminate the influence of the mounting errors of the W-side ball on the eccentricities of the circular trajectories, measurements for the B axis should be performed in Cartesian coordinate system and those for the C axis should be performed in cylindrical coordinate system. It is the first time to measure the geometric deviations related to a swivel spindle in Cartesian coordinate system.
4. Through the relationship between the geometric deviations and the eccentricities of the measured trajectories, it is found that the circular trajectories of the B axis X direction, B axis Y direction, C axis radial direction and C axis axial direction are adequate to identify the geometric deviations by designing an appropriate measuring procedure.

Chapter 3 Compensation method based on kinematic chain of the targeted machine tool

3.1 Preface

The compensation of the geometric deviations is the final and important step to calibrate the geometric deviations and improve the accuracy of the machine tool. Therefore, it needs to develop an effective method to compensate the influence of the geometric deviations on the trajectory of tool center point. The presence of the rotary axis makes the kinematic module highly nonlinear, and it becomes rather difficult to derive the actual inverse kinematic module that considers geometric deviations. Thus, many researchers focus on developing different algorithms and verifying their effectiveness on compensating the geometric deviations. According to the special topological structure, a simple and operable compensation method needs to be determined for the multi-tasking machine tool.

In this chapter, many compensation methods for the rotary axis of five-axis machining center are discussed in Section 3.2. In Section 3.3, based on the idea of screw theory, the compensation algorithm is determined and the formulae to generate the modified NC code are derived for the targeted multi-tasking machine tool according to the homogenous transformation matrix.

3.2 Compensation method for rotary axis

In order to improve the manufacturing accuracy, the identified geometric deviations inherent to the multi-tasking machine tool need to be compensated. A reasonable compensation method is an important and critical step in the development of calibration techniques for the geometric deviations of the machine tool.

The quality of the machine tool is enhanced by eliminating the geometric errors in terms of hardware in the design and manufacturing stages. With the long-term use of the machine tool, the accuracy is guaranteed by compensating the geometric errors in the CNC system. The compensation can mainly be carried out by the following four methods: additional embedded software module, control parameter modifications, post-processor

modification, and NC program modification [57]. In this study, the NC program modification method is adopted to create a new NC code that will give better performance considering the geometric deviation information.

To compensate geometric deviations, the existing of the rotary axis makes the forward kinematic module, including geometric deviation matrices, highly nonlinear and it becomes rather difficult to derive the actual inverse kinematic module which should consider the geometric deviations. Thus, many researchers used approximate linearized method or iterative method to conduct the compensation.

In [58], it was focused on using an approximate linearized mothed to compensate the geometric deviations of a five-axis machine tool. The relationship between the small variations of tool center point in the workpiece coordinate system and the differential change of drives' motions in the machine coordinate system was assumed to be linear. Due to the small geometric deviations, the correction motion positions could be simply calculated by multiplying the geometric deviation vectors in the workpiece coordinate system by the inverse Jacobian matrix that was derived through solving the ideal forward kinematics functions for the particular machine topology. In [59], a decoupled method was developed to compensate the geometric deviations of five-axis machine tools. The sequence of the compensation was emphasized that the geometric deviations of translational axes should be compensated before those related to rotary axes. However, in [60], the relationship between the workpiece coordinate system and the machine coordinate system was pointed out highly nonlinear. Therefore, it was necessary to use iterative calculation to achieve more accurate solution. A total differential algorithm was applied to improve the calculation speed and reduce the difficulty of the actual inverse kinematic solution. The iterative calculation ended when an acceptable tolerance was reached.

In Chapter 2, the homogenous transformation matrix is used to establish the mathematical model of the simultaneous three-axis motions. The homogeneous transformation matrix is developed and commonly used according to a kinematic model whereby a reference coordinate system is associated with each drive axis in the serial kinematic chain [61]. For a multi-tasking machine tool, by using the required translations and rotations relative to the previous coordinate system in the kinematic chain, the coordinate systems are associated with each drive axis in sequence. Therefore, after identifying the geometric deviations of the machine tool, the actual twist coordinates can be directly calculated by the homogenous transformation matrix considering the identified values of geometric deviations. Thus, the actual inverse kinematic solution can be simply obtained without any iteration.

The screw theory [62], known since the early 1900s, is an effective mathematical tool to model kinematics of five-axis machine tools. It provides an alternative to the traditional method of Denavit–Hartenberg (DH) for the forward and inverse kinematics. The way of representing the matrix as Twist and Screw has two advantages. The first is that they allow a comprehensive description of the motion of a rigid body which does not suffer from the singularities that arise when using local coordinates. The second is that a geometric description of the movements is obtained, which greatly simplifies the analysis of mechanisms. The steps to get the forward kinematics are described.

a) Define the placement of the coordinate systems S and G, where the first is the global reference system, and the later one is the final effector system.

b) Locate the ω_i on each joint, those are R^3 unitary vectors that are over the rotation or displacement axis depending on the kind of joint.

c) Select the q_i points needed, those must be placed over one or more axis in order to let the Twist creation.

d) With the ω_i and q_i the Twists are calculated, represented by the Greek letter ξ_i , which can be in two ways depending on the joint's kind, as in the next equation.

Rotary axis: $$\xi_i = \begin{bmatrix} -\omega_i \times q_i \\ \omega_I \end{bmatrix} \tag{3.1}$$

Translational axis: $$\xi_i = \begin{bmatrix} \omega_i \\ 0 \end{bmatrix} \tag{3.2}$$

e) The $g_s^G(0)$ homogeneous matrix is obtained which represent the position and orientation of the final effector G seen from the reference system S, where all values of the articular variables are default.

f) The matrix's exponentials $e^{\hat{\xi}_i \theta_i}$ are generated from the Twists, which represent the homogeneous transformation matrix equivalent for the joint.

g) At last, calculate the forward kinematics, by multiplying all the $e^{\hat{\xi}_i \theta_i}$ and the matrix $g_s^G(0)$, getting the $g_s^G(\theta)$ as shown in Eq. (3.3) where n is the number of joins.

$$g_s^G(\theta) = e^{\xi_1 \omega_1} e^{\xi_2 \omega_2} \cdots e^{\xi_i \omega_i} g_s^G(0) \qquad i = 1,2,\cdots,n \tag{3.3}$$

Until now, there is only limited use of the screw theory for machine tools' geometric deviations modeling although it has been widely used in the robotics area. In [63], the screw theory has been used to separate the source errors affecting the compensated and uncompensated pose accuracy of the machine tool. In [64], the identification and correction of the five-axis machine tools are presented based on the screw theory by a generalized Jacobian function.

In this study, based on the idea of screw theory, machine coordinate system is

considered as a global reference system. The angular and positional geometric deviations are treated as vectors of rotation and movement by using homogenous transformation matrix to model the transformation of coordinates between adjacent axes by considering the identified inherent geometric deviations. Since the rigid body motion is descripted in a global reference system, the geometric deviations are easy to be compensated approximately and directly in the actual inverse kinematic solution based on the homogenous transformation matrix. So, the compensation for geometric deviations of the multi-tasking machine tool is proposed by using the homogenous transformation matrix.

3.3 Compensation for the geometric deviations of the targeted multi-tasking machine tool

Figure 3.1 explains the basic compensation concept. The ideal tool center position, embedded in the corresponding NC code, is expressed by point P, while the actual position of tool center point, which is affected by the geometric deviations inherent to the multi-tasking machine tool is expressed by point P'. The compensated tool center position is expressed by point P^C, driven by the modified NC code. If the machine tool is running by the modified NC code, the actual position of tool center point can be reached to the desired position, because the influence of the geometric deviations is compensated. Thus, the geometric deviations are compensated.

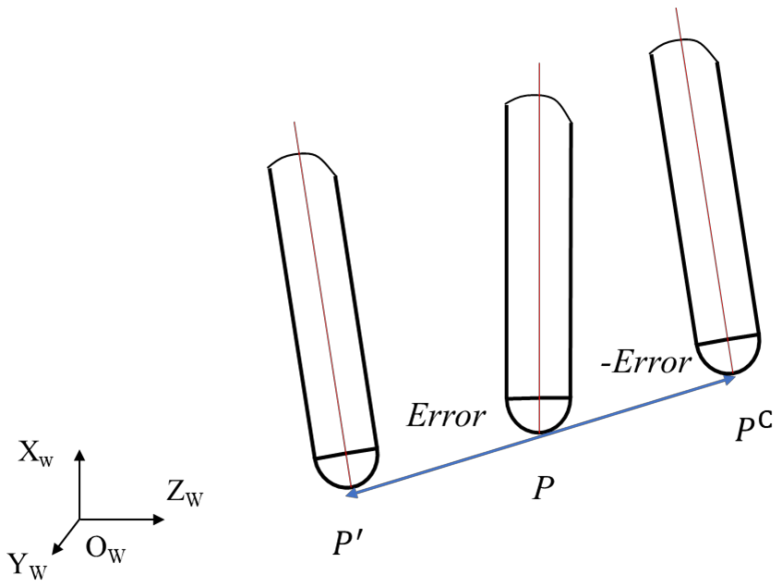

Figure 3.1 Basic concept of geometric deviations compensation

The idea of screw theory is adopted in this study to consider the compensation method for geometric deviations of the targeted machine tool.

A multi-tasking machine tool is similar to two cooperating robots, one robot carrying the workpiece and the other carrying the tool. Therefore, a kinematic chain of the multi-tasking machine tool is treated as a unified kinematic chain of two collaborative robots in order to formulate a kinematic module of the machine tool.

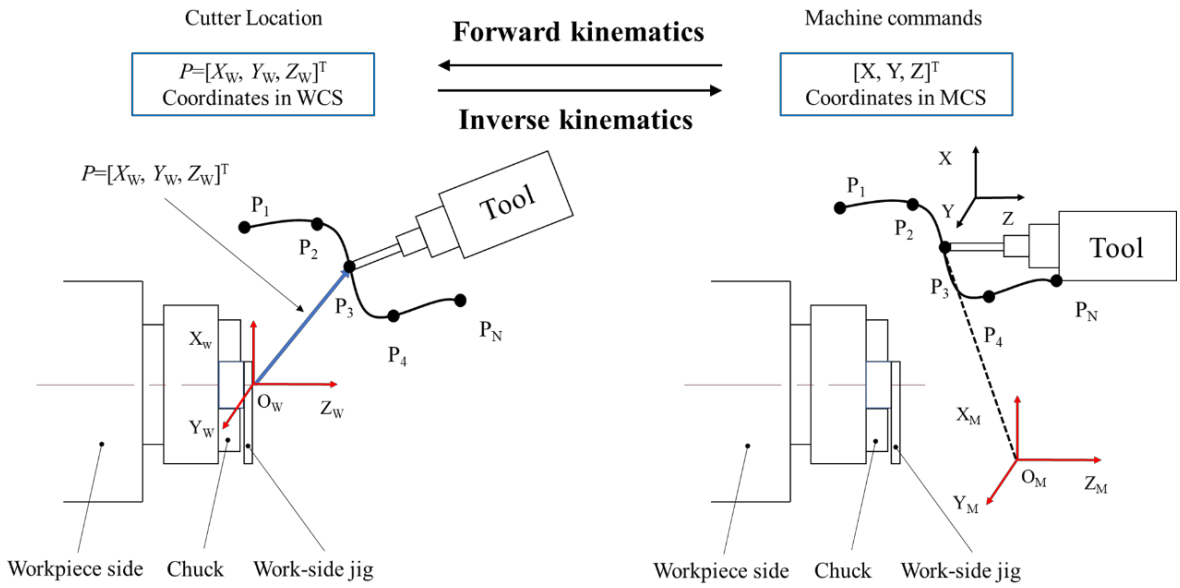

Figure 3.2 Forward and inverse kinematics

The kinematic module of the multi-tasking machine tool, which includes the forward and inverse kinematics as shown in Fig. 3.2, is the basic idea to compensate the geometric deviations. The forward kinematic describes the cutter location in the workpiece coordinate system as a function of three linear drives' displacements in the machine coordinate system. On the contrary, the inverse kinematic is used to calculate the commands of three translational axes from the cutter location. In the information flow of the multi-tasking machine tool, the forward and inverse kinematics are performed at different levels. For convenience, the kinematic module ignoring the geometric deviations is named as the ideal kinematic module, while the one considering the geometric deviations is named as the actual kinematic module.

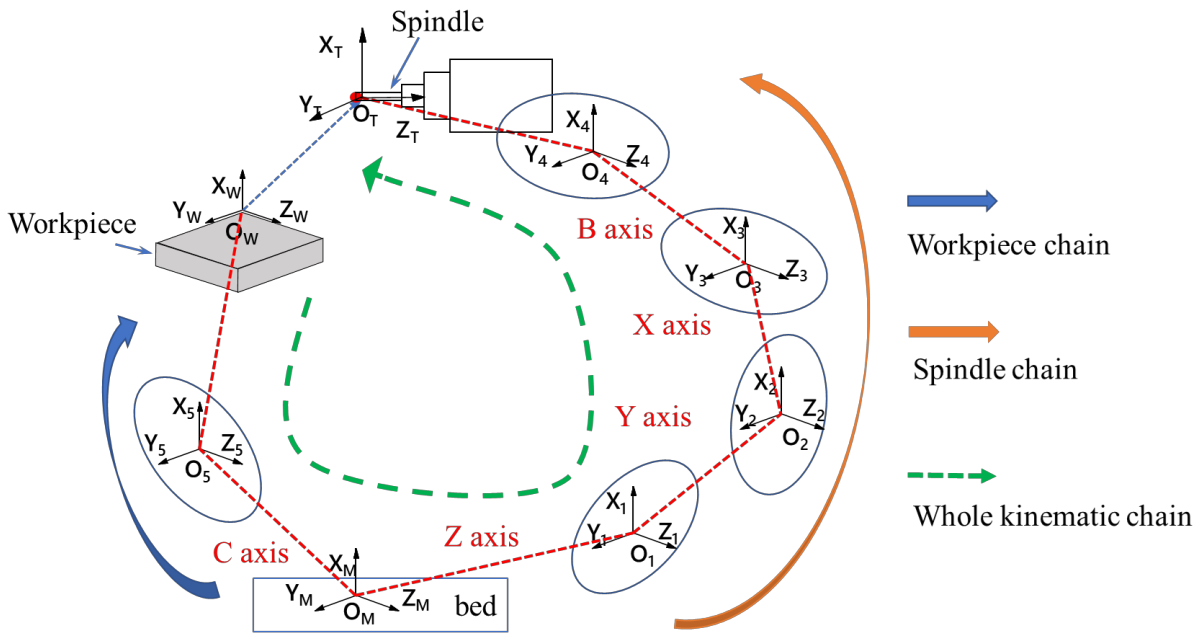

Figure 3.3 Kinematic chains of a multi-tasking machine tool

Based on the topological structure of the targeted multi-tasking machine tool (Fig. 2.1), the kinematic chains in details are illustrated in Fig. 3.3. The workpiece chain is from the reference coordinate system to C axis and finally the workpiece located on the table of C axis. The spindle chain is from the reference coordinate system to Z axis, Y axis, X axis, B axis, and the cutting spindle attached to B axis. The whole kinematic chain is from the workpiece to C axis, reference coordinate system, Z axis, Y axis, X axis, then to B axis and the cutting spindle. The reference coordinate system O_M-$X_MY_MZ_M$ is attached to the machine bed and designed by the manufacture when the movements of all axes are zero. The workpiece coordinate system Ow-XwYwZw and tool coordinate system O_T-$X_TY_TZ_T$ are each attached to the workpiece and the cutting spindle, respectively.

The compensation algorithm for the multi-tasking machine tool is shown in Fig 3.4.

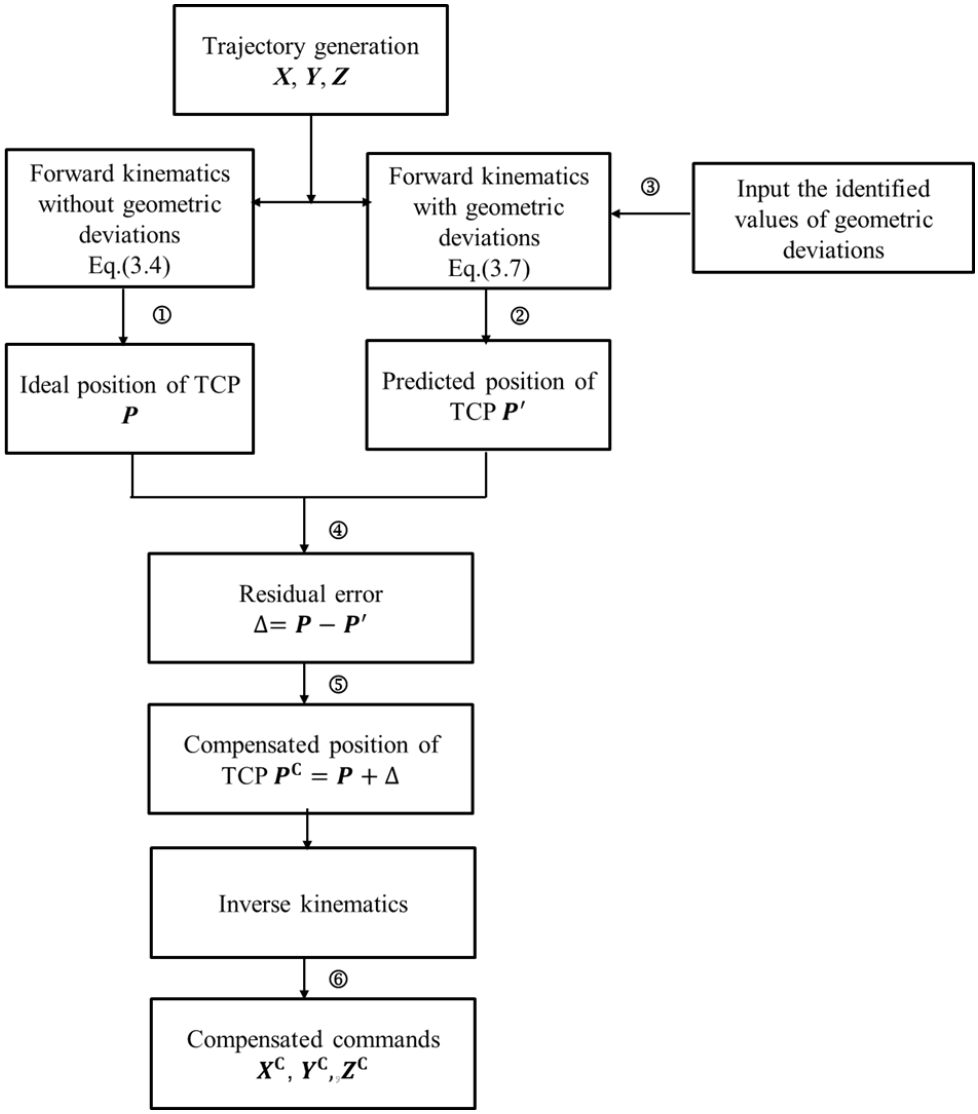

Figure 3.4 Compensation algorithm

In order to compensate the influence of geometric deviations on the positioning accuracy of the tool center point, other error sources described in Table 1.1 are ignored and not considered in this study. If the geometric deviations are all zero, the measured trajectory of the spindle controlled by the interpolated X, Y, and Z coordinate values will meet the desired circular trajectory controlled by a rotary axis. Thus, the eccentricity of the trajectory will be zero in theory. However, in the actual measurement, the trajectory of the spindle is not completely consistent with the theoretical circular trajectory because the geometric deviations are not zero. Therefore, there is an amount of eccentricity.

The main idea of the compensation is to add the opposite value of geometric deviation obtained from the first identification step to the homogenous transformation matrix to eliminate its influence on the eccentricity of the trajectory. Thus, the NC code of the interpolated circular trajectory after the compensation is the corrected NC code. For example, if the identified value of α_{XB} is +32 arcsecond, -32 arcsecond is substituted to

M_{XB} to calculate the compensated X, Y, and Z coordinate values for modifying the NC code to improve the positioning accuracy of the spindle.

The ideal kinematic module, which gives explicit solution for both forward and inverse kinematics module for the targeted machine configuration, is briefly reviewed at first because it is the basis of compensating the geometric deviations [65].

The forward kinematic formula is adopted to evaluate the position of TCP from three linear drives' displacements (Step 1 in Fig. 3.4). Equation (3.4) is to transform *X*, *Y* and *Z* coordinates of the TCP position in the machine coordinate system to X_{WI}, $Y_{WI}$and Z_{WI} in the workpiece coordinate system based on the forward kinematic. In there, X_{WI}, $Y_{WI}$and Z_{WI} are the coordinates of the ideal position of TCP, ignoring the geometric deviations of the machine tool.

$$P = \begin{bmatrix} X_{WI} \\ Y_{WI} \\ Z_{WI} \\ 1 \end{bmatrix} = E_{\mathrm{C}}^{-1} E_{\mathrm{B}} \begin{bmatrix} X \\ Y \\ Z \\ 1 \end{bmatrix} \tag{3.4}$$

Where, E_{C}^{-1} and E_{B} are the forward kinematic transformation matrices of the machine tool. The whole kinematic chain is counted from the workpiece towards the cutting spindle. Thus, in the forward kinematic E_{B} represents the displacement when B axis is rotated at the angle $\emptyset$, shown in Eq. (3.5). Due to the topological structure of the targeted machine tool, shown in Fig. 2.1, C rotary axis as the workpiece table is on the opposite side of the spindle. Therefore, the forward kinematic transformation matrix E_{C}^{-1} is calculated from the inverse of transformation matrix E_{C} which is the displacement when C axis is rotated at the angle θ. The E_{C}^{-1} is expressed in Eq. (3.6).

$$E_{\mathrm{B}} = \begin{bmatrix} \cos\emptyset & 0 & \sin\emptyset & 0 \\ 0 & 1 & 0 & 0 \\ -\sin\emptyset & 0 & \cos\emptyset & 0 \\ 0 & 0 & 0 & 1 \end{bmatrix} \tag{3.5}$$

$$E_{\mathrm{C}}^{-1} = \begin{bmatrix} \cos\theta & -\sin\theta & 0 & 0 \\ \sin\theta & \cos\theta & 0 & 0 \\ 0 & 0 & 1 & 0 \\ 0 & 0 & 0 & 1 \end{bmatrix}^{-1} = \begin{bmatrix} \cos\theta & \sin\theta & 0 & 0 \\ -\sin\theta & \cos\theta & 0 & 0 \\ 0 & 0 & 1 & 0 \\ 0 & 0 & 0 & 1 \end{bmatrix} \tag{3.6}$$

However, the actual position of TCP becomes P' due to the geometric deviations which can be predicted by the forward kinematics of the machine tool (Step 2 in Fig. 3.4). Equation (3.7) is to calculate the actual position in the workpiece coordinate system by inputting the identified values of the geometric deviations existing in the machine tool to the forward kinematic (Step 3 in Fig. 3.4).

$$P' = \begin{bmatrix} X_{WA} \\ Y_{WA} \\ Z_{WA} \\ 1 \end{bmatrix} = E_{\mathrm{C}}^{-1} M_{\mathrm{CZ}}^{-1} M_{\mathrm{XB}} E_{\mathrm{B}} M_{\mathrm{BT}} \begin{bmatrix} X \\ Y \\ Z \\ 1 \end{bmatrix} \tag{3.7}$$

Where, X_{WA}, Y_{WA} and Z_{WA} are the coordinates of the actual position of TCP, considering the geometric deviations of the machine tool. M_{CZ} is an HTM of the geometric deviations between C axis and the bed of the machine tool, and M_{XB} is an HTM of the geometric deviations between B and the X axes, and M_{BT} is an HTM of the geometric deviations between the spindle and B axis. The M_{CZ}^{-1}, inverse of the transformation matrix M_{CZ}, is used in Eq. (3.7) by analyzing the whole kinematic chain that is counted from the workpiece towards the cutting spindle. The reason is that the geometric deviations between C axis and the bed of the machine tool are on the opposite side of the spindle. By ignoring the higher-order terms, the M_{CZ}^{-1}, M_{XB}, and M_{BT} are expressed in Eqs. (3.8) - (3.10).

$$M_{\mathrm{CZ}}^{-1} = \begin{bmatrix} 1 & 0 & \beta_{\mathrm{CZ}} & \delta x_{\mathrm{CZ}} \\ 0 & 1 & -\alpha_{\mathrm{CZ}} & \delta y_{\mathrm{CZ}} \\ -\beta_{\mathrm{CZ}} & \alpha_{\mathrm{CZ}} & 1 & 0 \\ 0 & 0 & 0 & 1 \end{bmatrix}^{-1} = \begin{bmatrix} 1 & 0 & -\beta_{\mathrm{CZ}} & -\delta x_{\mathrm{CZ}} \\ 0 & 1 & \alpha_{\mathrm{CZ}} & -\delta y_{\mathrm{CZ}} \\ \beta_{\mathrm{CZ}} & -\alpha_{\mathrm{CZ}} & 1 & 0 \\ 0 & 0 & 0 & 1 \end{bmatrix} \tag{3.8}$$

$$M_{\mathrm{XB}} = \begin{bmatrix} 1 & -\gamma_{\mathrm{XB}} & \beta_{\mathrm{XB}} & 0 \\ \gamma_{\mathrm{XB}} & 1 & -\alpha_{\mathrm{XB}} & 0 \\ -\beta_{\mathrm{XB}} & \alpha_{\mathrm{XB}} & 1 & 0 \\ 0 & 0 & 0 & 1 \end{bmatrix} \tag{3.9}$$

$$M_{\mathrm{BT}} = \begin{bmatrix} 1 & 0 & 0 & \delta x_{\mathrm{BT}} \\ 0 & 1 & -\alpha_{\mathrm{BT}} & 0 \\ 0 & \alpha_{\mathrm{BT}} & 1 & \delta z_{\mathrm{BT}} \\ 0 & 0 & 0 & 1 \end{bmatrix} \tag{3.10}$$

The predicted position with geometric deviations (P′) are compared against the ideal desired trajectory (P) to predict the error components Δ, shown as Eq. (3.11) (Step 4 in Fig. 3.4).

$$\Delta = P - P' = \begin{bmatrix} X_{WI} \\ Y_{WI} \\ Z_{WI} \\ 1 \end{bmatrix} - \begin{bmatrix} X_{WA} \\ Y_{WA} \\ Z_{WA} \\ 1 \end{bmatrix} \tag{3.11}$$

The error components are added to the desired trajectory (P) to generate a new position of TCP (P^{C}) with the compensation of geometric deviations, shown as Eq. (3.12) (Step 5 in Fig. 3.4).

$$P^{\mathrm{C}} = \begin{bmatrix} X_W^C \\ Y_W^C \\ Z_W^C \\ 1 \end{bmatrix} = \begin{bmatrix} X_{WI} \\ Y_{WI} \\ Z_{WI} \\ 1 \end{bmatrix} + \Delta \tag{3.12}$$

Where, X_W^C, Y_W^C and Z_W^C are the coordinates of the compensated position of TCP in the

workpiece coordinate system.

The new position of TCP (P^{C}) is passed through the inverse kinematic of the machine tool to generate the commands with the compensation of geometric deviations components ($X^{\mathrm{C}}, Y^{\mathrm{C}}, Z^{\mathrm{C}}$) in the machine coordinate system, shown as Eq. (3.13) (Step 6 in Fig. 3.4).

$$\begin{bmatrix} X^C \\ Y^C \\ Z^C \\ 1 \end{bmatrix} = M_{\mathrm{BT}}^{-1} E_{\mathrm{B}}^{-1} M_{\mathrm{XB}}^{-1} M_{\mathrm{CZ}} E_{\mathrm{C}} P^{\mathrm{C}} = M_{\mathrm{BT}}^{-1} E_{\mathrm{B}}^{-1} M_{\mathrm{XB}}^{-1} M_{\mathrm{CZ}} E_{\mathrm{C}} \begin{bmatrix} X_W^C \\ Y_W^C \\ Z_W^C \\ 1 \end{bmatrix} \tag{3.13}$$

Where, M_{BT}^{-1}, E_{B}^{-1}, and M_{XB}^{-1} are the inverse of the transformation matrices M_{BT}, E_{B}, and M_{XB}, respectively. Since B and C rotary axes exist on both sides of the bed in the multi-tasking machine tool respectively, the inverse of the transformation matrices, M_{BT}^{-1}, E_{B}^{-1}, and M_{XB}^{-1}, are used to reflect the geometric deviations and rotation of B axis, while the transformation matrices, M_{CZ} and E_{C}, are used to reflect the geometric deviations and rotation of C axis in the inverse kinematics.

However, this linear method does not compensate all the errors because of the nonlinear kinematic of the multi-tasking machine tool. If the geometric deviations are large, a second iteration may be needed.

3.4 Conclusion

In this chapter, to compensate the geometric deviations which exist in a multi-tasking machine tool, the current algorithms and compensation methods for five-axis machining centers are investigated firstly. Then, a simple compensation method without any iteration is established based on the idea of screw method. Conclusions are summarized as follows.

1. Based on the analysis of the compensation methods for five-axis machining centers, the idea of screw method is used to model kinematics of the targeted multi-tasking machine tool.
2. The forward and inverse kinematics are analyzed in detail for the targeted machine tool. According to the topological structure, the formulae for the compensation are derived and they can be used to modify the NC code for compensating the influence of the geometric deviations on the position of tool center point.

Chapter 4 Identification and compensation with a ball bar

4.1 Preface

Referring to the simulation results in Chapter 2, if B axis is measured in the Cartesian coordinate system and C axis is measured in the cylindrical coordinate system, the mounting error of the workpiece side ball for a measuring instrument does not affect the eccentricity of the trajectory. Therefore, to eliminate the influence of the mounting errors on the eccentricity of trajectory, B axis measurements in the Cartesian coordinate system and C axis measurements in the cylindrical coordinate system are adopted in this study.

In this chapter, a ball bar is used to identify the geometric deviations of a multi-tasking machine tool, which has a swivel spindle head in the horizontal position. In Section 4.2, a measuring procedure is designed based on the analysis of the influence factors on circular trajectories in case of four measuring patterns. In Section 4.3, the measuring procedure is applied in a common multi-tasking machine tool and the geometric deviations are identified by using the eccentricities of trajectories. In Section 4.4, according to the compensation method in Chapter 3, the NC code is modified to make the actual position of the spindle side ball reach the desired position. The influence of the existing geometric deviations on the eccentricities of measuring trajectories is compensated and the position error of tool center point (TCP) is reduced.

4.2 Measuring procedure with a ball bar

4.2.1 Introduction of ball bar

A ball bar is one of the measuring instruments used to identify the geometric deviations. Figure 4.1 shows the configuration of the ball bar system. The ball bar system consists of a ball bar and two magnet sockets. The ball bar is essentially a one-dimensional ultra-high-precision telescopic linear sensor with a precision ball at each end, with one fixed and the other spring-loaded. These two steel balls are magnetically supported by a magnet socket with a built-in permanent magnet. Two magnet sockets are attached to the work side and the spindle side, respectively. In addition, the socket on the spindle side has a screw mechanism for aligning the center of the spindle side ball with the center of the spindle.

Figure 4.2 shows the measurement by using the ball bar system. The two steel balls at both ends of the ball bar are attached to the work side socket and the spindle side socket, respectively. When the straight shaft and the swivel shaft are simultaneously controlled and moved, the relative distance between the two balls is kept constant. And the change in the relative distance can be measured and recorded as expansion and contraction with respect to the reference length.

The ball bar used in this study is QC20-W manufactured by Renishaw, and the specification of the ball bar system is shown in Table 4.1. The QC20-W has a sphere diameter of 12.7 mm and has a built-in battery. The measurement results can be transmitted to the PC by wireless communication via Bluetooth. The reference length can be changed to 50 mm, 100 mm, and 150 mm by using the extension bar.

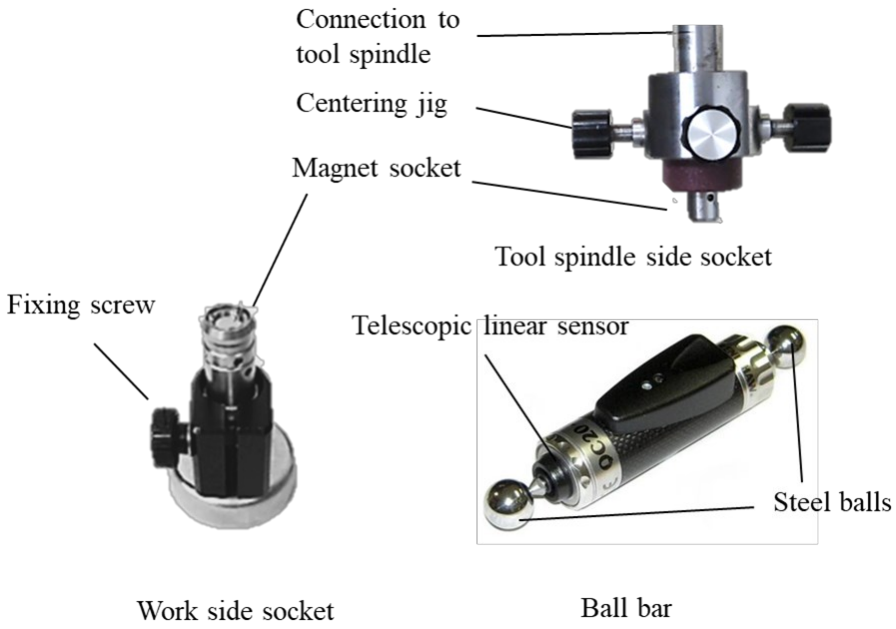

Figure 4.1 Configuration of Ball bar system (QC20-W, Renishaw)

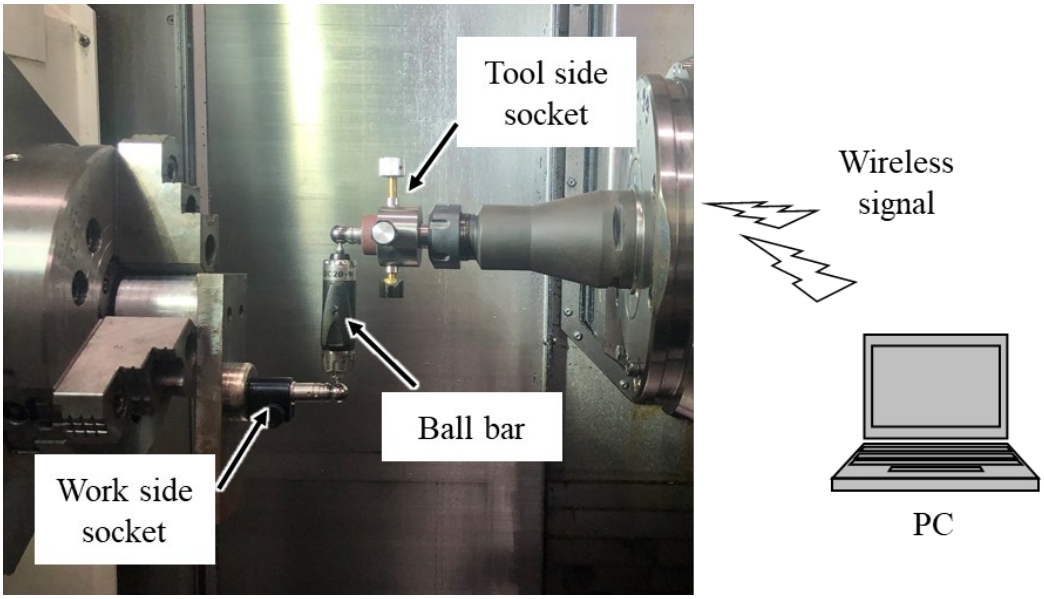

Figure 4.2 Measurement by using ball bar system

Table 4.1 Specification of ball bar system (QC20-W, Renishaw)

Sensor resolution	0.1 μm
Ball bar measurement accuracy (at 20°C)	±0.5 μm
Ball bar measuring range (at 20°C)	±1.25 μm
Sensor stroke	±1.0 mm
Maximum sample rate	1000 Hz
Data transmission range (Bluetooth, Class 2)	10 m typical
Operating temperature range	0°C~ 40°C
Reference length	100 mm (50mm, 150mm, 300 mm with extension)

4.2.2 Preparation before measurement

Before conducting the measuring procedure, centering check and distance measurement are necessary to ensure accurate measurement values and prepare for the calculation of the geometric deviations. The operation in detail is explained as follows.

1. Chucking of centering jig and fixing of work-side jig

(1) Insert the tool-side centering jig into the collet chuck and tighten it sufficiently with a special tool so that it can be attached to the spindle. The chucking of the centering jig is shown in Fig. 4.3.

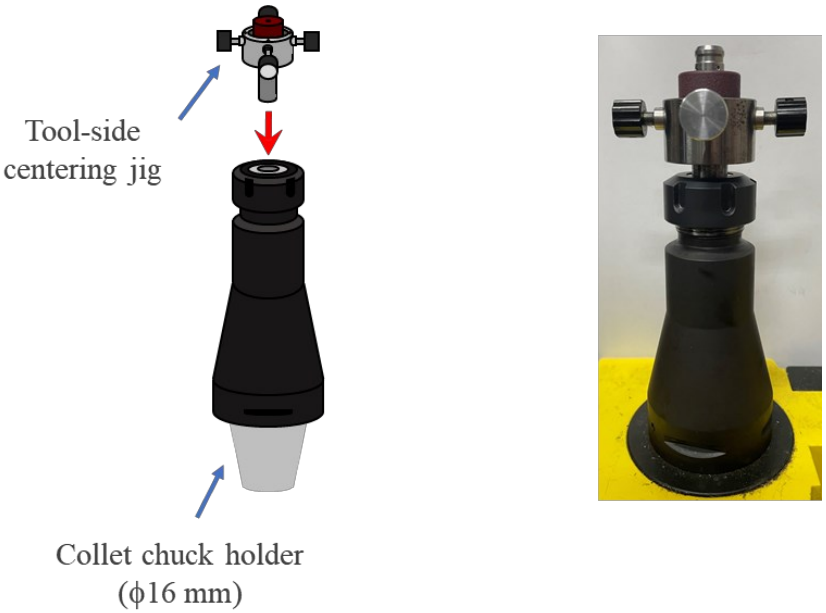

Figure 4.3 Chucking of tool-side centering jig

(2) Fix the cylindrical part of the work-side jig to the three-jaw chuck. This step is shown in Fig. 4.4.

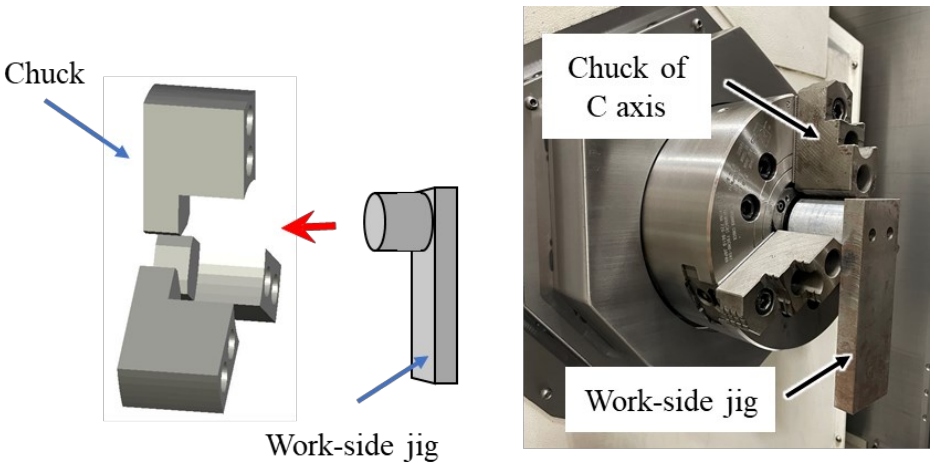

Figure 4.4 Fixing of work-side jig

2. Measurement of tool length R_B

The measurement of tool length R_B is shown in Fig. 4.5.

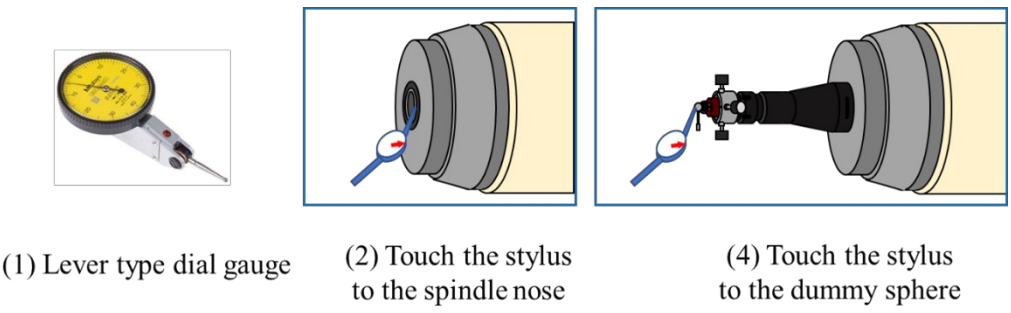

Figure 4.5 Measurement of tool length R_B

(1) Mount the magnet base equipped with the lever type dial gauge at the appropriate position of the work-side jig fixed to the chuck.

(2) While adjusting X axis and Y axis, move the spindle head in the negative direction of Z axis, and touch the stylus of the dial gauge to the spindle nose. Take the reading of the dial gauge, Z_G, and record the machine coordinate Z_N of Z axis. The dial gauge may be set to zero.

(3) Without moving the dial gauge, move the spindle head in the positive direction of Z axis, attach the collet chuck chucking the centering jig to the spindle, and then attach the dummy sphere.

(4) Carefully move the spindle head so that the dummy sphere touch the dial gauge stylus and adjust the X and Y axes to find the X and Y positions that maximize the dial gauge reading. Carefully move the spindle head at that position until the dial gauge reads Z_G. The machine coordinate Z_D of this Z axis is recorded.

(5) Tool length R_B is the difference between Z_N and ($Z_D - r$). Here, r is the diameter of the dummy sphere.

3. Centering check

The operation of aligning the spindle side ball with the rotation center of the spindle is important to reduce the measurement error. This error has a significant effect on the measured eccentricities.

(1) Fix the collet chuck holder to the spindle bore, and then attach a dummy sphere to the too spindle side socket. The work side socket is mounted on the work-side jig by visual inspection.

(2) Move the spindle by the handwheel to make the dummy sphere docked to the work side socket. The work side socket is clamped, and the coordinate values (X_0, Z_0) in the machine coordinate system are recorded. Here, X_0 is the coordinate value of X axis, and Z_0 is the coordinate value of Z axis. This step is shown in Fig. 4.6.

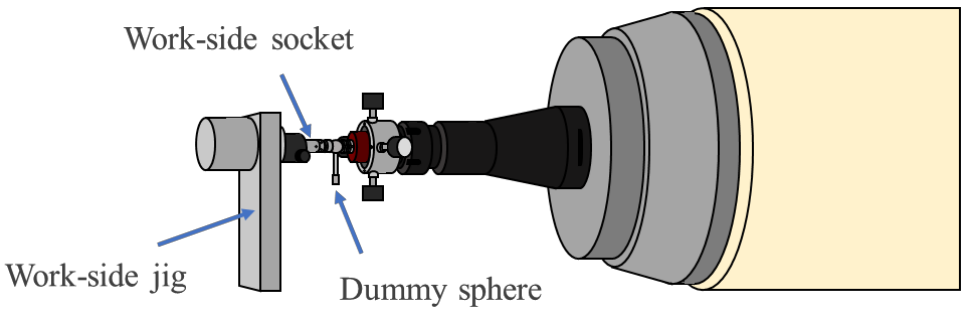

Figure 4.6 Determination of machine coordinate (X_0, Z_0)

(3) Move the spindle head away from the Z axis in the positive direction and move the X and Z axes to (X_0-100, Z_0) when the reference length of the ball bar is 100 mm.

(4) Set the spindle to “unclamp” to align the spindle side ball with the rotation center of the spindle. Set the ball bar between the spindle side socket and the work side socket.

(5) Turn the spindle slowly by hand and adjust the change in the distance between the two balls displayed on the PC screen to within $\pm 1\mu m$ by using the adjustment screws. This step is shown in Fig. 4.7.

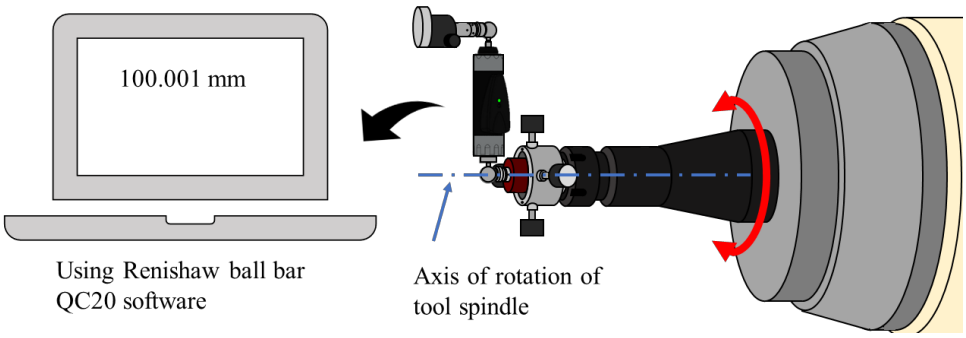

Figure 4.7 Setting ball bar and minute adjustment

4. Measurement of distance Z_C

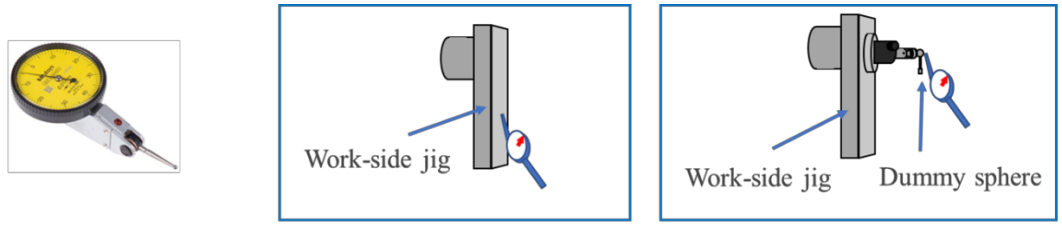

Figure 4.8 Measurement of the distance Z_C

The measurement of distance Z_C is shown in Fig. 4.8.

(1) Mount the magnet base equipped with the lever type dial gauge at the appropriate position of the tool setup stand.

(2) While adjusting X axis and Y axis, move the spindle head in the negative direction of Z axis, and touch the stylus of the dial gauge to the surface of the work-side jig. Take the reading of the dial gauge, Z_{DG}, and record the machine coordinate Z_W of Z axis. The dial gauge may be set to zero.

(3) Without moving the dial gauge, move the spindle head in the positive direction of Z axis, mount the work side socket on the work-side jig and clamp it, and then attach the dummy sphere.

(4) Carefully move the spindle head so that the dial gauge stylus touch the dummy sphere and adjust the X and Y axes to find the X and Y positions that maximize the dial gauge reading. Carefully move the spindle head at that position until the dial gauge reads

Z_{DG}. The machine coordinate Z_{DW} of this Z axis is recorded.

(5) The distance Z_C is the difference between ($Z_{DW}-r$) and Z_W. Here, r is the diameter of the dummy sphere.

4.2.3 Measuring patterns and relationship between eccentricities and geometric deviations

1. Pattern BX: B axis X direction measurement

The B axis X direction measurement is designed as shown in Fig. 4.9. It is named by the sensitive direction of ball bar during the measurement. The ball bar is placed horizontally along X axis and still stationary when B axis rotates from 0 degrees to 90 degrees around the spindle side ball. Since the sensitive direction of ball bar is always kept parallel to X axis, this measurement is named pattern BX. The influence of each geometric deviation on the eccentricity of pattern BX is analyzed as follows.

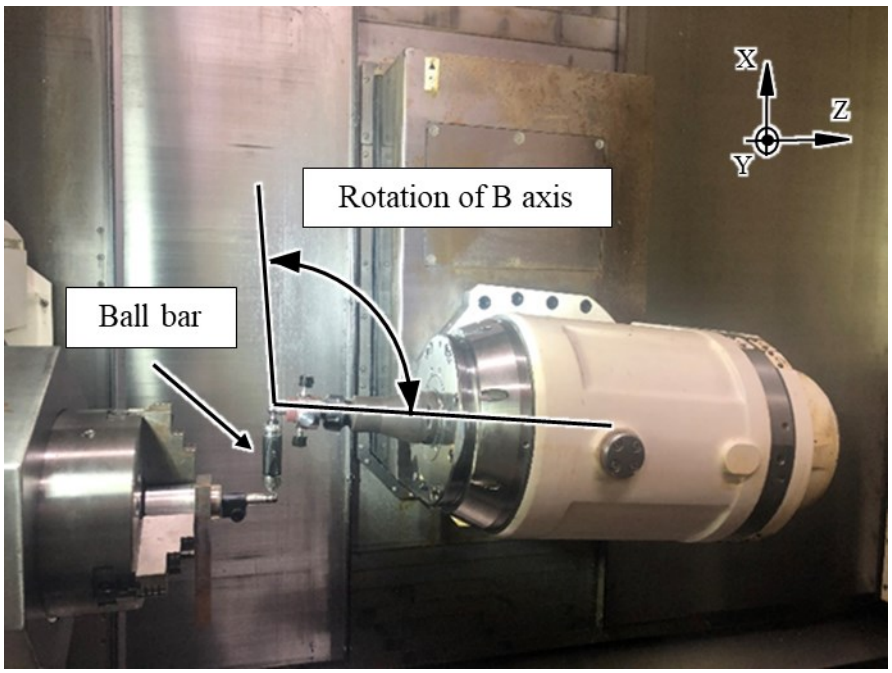

Figure 4.9 B axis X-direction measurement

(1) Positional deviation, δz_{BT}

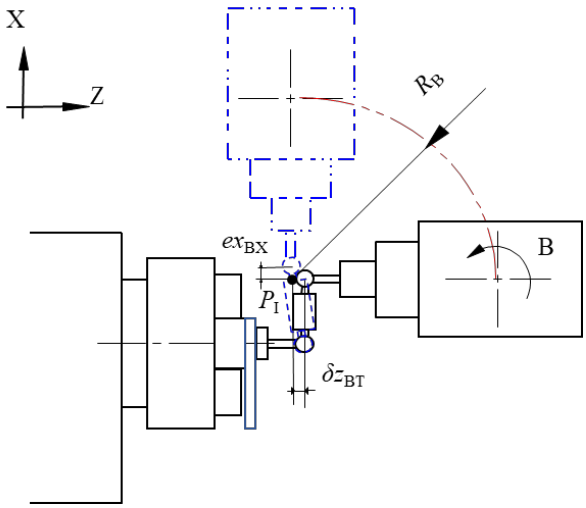

Figure 4.10 Influence of δz_{BT} on the eccentricity of BX measurement

δz_{BT} can be explained as an error in the Z direction of the center of spindle side ball with respect to the B axis origin. If $\delta z_{BT} > 0$ and supposing there are not any other geometric deviations, the center coordinate of spindle side ball should be shifted to the +X direction by the distance δz_{BT}, illustrated in Fig. 4.10. Therefore,

$$ex_{BX} = \delta z_{BT} \tag{4.1}$$

In there, ex_{BX} is the center eccentricity of the trajectory in the X direction when B axis X direction measurement is conducted. As δz_{BT} can be considered as the error of the tool length and is adjustable when measuring every time, the value of ex_{BX} is different according to the setting error of the spindle. Moreover, ex_{BX} can not be compensated by modifying the coordinates of X, Y and Z axes. Thus, ex_{BX} is not considered and the identification of δz_{BT} is not studied in this thesis.

(2) Angular deviation, β_{XB}

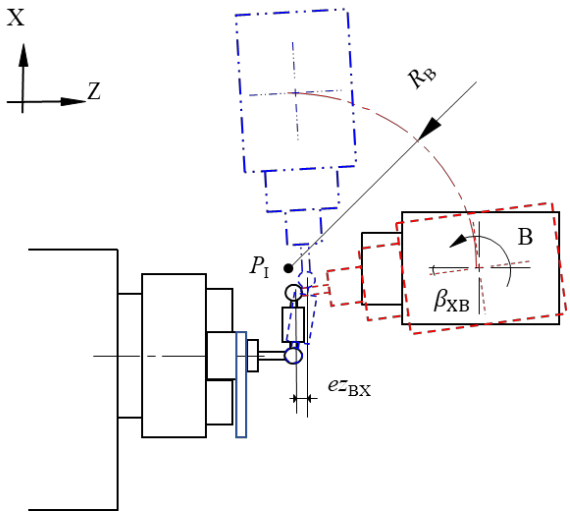

Figure 4.11 Influence of β_{XB} on the eccentricity of BX measurement

The influence of β_{XB} on the eccentricity is illustrated in Fig. 4.11. Because of the inclination of B axis by β_{XB} around Y axis, supposing $\beta_{XB} > 0$, the center coordinate of spindle side ball will differ in +Z direction by the distance $R_B\beta_{XB}$. Thus, the eccentricity of the trajectory in the Z direction ez_{BX} will occur, shown in Eq. (4.2).

$$ez_{BX} = R_B\beta_{XB} \tag{4.2}$$

In there, R_B represents the tool length.

2. Pattern BY: B axis Y direction measurement

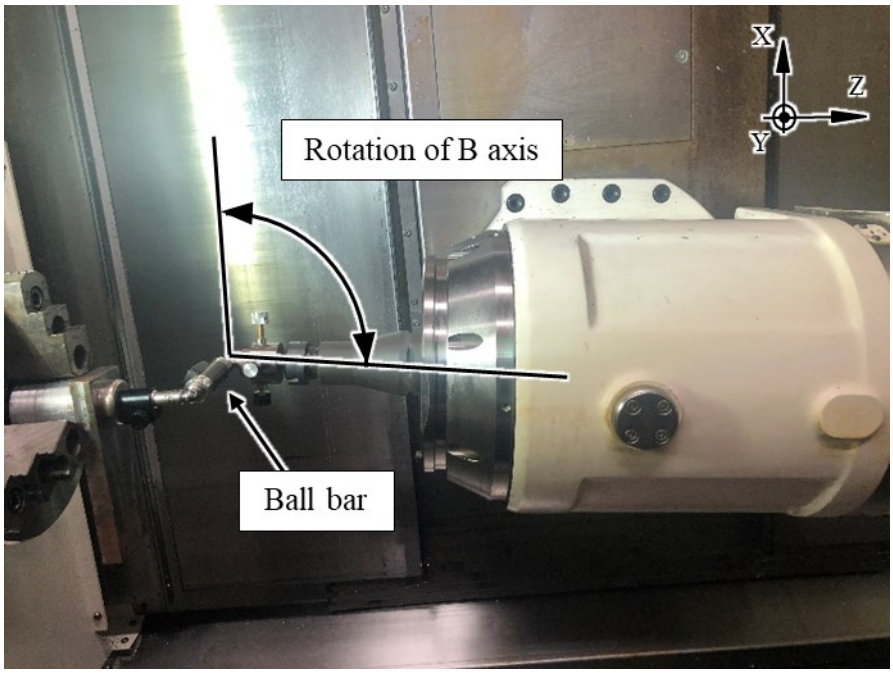

Figure 4.12 B axis Y-direction measurement

Figure 4.12 shows B axis Y direction measurement. During this measurement, B axis is rotated from 0 degrees to 90 degrees around the spindle side ball, and the motions of B, X and Z axes are driven analogously as those in the pattern BX. However, the sensitive direction of the ball bar is set as parallel to Y axis. Therefore, it is called B axis Y direction measurement. The influence of each geometric deviation on the eccentricity of the trajectory is analyzed as follows.

(1) Angular deviation, γ_{XB}

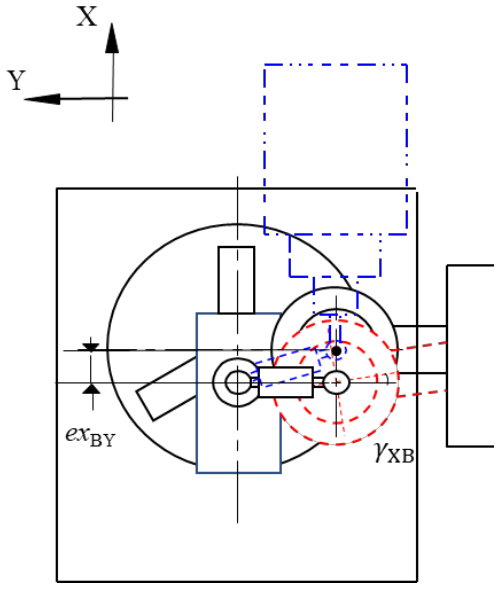

Figure 4.13 Influence of γ_{XB} on the eccentricity of BY measurement

The influence of γ_{XB} on the eccentricity of the BY measurement is illustrated in Fig. 4.13. Because of the inclination of B axis by γ_{XB} around Z axis, supposing $\gamma_{XB} > 0$ and there are not any other geometric deviations, the B axis origin is shifted to the -X direction by the distance $R_B\gamma_{XB}$. Thus, the center eccentricity of the trajectory in -X direction can be expressed as Eq. (4.3).

$$ex_{BY} = -R_B\gamma_{XB} \tag{4.3}$$

(2) Angular deviation, α_{XB}

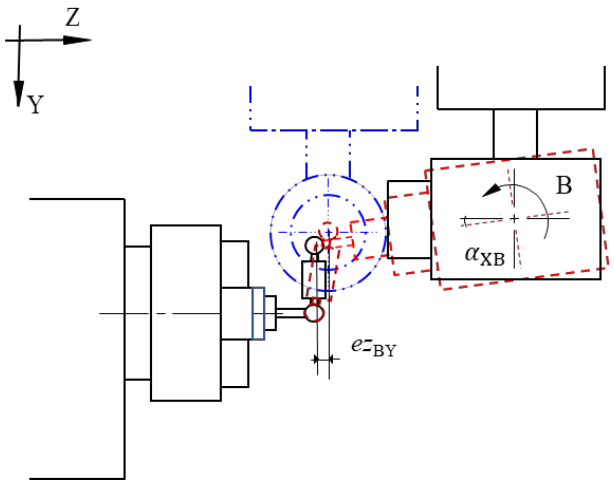

Figure 4.14 Influence of α_{XB} on the eccentricity of BY measurement

The influence of α_{XB} on the eccentricity of the BY measurement is illustrated in Fig. 4.14. Similarly, because of the inclination angle α_{XB} of B axis around X axis, supposing $\alpha_{XB} > 0$, the center coordinate of spindle side ball should be shifted in the YZ plane to the +Z direction by the distance $R_B\alpha_{XB}$, shown in Eq. (4.4).

$$ez_{\mathrm{BY}} = R_{\mathrm{B}}\alpha_{\mathrm{XB}} \tag{4.4}$$

3. Pattern CR: C axis radial direction measurement

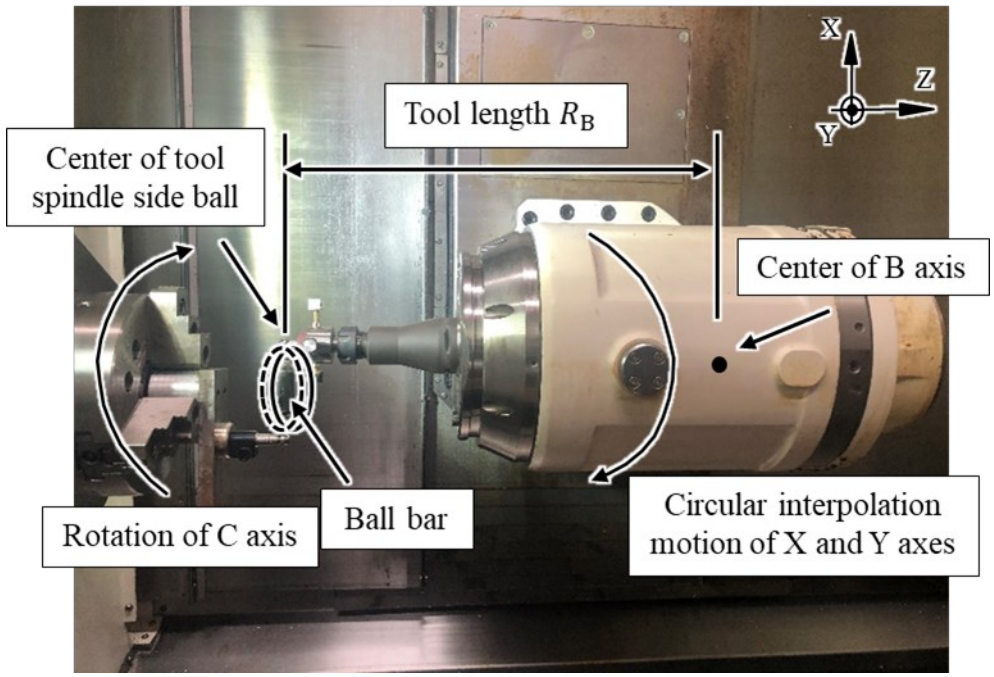

– – – Trajectory of workpiece side ball; —— Trajectory of spindle side ball

Figure 4.15 C axis radial direction measurement

Figure 4.15 shows C axis radial direction measurement, which is called pattern CR. In this figure, the dashed circle represents the trajectory of workpiece side ball driven by C axis rotation. The solid circle represents the circular interpolation motion of spindle side ball driven by X and Y axes. R_{B} is the length of the tool. The workpiece side ball reflects the rotation of C axis from 0 degrees to 360 degrees, and the spindle side ball moves under a circular interpolation motion of X and Y axes in the XY plane. The ball bar is used to measure the distance between these two balls. The sensitive direction of the ball bar is always consistent with the radial direction of the circular trajectory, so this measuring pattern is called C axis radial direction measurement, abbreviated by pattern CR. The influence of each geometric deviation on the eccentricity of this trajectory is analyzed as follows.

(1) Deviations δx_{BT}, δx_{CZ}, β_{XB}, and β_{CZ}

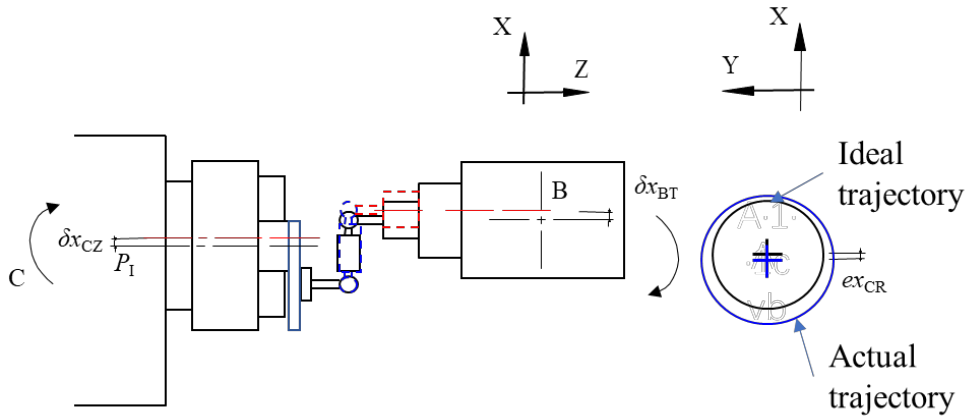

Figure 4.16 Influence of $(\delta x_{BT} - \delta x_{CZ})$ on the eccentricity of CR measurement

The influence of $(\delta x_{BT} - \delta x_{CZ})$ on the eccentricity is illustrated in Fig. 4.16. δx_{BT} is an X direction error of the spindle centerline with respect to the B axis origin. δx_{CZ} is an X direction error of the C axis centerline with respect to the machine coordinate system. The values of δx_{BT} and δx_{CZ} are included in the stretching and contraction change of ball bar. Because the workpiece side ball is mounted according to the position of the spindle side ball by a reference sphere, the values of δx_{BT} and δx_{CZ} can't be separated accurately. Therefore, the distance of $(\delta x_{BT} - \delta x_{CZ})$ can be measured as one unknown error that will affect the eccentricity of X direction.

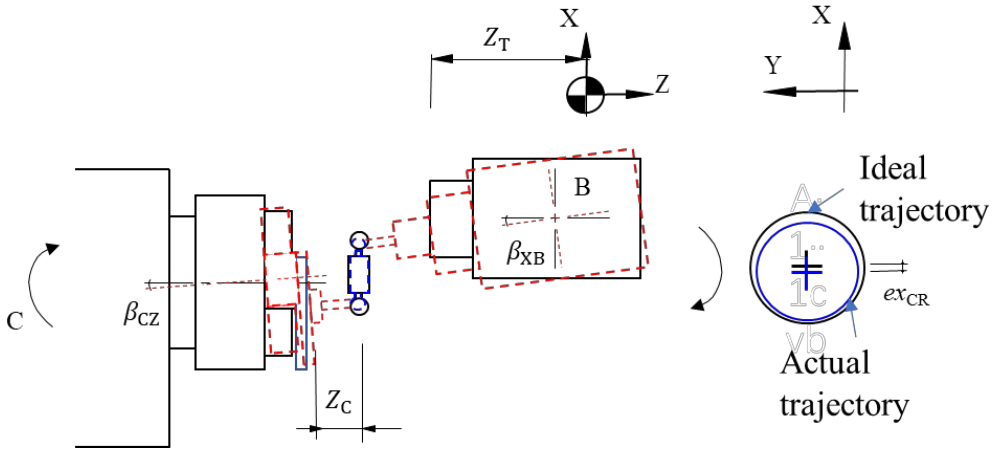

Figure 4.17 Influence of β_{XB} and β_{CZ} on the eccentricity of CR measurement

In Fig. 4.17, because of the inclination angle β_{XB} of B axis around Y axis, supposing $\beta_{XB} > 0$, the center coordinate of spindle side ball differs in -X direction by the distance $Z_T\beta_{XB}$. By the same analysis, the inclination angle β_{CZ} of C axis around Y axis causes the center coordinate of spindle side ball to differ in +X direction by the distance $Z_C\beta_{CZ}$. In conclusion, the eccentricity of the trajectory in X direction ex_{CR} is affected by $(\delta x_{BT} - \delta x_{CZ})$, β_{XB} and β_{CZ}, which is expressed as Eq. (4.5).

$$ex_{CR} = (\delta x_{BT} - \delta x_{CZ}) - Z_T \beta_{XB} + Z_C \beta_{CZ} \quad (4.5)$$

In there, Z_T indicates Z axis coordinate of the tool-holding spindle head in the machine coordinate system. Z_C indicates Z direction distance of the center position of the workpiece side ball to the surface of C axis table.

(2) Deviations δy_{CZ}, α_{XB}, α_{BT}, α_{CZ}, and γ_{XB}

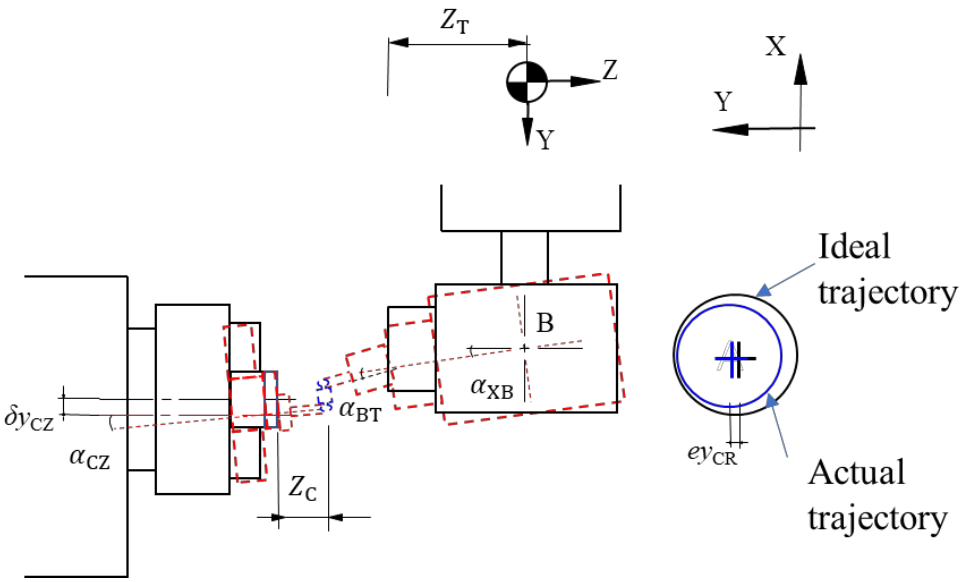

Figure 4.18 Influence of δy_{CZ} and α_{CZ}, α_{BT}, α_{XB} on the eccentricity of CR measurement

With the same analysis as the eccentricity of the trajectory in X direction, the eccentricity of the trajectory in Y direction ey_{CR} is affected by δy_{CZ}, α_{XB}, α_{BT}, α_{CZ}, and γ_{XB}, expressed as Eq. (4.6). As explained in Fig. 4.18, δy_{CZ} will cause the eccentricity in -Y direction. The eccentricity in +Y direction by the distance $Z_T(\alpha_{XB}+\alpha_{BT})$ will occur under the influence of α_{XB} and α_{BT}. In the table side, the angular deviation α_{CZ} causes the center coordinate of spindle side ball to shift to -Y direction by the distance $Z_C\alpha_{CZ}$. In the XY plane, illustrated in Fig. 4.19, the geometric deviation γ_{XB} causes the center coordinate of spindle side ball to shift to the -Y direction by the distance $X_T\gamma_{XB}$. In conclusion, the contributors of the eccentricity in Y direction ey_{CR} is expressed as Eq. (4.6).

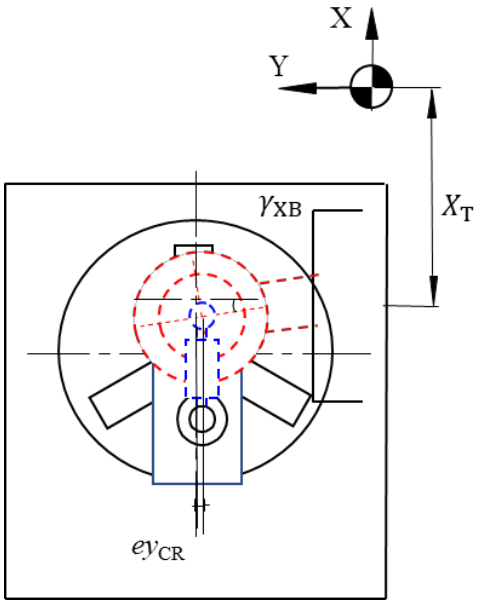

Figure 4.19 Influence of γ_{XB} on the eccentricity of CR measurement

$$ey_{CR} = -\delta y_{CZ} + Z_T\,(\alpha_{XB} + \alpha_{BT}) - Z_C\alpha_{CZ} - X_T\gamma_{XB} \tag{4.6}$$

In there, X_T indicates X axis coordinate of the tool-holding spindle head in the machine coordinate system.

4. Pattern CA: C axis axial direction measurement

C axis axial direction measurement is carried out as Fig. 4.20. In there, the dashed circle represents the trajectory of workpiece side ball driven by C axis rotation. The solid circle represents the circular interpolation motion of spindle side ball driven by X and Y axes. Because the sensitive direction of ball bar is always consistent to the axial direction of C axis during its rotation, this measuring pattern is called C axis axial direction measurement.

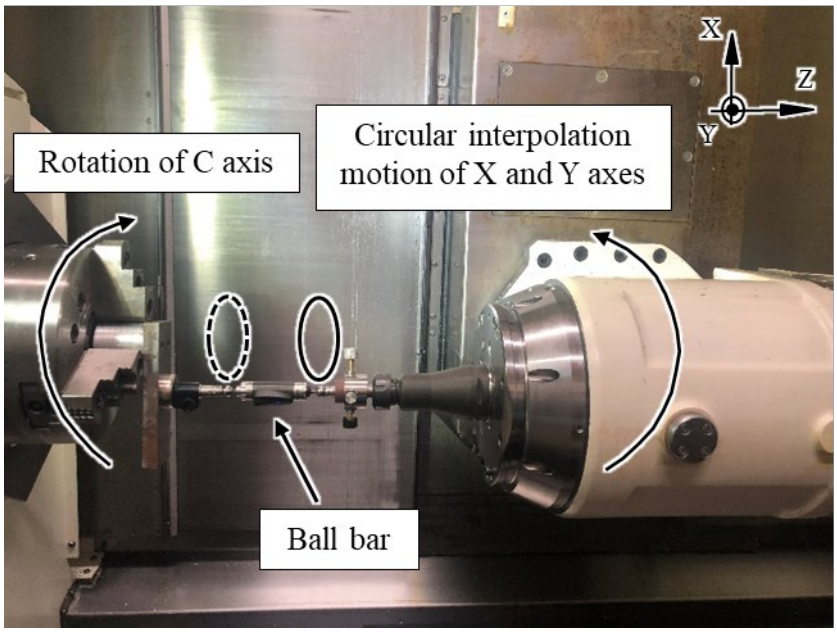

– – – Trajectory of workpiece side ball; —— Trajectory of spindle side ball

Figure 4.20 C axis axial direction measurement

The influence of each geometric deviation on the eccentricity of this circular trajectory is analyzed as follows.

(1) Angular deviation, β_{CZ}

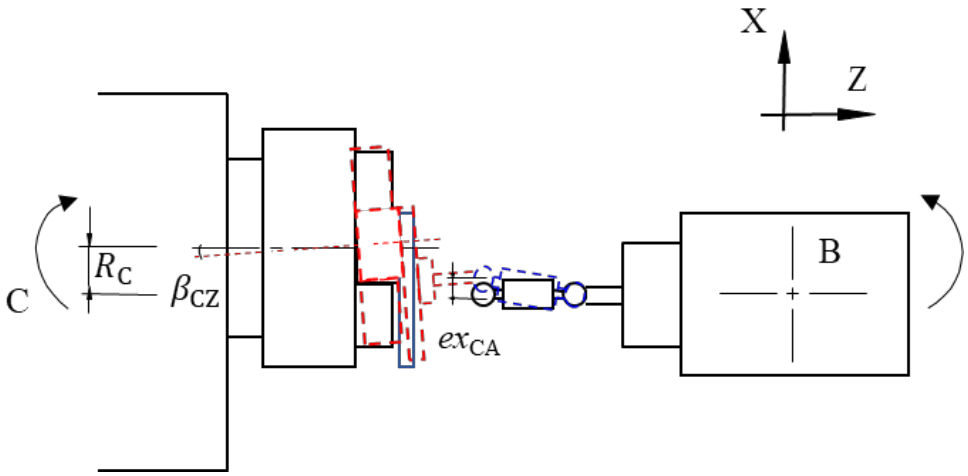

Figure 4.21 Influence of β_{CZ} on the eccentricity of CA measurement

In this measurement, the eccentricity of the trajectory in X direction ex_{CA} is influenced by angular deviation β_{CZ}. As shown in Fig. 4.21, supposing $\beta_{CZ} > 0$, the center coordinate of workpiece side ball is shifted to +X direction by the distance $R_C\beta_{CZ}$. Therefore, ex_{CA} can be expressed as Eq. (4.7).

$$ex_{CA} = R_C\beta_{CZ} \tag{4.7}$$

In there, R_C is the radius of the circular trajectory.

(2) Angular deviation, α_{CZ}

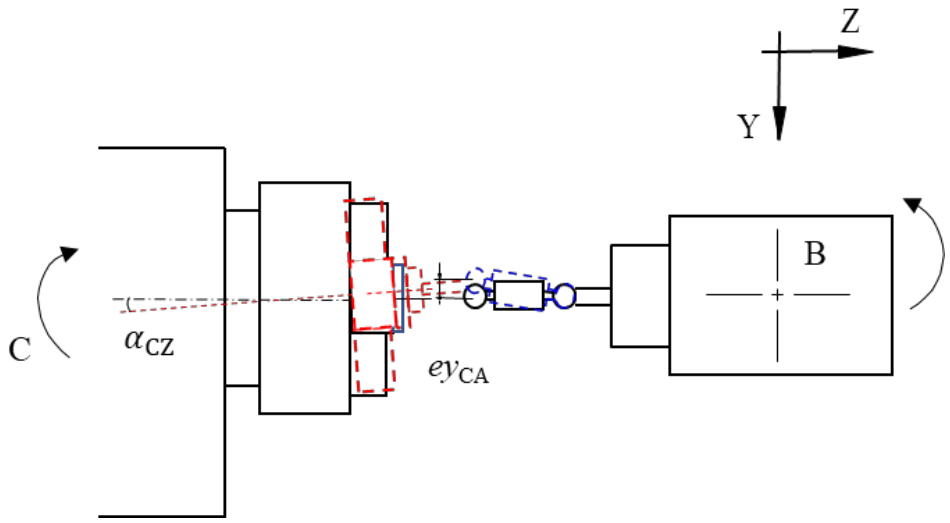

Figure 4.22 Influence of α_{CZ} on the eccentricity of CA measurement

The eccentricity of the trajectory in Y direction ey_{CA} is influenced by angular

deviation α_{CZ} in the YZ plane. As shown in Fig. 4.22, supposing $\alpha_{CZ} > 0$, the center coordinate of workpiece side ball is shifted to -Y direction by the distance $R_C\alpha_{CZ}$. Therefore, ey_{CA} can be expressed as Eq. (4.8).

$$ey_{CA} = -R_C\alpha_{CZ} \tag{4.8}$$

4.2.4 Measuring procedure

To calculate eight unknown parameters (α_{CZ}, β_{CZ}, α_{XB}, β_{XB}, γ_{XB}, α_{BT}, (δx_{CZ}-δx_{BT}), δy_{CZ}), pattern CR is needed to be measured again by changing the value of parameter R_B to get another independent expression. The reason is that only seven expressions of the eccentricities (from Eq. (4.2) to Eq. (4.8)) can be used to calculate geometric deviations through carrying out above four measuring patterns. They are not enough to calculate eight unknown parameters. Therefore, the measuring procedure is designed as follows.

Step 1: Set the ball bar parallel to X axis and carry out the B axis X direction measurement. The simultaneous B, X and Z axis movement is controlled by the generated NC code under the measured tool length R_B.

Step 2: Set the ball bar parallel to Y axis and carry out the B axis Y direction measurement by using the same simultaneous B, X and Z axis movement as step 1.

Step 3: Move the workpiece side ball to the position R_C, which is the distance from the centerline of C axis to the center of the workpiece side ball and carry out the C axis radial direction measurement. The NC code is changed to drive simultaneous C, X and Y axis movement.

Step 4: Set the ball bar parallel to Z axis without moving the workpiece side ball and carry out the C axis axial direction measurement. The simultaneous movement of C, X and Y axes always makes the sensitive direction of ball bar parallel to the Z axis direction.

Step 5: Attach a 50 mm extension bar at the spindle side to change the tool length from R_B to R'_B. Since the center of the spindle side ball is shifted by attaching the extension bar, the alignment operation of the spindle side ball with the rotation center of the spindle is required. Then, the tool length R'_B should be measured again and the parameter Z_T is correspondingly changed to Z'_T. After these pretreatments, C axis radial direction measurement is performed again under the modified NC code by using the measured tool length R'_B. This step is depicted in Fig. 4.23. Compared with Fig. 4.15, the tool length is changed from R_B to R'_B by using the extension bar.

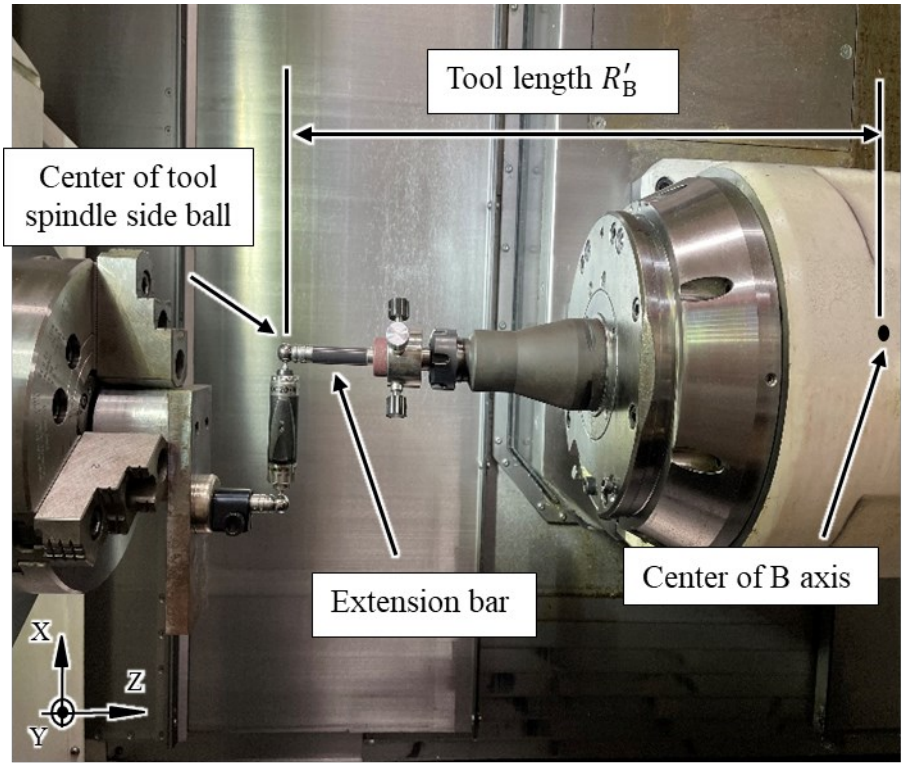

Figure 4.23 C axis radial direction measurement at the conditions of R'_B

According to Eq. (4.6) of Section 4.2.3, the measured Y direction eccentricity of circular trajectory in this step can be expressed as follows.

$$ey'_{CR} = -\delta y_{CZ} + Z'_T(\alpha_{XB} + \alpha_{BT}) - Z_C\alpha_{CZ} - X_T\gamma_{XB} \tag{4.9}$$

4.2.5 Formulae to identify geometric deviations

According to the eccentricities of measured circular arcs or circles trajectory, eight geometric deviations can be calculated and identified as follows.

Observing the Eqs. (4.2) to (4.9), there is only one unknown geometric deviation in Eqs. (4.2), (4.3), (4.4), (4.7), and (4.8). Therefore, the unknown geometric deviation can be directly calculated according to the related equations. Thus, five geometric deviations are derived, shown in the following Eqs. (4.10) to (4.14).

$$\alpha_{CZ} = -\frac{ey_{CA}}{R_C} \tag{4.10}$$

$$\beta_{CZ} = \frac{ex_{CA}}{R_C} \tag{4.11}$$

$$\alpha_{XB} = \frac{ez_{BY}}{R_B} \tag{4.12}$$

$$\beta_{XB} = \frac{ez_{BX}}{R_B} \tag{4.13}$$

$$\gamma_{XB} = -\frac{ex_{BY}}{R_B} \tag{4.14}$$

Then, substituting the results of Eqs. (4.11) and (4.13) into Eq. (4.5), the deviation (δx_{CZ}-δx_{BT}) can be determined as Eq. (4.15).

$$(\delta x_{CZ} - \delta x_{BT}) = -ex_{CR} + Z_C \frac{ex_{CA}}{R_C} - Z_T \frac{ez_{BX}}{R_B} \tag{4.15}$$

Finally, substituting the results of Eqs. (4.10), (4.12), and (4.14) into Eqs. (4.6) and (4.9), the following two relationships are obtained.

$$\begin{cases} \delta y_{CZ} - Z_T \alpha_{BT} = \frac{Z_T ez_{BY} + X_T ex_{BY}}{R_B} + \frac{Z_C}{R_C} ey_{CA} - ey_{CR} \\ \delta y_{CZ} - Z'_T \alpha_{BT} = \frac{Z'_T ez_{BY} + X_T ex_{BY}}{R_B} + \frac{Z_C}{R_C} ey_{CA} - ey'_{CR} \end{cases} \tag{4.16}$$

Therefore, the other two geometric deviations are calculated by the following Eqs (4.17) and (4.18).

$$\alpha_{BT} = \frac{ey'_{CR} - ey_{CR}}{Z'_T - Z_T} - \frac{ez_{BY}}{R_B} \tag{4.17}$$

$$\delta y_{CZ} = Z_C \frac{ey_{CA}}{R_C} + \frac{Z_T ey'_{CR} - Z'_T ey_{CR}}{Z'_T - Z_T} + X_T \frac{ex_{BY}}{R_B} \tag{4.18}$$

4.3 Identified results

4.3.1 Parameters of the targeted multi-tasking machine tool

The targeted machine tool in this study is INTEGREX i-200, a multi-tasking machine tool manufactured by Yamazaki Mazak Corporation, as shown in Fig. 4.24. It integrates turning and milling functionalities by adding a swivel spindle head to a turning machine tool. The specifications are shown in Table 4.2.

Figure 4.24 Multi-tasking machine tool (INTEGREX i-200)

Table 4.2 Specification of INTEGREX i-200

Specification		Bed Length – 1000U in
Capacity	Maximum Machining Diameter	658 mm
	Maximum Bar Work Capacity	65 mm
	Maximum Machining Length	1011 mm
Main Spindle	Chuck Size	8 in
	Maximum Speed	5000 rpm
	Motor Output (30 minute rating)	22 kw / 30.0 hp
Milling Spindle	B-Axis Travel	240°
	Maximum Speed	12000 rpm
	Motor Output (20 ED Rating)	22 kw / 30 hp
	Travel (X Axis)	615 mm
	Travel (Y Axis)	250 mm
	Travel (Z Axis)	1077 mm

4.3.2 Measured circular trajectories

Due to the limit of Y axis movable range shown in Table 4.2, the distance between the center line of C axis and the center of the workpiece side ball is set as $R_C = 50\,mm$ for pattern CR and CA measurements. The reference length of ball bar is 100 mm. Feed speed is set to 1000 mm/min. The measuring conditions during each step are shown in Table 4.3.

Table 4.3 Measuring conditions

Measuring steps	R_B (mm)	Z_C (mm)	Z_T (mm)	X_T (mm)
1. Pattern BX	356.3945	65.5348	112.2877	490
2. Pattern BY	356.3945	65.5348	112.2877	490
3. Pattern CR	356.3945	65.5348	112.2877	490
4. Pattern CA	356.3945	65.5348	112.2877	490
5. Pattern CR (R'_B, Z'_T)	406.4608	65.5348	62.2491	490

Where, R_B is the tool length. Z_C is Z axis coordinate of the center position of the workpiece side ball in table coordinate system. Z_T is Z axis coordinate of the tool-holding spindle head in machine coordinate system. X_T is X axis coordinate of the tool-holding spindle head in machine coordinate system.

The B axis measurement results in the Cartesian coordinate system are shown in Figs. 4.25. and 4.26. The C axis measurement results in the cylindrical coordinate system are

shown in Figs. 4.27 and 4.29. Among them, Fig. 4.29 shows the result of C axis radial direction measurement again when the tool length R_B is changed to R'_B.

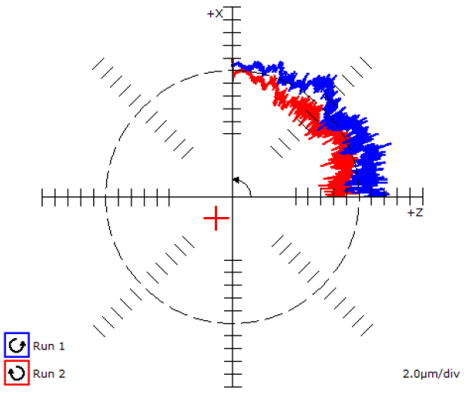

Figure 4.25 B axis X-direction

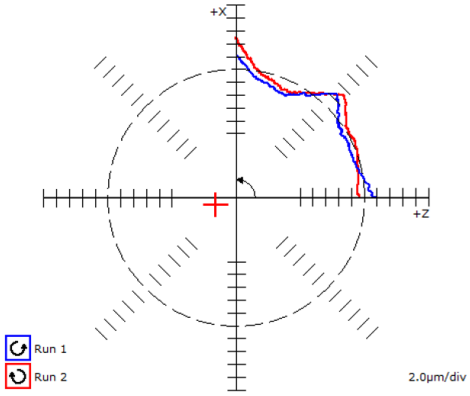

Figure 4.26 B axis Y-direction

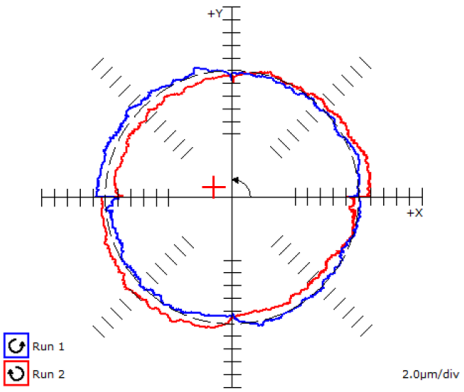

Figure 4.27 C axis radial direction

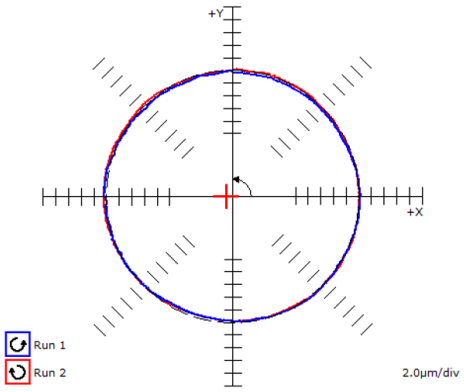

Figure 4.28 C axis axial direction

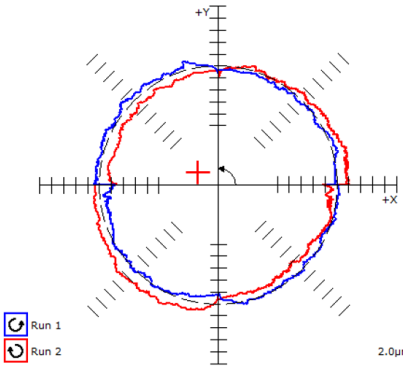

Figure 4.29 C axis radial direction (R'_B)

For each step, the measurement is conducted in the case of clockwise (CW) rotation and counterclockwise (CCW) rotation. In Figs 4.25-4.29, the red line represents the trajectory of CW measurement, and the blue line represents the trajectory of CCW measurement. The average value of CW and CCW eccentricities is used to identify geometric deviations and represented by the red cross in Figs 4.25-4.29.

Except for geometric deviations, the motion accuracy and synchronization error can be also explored from the measured trajectory.

Viewing from the B axis X-direction measurement in Fig. 4.25, the CW and CCW trajectories are greatly different because of the synchronization error. The synchronization error is the difference between the speeds of the circular interpolation motion of X and Z axes and the rotary motion of B axis, which is caused by the mismatch between backlash and position loop gain. In addition, the pitch error is found in the trajectory, which is a periodical vibration observed during the rotation of the swivel B axis. It is manifested by the meshing of the worm gear. In the B axis X-direction measurement, the amplitude of the pitch error is not constant because the sensitive direction of ball bar changes with respect to the rotation direction of B axis.

Viewing from the C axis radial direction measurement in Figs. 4.27 and 4.29, quadrant protrusion can be found, which is the error appeared when the movement direction of translational axis is switched during the circular interpolation motion. In fact, the quadrant protrusion does not affect the eccentricity of the trajectory. Therefore, it can be ignored when identifying the geometric deviations by using the measured eccentricity.

4.3.3 Discussion about the repeatability of eccentricities

The eccentricity of the circular trajectory is summarized in Table 4.4. In order to reduce the influence of random error on the measured results, the procedure is repeated three times and the average value and the standard deviation (σ) are calculated.

Table 4.4 Eccentricity of circular trajectory for each step

Measurement steps and directions	Eccentricity	Measurement number			Average (μm)	Standard deviation (σ) (μm)
		1 (μm)	2 (μm)	3 (μm)		
1. BX	ex	-51.4	-52.1	-51.6	-51.70	0.29
	ez	-41.3	-42	-41.7	-41.67	0.29
2. BY	ex	-9.4	-10	-9.8	-9.73	0.25
	ez	-35.4	-36.7	-36.2	-36.10	0.54
3. CR	ex	-47.9	-48	-48.1	-48.00	0.08
	ey	25.4	25.9	26	25.77	0.26
4. CA	ex	-6.1	-6.1	-6.1	-6.10	0.00
	ey	-0.3	-0.3	-0.2	-0.27	0.05
5. CR (R'_B)	ex	-57.6	-57.8	-57.8	-57.73	0.09
	ey	28.5	28.4	28.6	28.50	0.08

The standard deviation (σ) is used to estimate the positioning repeatability at a position.

In Table 4.4, the maximum standard deviation is 0.54 μm. Except for 0.54 μm, other standard deviations are smaller than the ball bar measurement accuracy 0.5 μm shown in Table 4.1. It is concluded that the measured eccentricities are stable and reliable, and they can be used to calculate the geometric deviations.

4.3.4 Identified geometric deviations

Eight geometric deviations are identified by substituting the average values of the obtained eccentricities into Eqs. (4.10) - (4.15), (4.17), and (4.18). The identified results are shown in Table 4.5.

Table 4.5 Identified geometric deviations exiting in the machine tool

Deviation	Identified value	Deviation	Identified value
α_{CZ} ($''$)	1.10	γ_{XB} ($''$)	5.63
β_{CZ} ($''$)	-25.16	α_{BT} ($''$)	9.63
α_{XB} ($''$)	-20.89	$(\delta x_{CZ} - \delta x_{BT})$ (μm)	53.13
β_{XB} ($''$)	-24.11	δy_{CZ} (μm)	-45.63

Since the spindle of the targeted multi-tasking machine tool is in the horizontal position, the gravity will greatly cause the geometric deviations of XZ plane and the positional deviation in X axis direction. Therefore, it is discovered that angular geometric deviations (β_{CZ} and β_{XB}) of XZ plane are larger than other angular geometric deviations (α_{CZ}, α_{XB}, α_{BT} and γ_{XB}) of YZ and XY planes. In regard to the positional deviations of C axis, the offset value in X axis direction is larger than that in Y axis direction.

4.4 Compensated results

4.4.1 NC codes before and after compensation

The compensation method of the geometric deviations existing in the targeted machine tool is proposed in Chapter 3 based on the screw theory. Based on the proposed compensation idea, the modified NC code after compensation is generated by substituting the identified values of the geometric deviations into Eq. (3.10). The calculation is conducted by MATLAB. For an example, the original and compensated NC codes of B axis X direction measurement are shown in Fig. 4.30.

```
G01 X-390.0000 Y0.0000 Z-112.2605 B0.0000 C0.0000 F2000↵
G01 X-388.2722 Y0.0000 Z-112.2647 B0.2778 C0.0000 F2000↵
G01 X-386.5444 Y0.0000 Z-112.2773 B0.5556 C0.0000 F2000↵
G01 X-384.8166 Y0.0000 Z-112.2982 B0.8333 C0.0000 F2000↵
G01 X-383.0890 Y0.0000 Z-112.3275 B1.1111 C0.0000 F2000↵
G01 X-381.3616 Y0.0000 Z-112.3652 B1.3889 C0.0000 F2000↵
G01 X-379.6344 Y0.0000 Z-112.4113 B1.6667 C0.0000 F2000↵
G01 X-377.9074 Y0.0000 Z-112.4657 B1.9444 C0.0000 F2000↵
G01 X-376.1807 Y0.0000 Z-112.5285 B2.2222 C0.0000 F2000↵
G01 X-374.4543 Y0.0000 Z-112.5997 B2.5000 C0.0000 F2000↵
```

(a) Original NC code

```
G01 X-390.0131 Y0.0000 Z-112.2421 B0.0000 C0.0000 F2000↵
G01 X-388.2854 Y0.0000 Z-112.2465 B0.2778 C0.0000 F2000↵
G01 X-386.5577 Y0.0000 Z-112.2593 B0.5556 C0.0000 F2000↵
G01 X-384.8302 Y0.0000 Z-112.2804 B0.8333 C0.0000 F2000↵
G01 X-383.1027 Y0.0000 Z-112.3099 B1.1111 C0.0000 F2000↵
G01 X-381.3754 Y0.0000 Z-112.3478 B1.3889 C0.0000 F2000↵
G01 X-379.6483 Y0.0000 Z-112.3941 B1.6667 C0.0000 F2000↵
G01 X-377.9214 Y0.0000 Z-112.4487 B1.9444 C0.0000 F2000↵
G01 X-376.1949 Y0.0000 Z-112.5117 B2.2222 C0.0000 F2000↵
G01 X-374.4686 Y0.0000 Z-112.5831 B2.5000 C0.0000 F2000↵
```

(b) Compensated NC code

Figure 4.30 Original and compensated NC codes for B axis X direction measurement

4.4.2 Comparison with the eccentricities before and after the compensation

The influence of geometric deviations on TCP after the compensation is investigated to evaluate the eccentricities by using the same formula. Four measuring patterns of ball bar are performed again under the modified NC code. The eccentricities after the compensation are shown in Table 4.6. The trajectories of each measuring pattern before and after the compensation are compared in Figs. 4.31 and 4.32. In the figures, the red line represents the trajectory before the compensation and the blue line represents the trajectory after the compensation. The centers of each trajectory are also represented by the red and blue lines, respectively.

Table 4.6 Eccentricity of circular trajectory after compensation

Measurement steps and directions	Eccentricity	Measured values after compensation(μm)
1. BX	ex	-27.8
	ez	-3.8
2. BY	ex	-0.7
	ez	0.4
3. CR	ex	-0.8
	ey	2.7
4. CA	ex	0.3
	ey	-0.2
5. CR (R'_B)	ex	-5.8
	ey	0.5

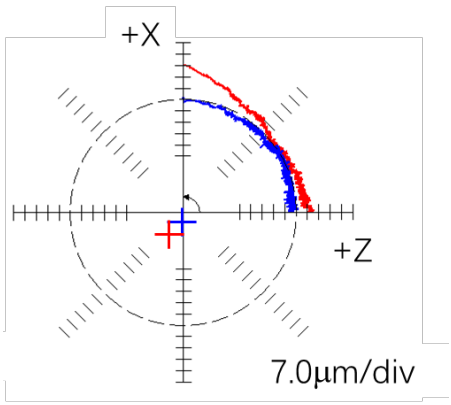

B axis X-direction

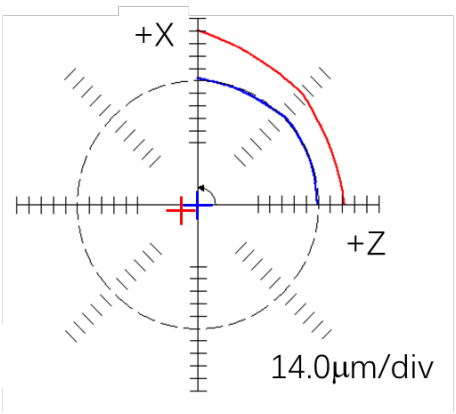

B axis Y-direction

Figure 4.31 Measured trajectories of B axis before and after compensation

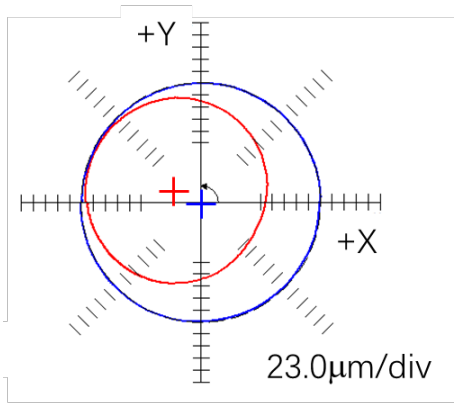

C axis radial direction

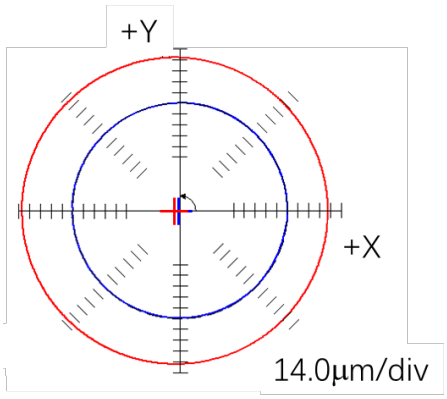

C axis axial direction

Figure 4.32 Measured trajectories of C axis before and after compensation

The measured eccentricities after the compensation are compared with those before the compensation, shown in Fig. 4.33. It is found that the absolute values of the eccentricities after the compensation are not over 5.8 μm except for the eccentricity ex_{BX}. As mentioned in the Section 4.2.3, the eccentricity ex_{BX} is strongly affected by the value of tool length R_{B}. Thus, it is depended on the positioning error of the spindle side ball before the measurement. Therefore, the eccentricities ex_{BX} before and after the compensation are not considered in this study. As a result, it is concluded that the trajectories after the compensation are accurate enough to meet the requirement of the conventional machining.

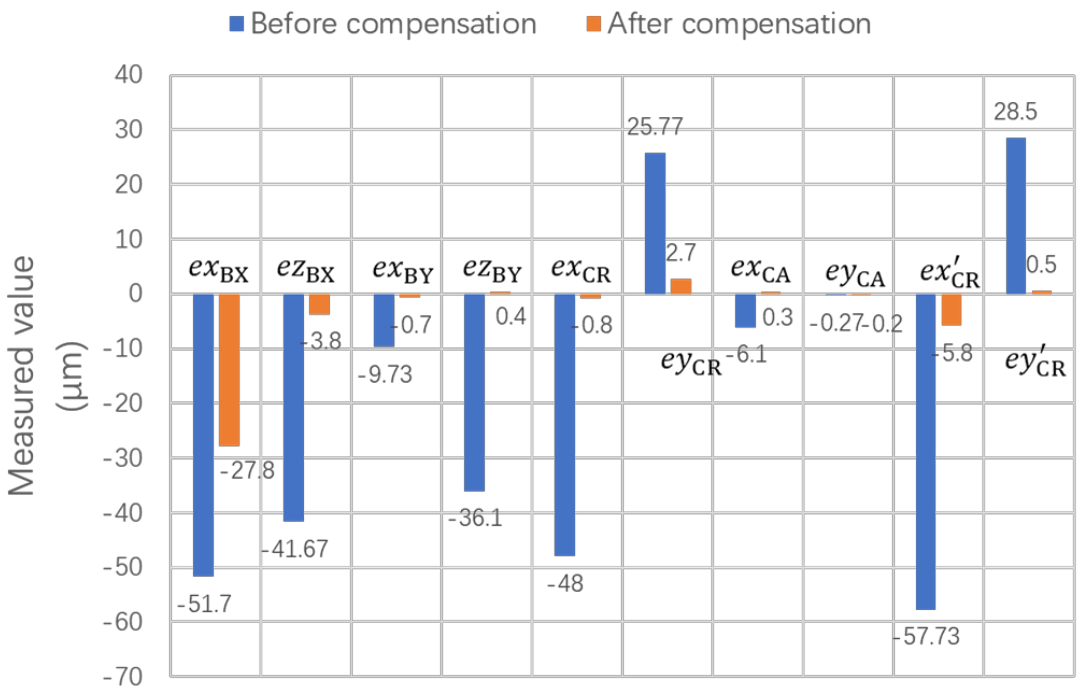

Figure 4.33 Comparison of eccentricities before and after compensation

4.4.3 Comparison with the identified geometric deviations before and after the compensation

Table 4.7 summarizes the corresponding geometric deviations after compensating the influence of the geometric deviations on TCP. Figure 4.34 shows that the corresponding values of angular geometric deviations after the compensation are not over 2.2 arcseconds except for α_{BT} and the corresponding values of positional geometric deviations are not over 2.4 micrometers. It is concluded that the influence of the geometric deviations on TCP is compensated effectively.

Table 4.7 Corresponding geometric deviations by compensating the influence of the geometric deviations on TCP

Deviations	Corresponding values	Deviations	Corresponding values
α_{CZ} (″)	0.83	γ_{XB} (″)	0.41
β_{CZ} (″)	1.24	α_{BT} (″)	8.84
α_{XB} (″)	0.23	$(\delta x_{CZ} - \delta x_{BT})$ (μm)	2.39
β_{XB} (″)	-2.20	δy_{CZ} (μm)	1.01

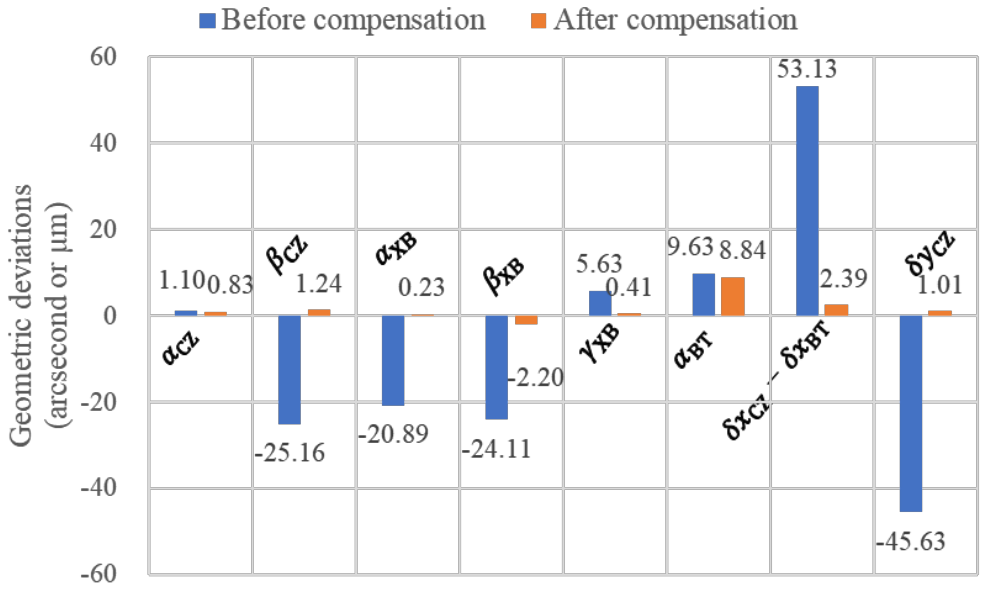

Figure 4.34 Comparison between identified geometric deviations before the compensation and their corresponding values after the compensation

It is also found that the influence of α_{BT} on TCP is scarcely reduced by this method. The reason is that the spindle axis is not controlled for angular positioning, and the compensation method is to correct the coordinate value of the spindle nose not to correct the center of stylus sphere. As shown in Fig. 4.35, the center coordinate of spindle side ball is calculated by adding the measured vertical distance L_1 to the coordinate (X_T, Y_T, Z_T) of spindle nose. Thus, the value of the angular geometric deviation α_{BT} about the spindle axis is not included in the modified NC code through the compensation method. Therefore, this method could not compensate the influence of the geometric deviation α_{BT} on TCP.

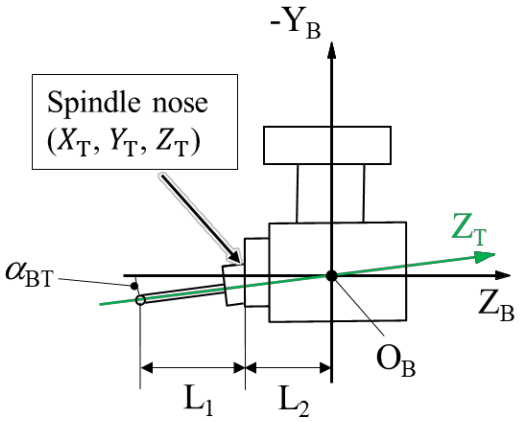

Figure 4.35 Influence of α_{BT} on TCP

4.5 Conclusion

In this chapter, a measuring procedure for identifying geometric deviations is investigated. The B axis measurements in the Cartesian coordinate system and the C axis measurements in the cylindrical coordinate system are conducted in a multi-tasking machine tool by a ball bar. An experiment modifying the NC code is also conducted to compensate the influence of the geometric deviations on TCP. Conclusions are summarized as follows.

1. A measuring procedure by a ball bar for identifying the geometric deviations is designed according to the analysis of the influence factors for each trajectory. Four measuring patterns are conducted to identify eight geometric deviations which are inherent to a multi-tasking machine tool.
2. The trajectories after the compensation by modifying the NC code are also measured and compared with those before the compensation.
3. From the experimental results, the geometric deviations about two rotary axes (B and C axes) could be compensated effectively. However, the geometric deviations of the spindle (α_{BT}, δx_{BT}, and δz_{BT}) could not be compensated by this method.
4. After modifying the NC code, the corresponding values of angular geometric deviations are not over 2.2 arcseconds except for α_{BT} and positional geometric deviations are not over 2.4 micrometers. Therefore, it is confirmed that the position error of TCP is reduced significantly after the compensation.

Chapter 5 Verification measurement with a touch-trigger probe

5.1 Preface

In order to verify the identification and compensation methods of the geometric deviations by a ball bar, another traditional and practical measurement instrument, a touch-trigger probe, is studied in this chapter.

In Section 5.2, a measuring procedure using a touch-trigger probe is devised to identify the geometric deviations for a multi-tasking machine tool with a swivel spindle head in a horizontal position. In addition, the formulae to calculate the geometric deviations are derived by analyzing the influence of the geometric deviations on the measurements for the respective rotations of B and C axes. In Section 5.3, the measuring procedure is applied in INTEGREX i-200, and the geometric deviations are identified by the proposed calculation method. The identified values are compared to those obtained from the ball bar measurements in Chapter 4. It can be concluded that the identification and compensation methods by a ball bar are effective to identify the angular geometric deviations related to the rotary B and C axes of a multi-tasking machine tool.

5.2 Measuring procedure by touch-trigger probe

5.2.1 Introduction of touch-trigger probe

The high-accuracy touch-trigger probe RMP600 by Renishaw is used for the measurement. This type of touch-trigger probe provides good characteristics for the measurement since it is suitable for process setting, in-process control and post-process monitoring.

The probe is a detector that captures three-dimensional coordinates by contacting the stylus with the measured workpiece. The probe is classified into two types, one is a touch-trigger type that captures discrete coordinate values and the other is a copy measurement form that captures continuous displacements. For the touch-trigger type, there are two general mechanisms. One is the kinematic structure, which has a mechanical three-point support structure shown in Fig. 5.1(a). Via a rigid shaft, the stylus sphere is attached to a stylus center equipped with a switch at each of its three bearing points. When the stylus is

contacted to the workpiece from a given direction, at least one of these switches will be opened. This is then further processed as a trigger signal. When the stylus separates from the workpiece, the spring set on the top of the stylus center can make the stylus sphere return to the original position accurately. The major disadvantage of this mechanism lies in the fact that the variation of probing forces according to the probing direction results in a stylus deflection of varying elasticity. This in turn results in a directional probing behavior which is difficult to correct.

The other is a strain gauge probe that uses the strain gauge as the detection device to convert mechanical signals to electrical ones, shown in Fig. 5.1(b). The measured pressure of the strain gauge probe is smaller than that of the first mechanical kinematic type because the slight displacement of the stylus is detected by the strain gauge. Therefore, when the stylus touches the measured workpiece, the signal can be output without slippage. Another advantage of this probe is that non-directional probing behavior can be achieved by using the strain gauge.

Figure 5.2 shows the touch-trigger probe RPM600 used in this study, which is a high-precision radio signal transduction probe manufactured by Renishaw. Table 5.1 shows its specifications. The advanced strain gauge technology is adopted in the RPM600. Since the influence of the sensor on the measuring uncertainty is minimal, highly accurate measurements can be achieved based on the high repeatability. Figure 5.3 shows the radio machine interface (RMI), which is a unit that integrates a wireless transceiver and an interface. This unit performs wireless communication between the touch-trigger probe and the measured machine tool, and the wireless interference can be eliminated by the frequency hopping (FHSS) wireless communication method.

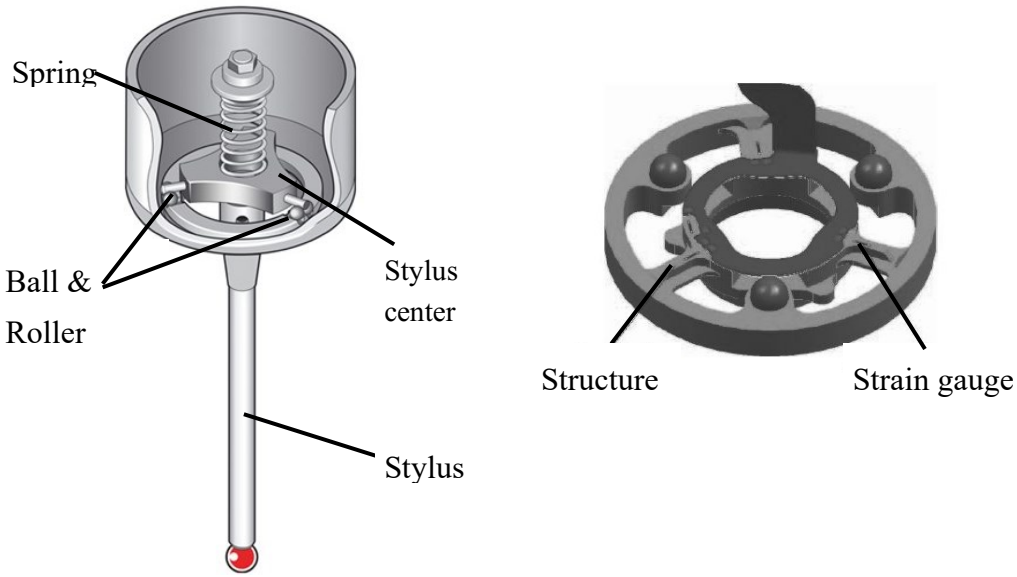

(a) Kinematic type (b) Strain gauge type

Figure 5.1 Principles of touch-trigger probe

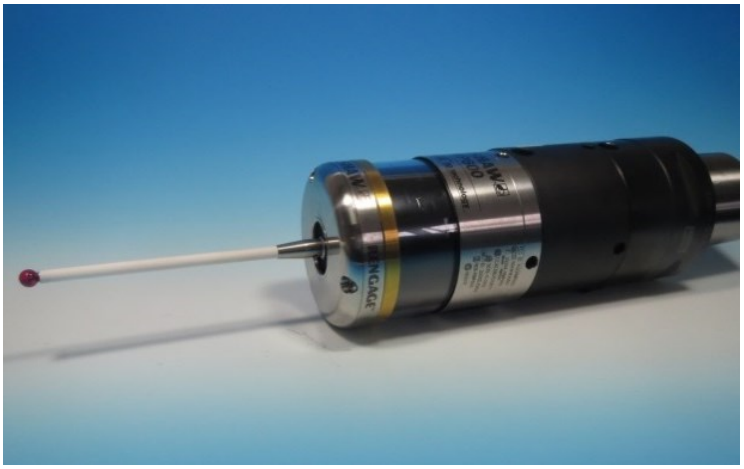

Figure 5.2 RMP600 manufactured by Renishaw

Figure 5.3 Radio machine interface (RMI) of the touch-trigger probe RMP600

Table 5.1 Specification of RMP600

Transmission type		Frequency hopping spread spectrum (FHSS) radio
Radio frequency		2400 MHz～2483.5 MHz
Weight without shank (including batteries)		1010 g
Sense directions		±X，±Y，+Z
Unidirectional repeatability	50mm stylus	0.25 μm
	100mm stylus	0.35 μm
Stylus trigger force	XY plane	0.2 N
	+Z direction	1.9 N
Stylus overtravel force	XY plane	2.8 N
	+Z direction	9.8 N
Minimum probing speed		3 mm/min
Sealing		IPX8（EN/IEC60529）

5.2.2 Preparation before measurement

Before conducting the measuring procedure, calibration of the stylus sphere of the touch-trigger probe from the spindle is necessary to ensure accurate measurement values and simplify the measuring procedure for identifying the geometric deviations [66]. The calibration is the work of correcting the misalignment when assembling the probe, stylus to the spindle holder, and measuring the length of the probe. It includes the following three steps.

Step 1: Checkup the runout of the stylus.

(1) Insert the stylus into the touch-trigger probe and tighten it sufficiently with a special tool so that it can be attached to the spindle. The completion of this step is shown in Fig. 5.4.

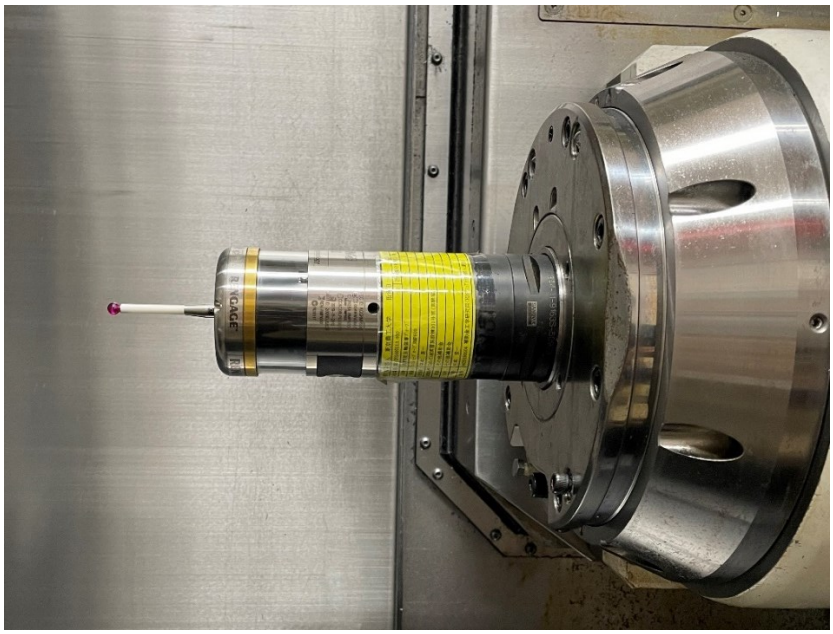

Figure 5.4 Attachment of the touch-trigger probe on the spindle

(2) Attach a lever type dial gauge to the workpiece table at an appropriate position. The lever type dial gauge should be able to read 1/1000 mm. Before setting the dial gauge, adjust the sensitivity to the extent to be touched lightly.

(3) Read the dial gauge while rotating the spindle slowly by hand. Adjust the change of the reading to within $\pm 2.5 \mu m$ by using the adjustment screws. This step is shown in Fig. 5.5.

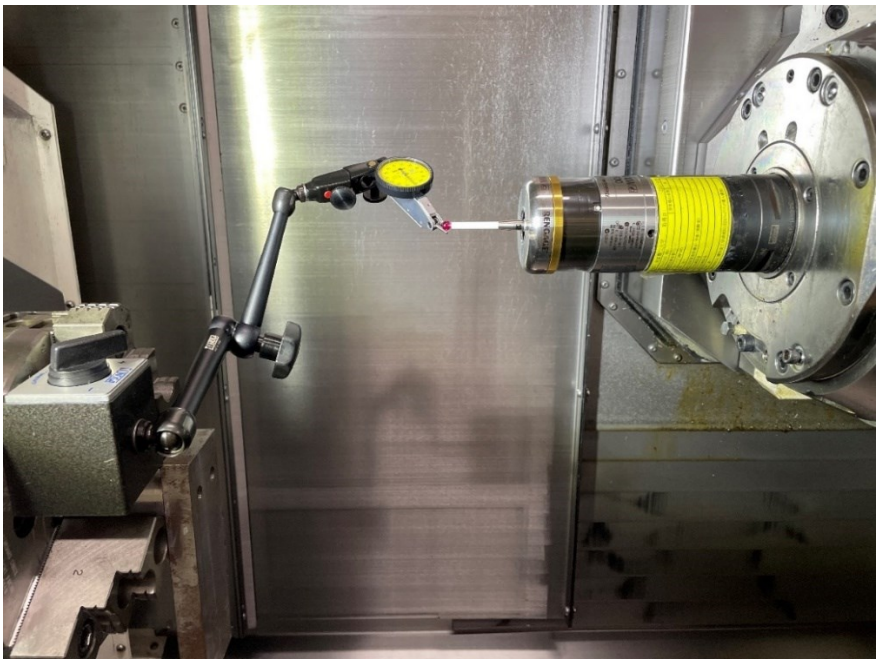

Figure 5.5 Checkup the runout of the stylus

Step 2: Measure the tool length R_B and set the origin of the work coordinate system in the Z axis direction.

The tool length is measured automatically by the “tool eye” function of the Integrex and record the tool length in the G54.1 command to complete the setting of work coordinate system in the Z axis direction. This step is shown in Fig. 5.6.

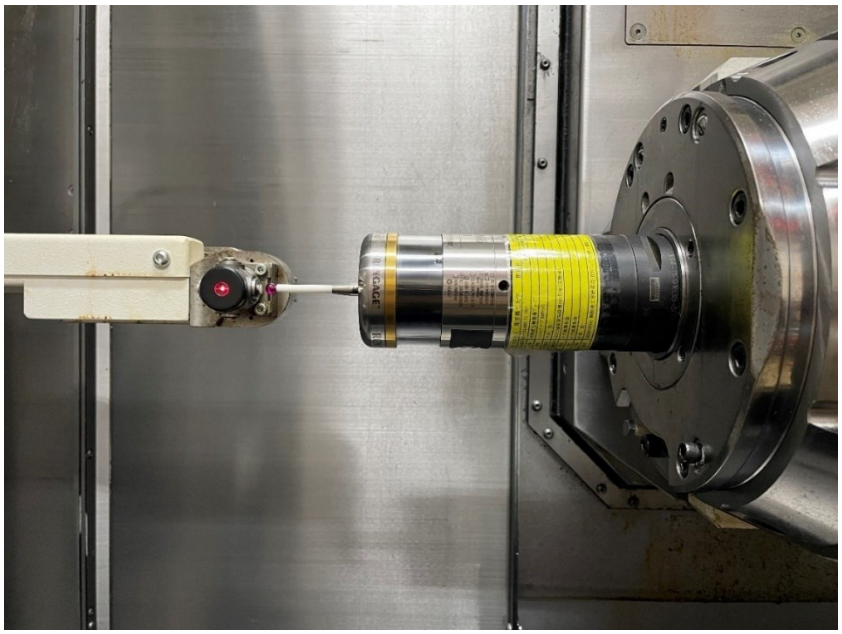

Figure 5.6 Measurement of the tool length

Step 3: Correct the positions of the touch-trigger probe in X and Y directions.

(1) Secure the reference sphere to the workpiece table.

(2) Mount the lever type dial gauge onto the spindle nose and slowly rotate the spindle until a constant reading is achieved over 360°. The change of the reading is to within $\pm 2\mu m$. This step is shown in Fig. 5.7.

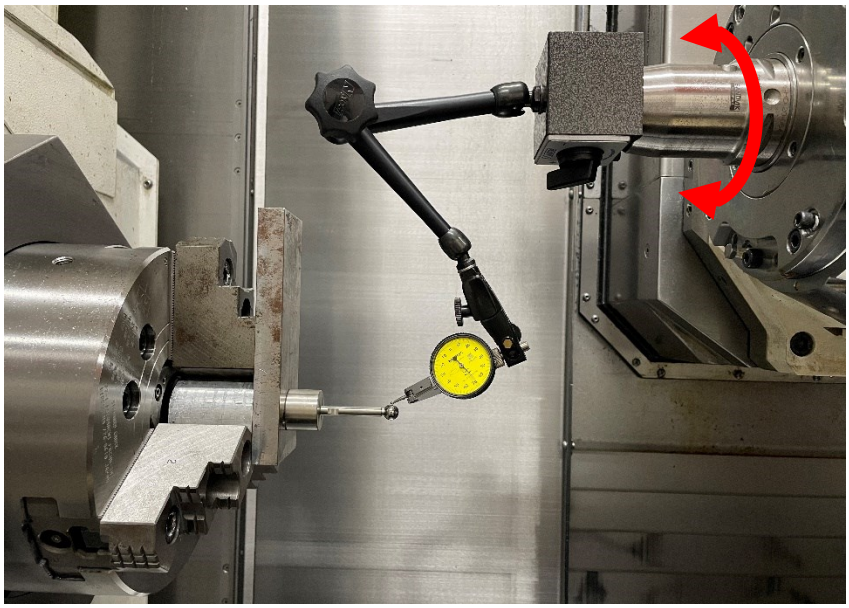

Figure 5.7 Aligning the reference sphere with the spindle

(3) Run the probe setting program to ensure the center of the reference sphere as the desired position. Set the work offset of X and Y axes in the G54.1 command to complete the setting of work coordinate system in the X- and Y- axis directions.

The distance between the center of the reference sphere and the workpiece table Z_C is another important parameter that should be measured before experiments. The measurement step is explained as follows, shown in Fig. 5.8.

(1) Mount the magnet base equipped with the lever type dial gauge at the appropriate position of the tool setup stand.

(2) While adjusting X axis and Y axis, move the spindle head in the negative direction of Z axis, and touch the stylus of the dial gauge to the surface of the work-side jig. Take the reading of the dial gauge, Z_{DG}, and record the machine coordinate Z_W of Z axis.

(3) Without moving the dial gauge, carefully move the spindle head so that the dial gauge stylus touch the reference sphere and adjust the X and Y axes to find the X and Y positions that maximize the dial gauge reading. Carefully move the spindle head at that position until the dial gauge reads Z_{DG}. The machine coordinate Z_{DW} of this Z axis is recorded.

(4) The distance Z_C is the difference between ($Z_{DW}-r$) and Z_W. Here, r is the diameter of the reference sphere.

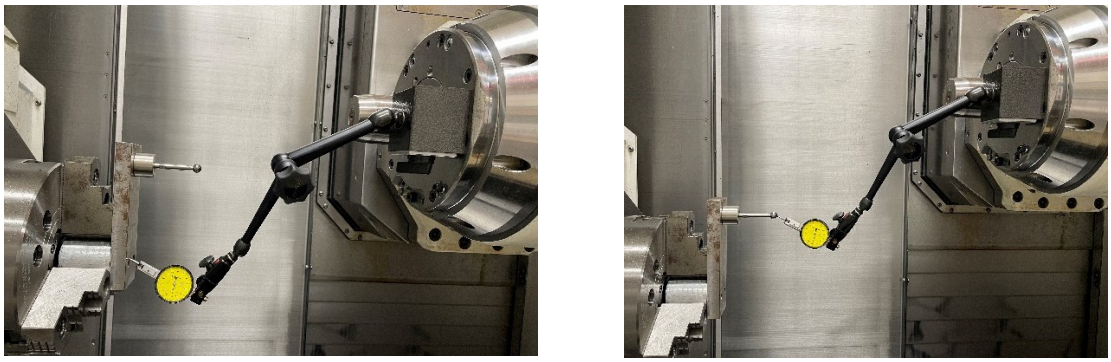

(a) Coordinate of the workpiece table (Z_W) (b) Coordinate of the reference sphere (Z_{DW})

Figure 5.8 Measurement of the distance Z_C

5.2.3 Measuring procedure

The measuring procedure to identify the geometric deviations of C axis is devised as follows.

Step 1: Insert a short stylus into the touch-trigger probe and calibrate the touch-trigger probe at C=0° and B=0°. Set the reference sphere at the position R_C=100 mm, which is the distance from the centerline of C axis to the center of the reference sphere. Therefore, after the calibration, the center position of reference sphere in case of C=0° and B=0° is regarded as the standard position. Measure the distance Z_C according to the steps described in Section 5.2.2.

Step 2: To exclude the influence of other geometric deviations, the measurement is performed only under the condition of the rotation of C axis. The position of the reference sphere is measured at C=0°, C=90°, C=180°, C=270°, respectively. For example, Fig. 5.9 shows the measurement in case of C=0°.

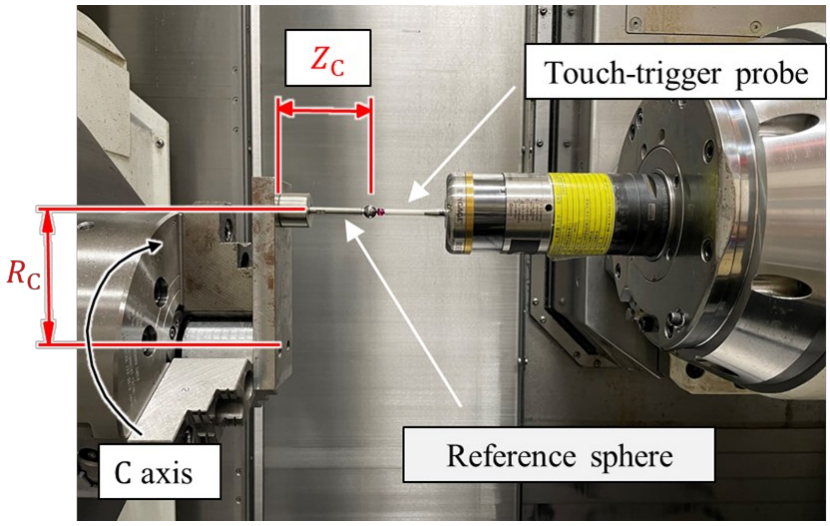

Figure 5.9 Measurement for C axis geometric deviations in case of C=0°

The measuring procedure to identify the geometric deviations of B axis is devised as follows.

Step 1: Set the reference sphere at the centerline of C axis. Conduct the step 3 of the calibration described in Section 5.2.2 to correct the X and Y positions of the reference sphere at C=0° and B=0°. Therefore, the center position of reference sphere is regarded as the standard position in case of C=0° and B=0°.

Step 2: To exclude the influence of other geometric deviations, the measurement is performed only under the condition of the rotation of B axis. The position of the reference sphere is measured at B=0° and B=90°. For example, Fig. 5.10 shows the measurement in case of B=90°.

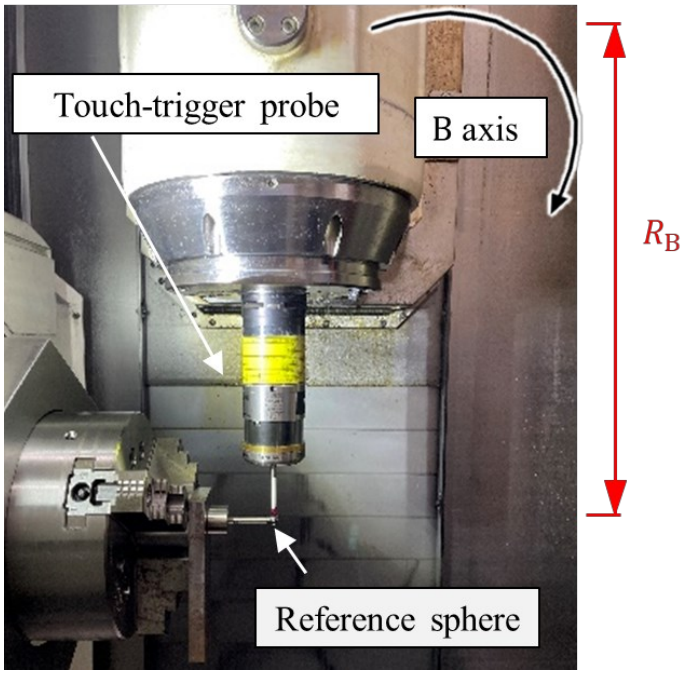

Figure 5.10 Measurement for B axis geometric deviations in case of B=90°

Step 3: Replace a long stylus into the touch-trigger probe to change the tool length from R_B to R'_B. The calibration of the touch-trigger probe is required again because the center of the stylus sphere is shifted. Therefore, the whole steps for the calibration should be conducted again.

Step 4: The position of the reference sphere is measured at B=0° and B=90° by the long stylus.

The measurement path at each position is created according to the machine simulator program developed by Mr. Shimada. By using a 3D model of the reference sphere created in advance, a measurement path of the sphere is designed as shown in Fig. 5.11. The center position of the reference sphere is obtained by measuring some discrete points distributed in

two perpendicular planes on the reference sphere surface. The touch-trigger probe approaches to the sphere surface in the direction normal to it. Therefore, the measurement path is designed from a 10 mm point along the normal direction of the measured point to the center of the reference sphere. When the contact of the probe sphere with the reference sphere is detected, a signal is sent to a CNC to stop the drive and record its position in the machine coordinate system. Thus, the coordinate value of the contact point is acquired. Due to the influence of geometric deviations, the measured coordinate value is different from the expected position.

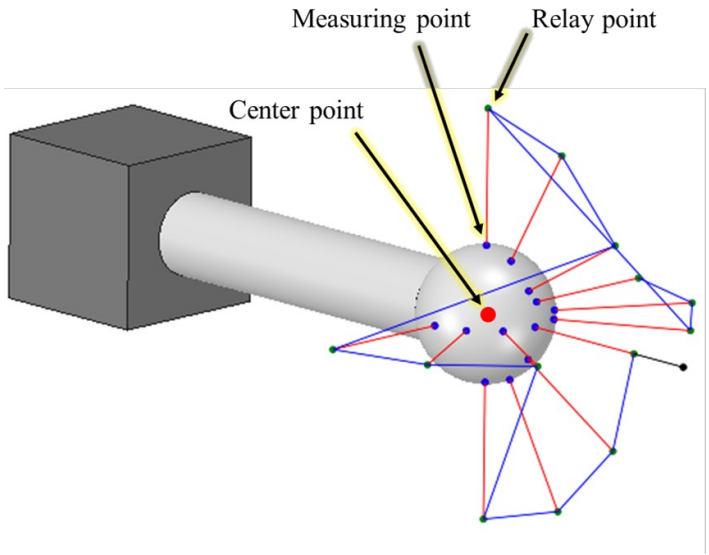

Figure 5.11 Generation of the measurement path

NC code is programmed based on the designed measurement path. For example, when the geometric deviation of C axis is identified, the NC code for measuring the reference sphere at the position of B=0° and C=0° is written as shown in Fig. 5.12.

The position of the contact point on the surface is calculated from the machine position and the approaching direction. The coordinate value of the measuring point in Fig. 5.12 is output as shown in Fig. 5.13.

```
<1010-1>(MEASURING-TEST)
G0 G18 G21 G40 G80 G90 G94 G97
POPEN
N1
G10.9 X0
M200
T23 M6(INTENEW)
G91 G0 G28 X0 Y0
G28 Z0
G90
G54.1 P5
G90 G43 G0 X-50. Y0. B0.0000 H23
DPRNT[Number*of*Points*40]
DPRNT[Feature*Model*PLANE]
G00 X-390.0000 Y0.0000 Z-452.0000 B0.0000 C0.0000
G00 X-390.0000 Y0.0000 Z-457.0000 B0.0000 C0.0000
G31 X-390.0000 Y0.0000 Z-472.0000 B0.0000 C0.0000 F100.0000
DPRNT[X#5001[4 4]*Y#5002[4 4]*Z#5003[4 4]*B#5004[4 4]*C#5005[4 4]]
G00 X-390.0000 Y0.0000 Z-457.0000 B0.0000 C0.0000
G00 X-394.6353 Y0.0000 Z-457.7342 B0.0000 C0.0000
G31 X-390.0000 Y0.0000 Z-472.0000 B0.0000 C0.0000 F100.0000
DPRNT[X#5001[4 4]*Y#5002[4 4]*Z#5003[4 4]*B#5004[4 4]*C#5005[4 4]]
G00 X-394.6353 Y0.0000 Z-457.7342 B0.0000 C0.0000
G00 X-398.8168 Y0.0000 Z-459.8647 B0.0000 C0.0000
G31 X-390.0000 Y0.0000 Z-472.0000 B0.0000 C0.0000 F100.0000
DPRNT[X#5001[4 4]*Y#5002[4 4]*Z#5003[4 4]*B#5004[4 4]*C#5005[4 4]]
G00 X-398.8168 Y0.0000 Z-459.8647 B0.0000 C0.0000
G00 X-402.1353 Y0.0000 Z-463.1832 B0.0000 C0.0000
G31 X-390.0000 Y0.0000 Z-472.0000 B0.0000 C0.0000 F100.0000
DPRNT[X#5001[4 4]*Y#5002[4 4]*Z#5003[4 4]*B#5004[4 4]*C#5005[4 4]]
```

Figure 5.12 NC code for B=0° and C=0° position

```
%
Number of Points 40
Feature Model PLANE
X-390.0000 Y0.0000 Z-464.5118 B0.0000 C0.0000
X-392.3406 Y0.0000 Z-464.7967 B0.0000 C0.0000
X-394.5199 Y0.0000 Z-465.7790 B0.0000 C0.0000
X-396.3313 Y0.0000 Z-467.4001 B0.0000 C0.0000
X-397.5836 Y0.0000 Z-469.5359 B0.0000 C0.0000
X-398.1191 Y0.0000 Z-472.0000 B0.0000 C0.0000
X-390.0000 Y2.3213 Z-464.8558 B0.0000 C0.0000
X-390.0000 Y4.4467 Z-465.8796 B0.0000 C0.0000
X-390.0000 Y6.1922 Z-467.5011 B0.0000 C0.0000
X-390.0000 Y7.3864 Z-469.5999 B0.0000 C0.0000
X-390.0000 Y7.8969 Z-472.0000 B0.0000 C0.0000
X-387.6988 Y0.0000 Z-464.9178 B0.0000 C0.0000
X-385.6247 Y0.0000 Z-465.9779 B0.0000 C0.0000
X-383.9443 Y0.0000 Z-467.6003 B0.0000 C0.0000
X-382.7995 Y0.0000 Z-469.6604 B0.0000 C0.0000
X-382.3193 Y0.0000 Z-472.0000 B0.0000 C0.0000
X-390.0000 Y-2.3213 Z-464.8558 B0.0000 C0.0000
X-390.0000 Y-4.4467 Z-465.8796 B0.0000 C0.0000
X-390.0000 Y-6.1922 Z-467.5011 B0.0000 C0.0000
X-390.0000 Y-7.3892 Z-469.5990 B0.0000 C0.0000
X-390.0000 Y-7.8969 Z-472.0000 B0.0000 C0.0000
%
```

Figure 5.13 Coordinate values when measuring at B=0° and C=0° position

The center of reference sphere at B=0° and C=0° position can be obtained based on the above measured contact points by MATLAB. If there are not any geometric deviations in the measured machine tool, the center position of the reference sphere should be same as the desired position. In fact, the measured value is different from the ideal value since the geometric deviations exist. Therefore, the geometric deviations can be identified by analyzing the difference between the measured value and the ideal value.

5.2.4 Calculation method

Two rotary B and C axes of the multi-tasking machine tool are separately located on the two sides of the bed, and they are not adjacent. Therefore, the geometric deviations related to these two rotary axes exist on both sides of the bed respectively. Thus, the geometric deviations of B and C axes are defined individually and the coupling effects of them are avoided. The calculation method of them is studied separately as follows.

To identify the four geometric deviations associated with C axis (δx_{CZ}, δy_{CZ}, α_{CZ}, β_{CZ}), a reference sphere is located at the position R_C=100 mm, which is the distance from the centerline of C axis to the center of the reference sphere. During the measurement, B axis is fixed at B=0° and C axis rotates by 360°. When C axis is rotated and stops at positions of C=0°, C=90°, C=180°, C=270°, the center of reference sphere is measured and calculated as descripted in Section 5.2.3 correspondingly. A trajectory in the space is obtained and it is projected onto X-Z and Y-Z planes as shown in Figs. 5.14 and 5.15.

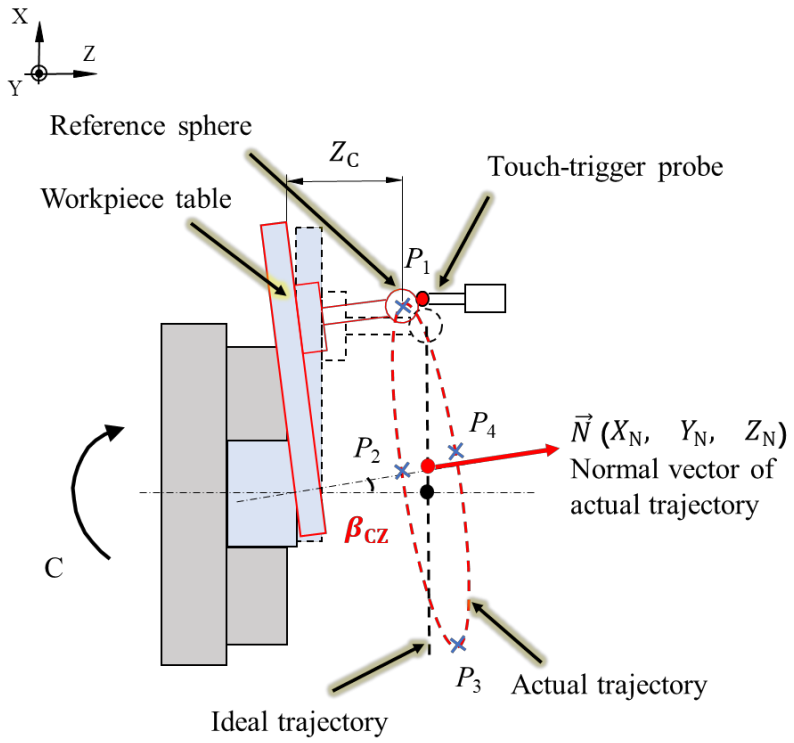

Figure 5.14 Influence of β_{CZ} on the center of trajectory in X-Z plane

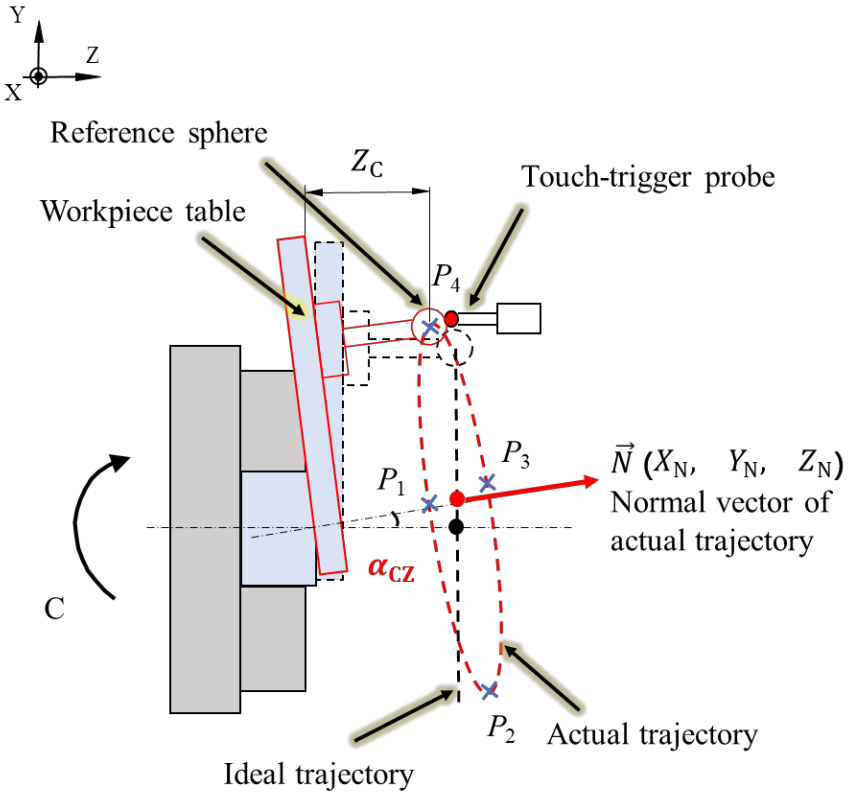

Figure 5.15 Influence of α_{CZ} on the center of trajectory in Y-Z plane

On the workpiece side, the black dotted line represents the ideal position of the workpiece without geometric deviations, and the red solid line represents the actual position of the workpiece with the influence of geometric deviations. About the projected trajectory, the black dotted line represents the ideal trajectory, and the red dotted line represents the actual trajectory. Through analysis, the center error of the reference sphere in X direction is caused by two geometric deviations (δx_{CZ} and β_{CZ}) and that in Y direction is caused by two geometric deviations (δy_{CZ} and α_{CZ}). These four geometric deviations are calculated as follows.

1. If the geometric deviations are zero, the measured trajectory projected onto the X-Z plane should be a line as the dotted black line. However, the actual trajectory projected onto the X-Z plane is not a line perpendicular to the centerline of C axis. The reason is that the geometric deviation β_{CZ} causes the workpiece table tilt as the red solid line shown in Fig. 5.14 and 5.15. Therefore, the normal vector is calculated firstly through the actual trajectory confirmed by the four measured positions. Then, the geometric deviation β_{CZ} is reflected and calculated from the angle between the normal vector and the ideal centerline of C axis.

In Figs. 5.14 and 5.15, points of P_1 (X_1, Y_1, Z_1), P_2 (X_2, Y_2, Z_2), P_3 (X_3, Y_3, Z_3), P_4 (X_4, Y_4, Z_4) represent the measured centers of reference sphere at positions of C=0°, C=90°, C=180°, C=270°, respectively. Thus, the normal vector of the trajectory $\vec{N}$ is calculated by

Eq. (5.1).

$$\vec{N} = \overrightarrow{P_1P_3} \times \overrightarrow{P_2P_4} = \begin{vmatrix} i & j & k \\ X_3 - X_1 & Y_3 - Y_1 & Z_3 - Z_1 \\ X_4 - X_2 & Y_4 - Y_2 & Z_4 - Z_2 \end{vmatrix} = (X_N, \quad Y_N, \quad Z_N) \tag{5.1}$$

Where, $$X_N = (Y_3 - Y_1) \times (Z_4 - Z_2) - (Y_4 - Y_2) \times (Z_3 - Z_1) \tag{5.2}$$

$$Y_N = (Z_3 - Z_1) \times (X_4 - X_2) - (Z_4 - Z_2) \times (X_3 - X_1) \tag{5.3}$$

$$Z_N = (X_3 - X_1) \times (Y_4 - Y_2) - (X_4 - X_2) \times (Y_3 - Y_1) \tag{5.4}$$

Therefore, in the X-Z plane shown in Fig. 5.14, $$\beta_{CZ} = \frac{X_N}{Z_N} \tag{5.5}$$

In the Y-Z plane shown in Fig. 5.15, $$\alpha_{CZ} = \frac{Y_N}{Z_N} \tag{5.6}$$

2. If the measured trajectory is straightened by the identified values of β_{CZ} and α_{CZ}, the positional deviations δx_{CZ} and δy_{CZ} are identified by excluding the error caused by the angular deviation β_{CZ} and α_{CZ} from the center errors in X and Y directions of the measured trajectory, respectively. Figure 5.16 explains the calculation method of these two positional deviations.

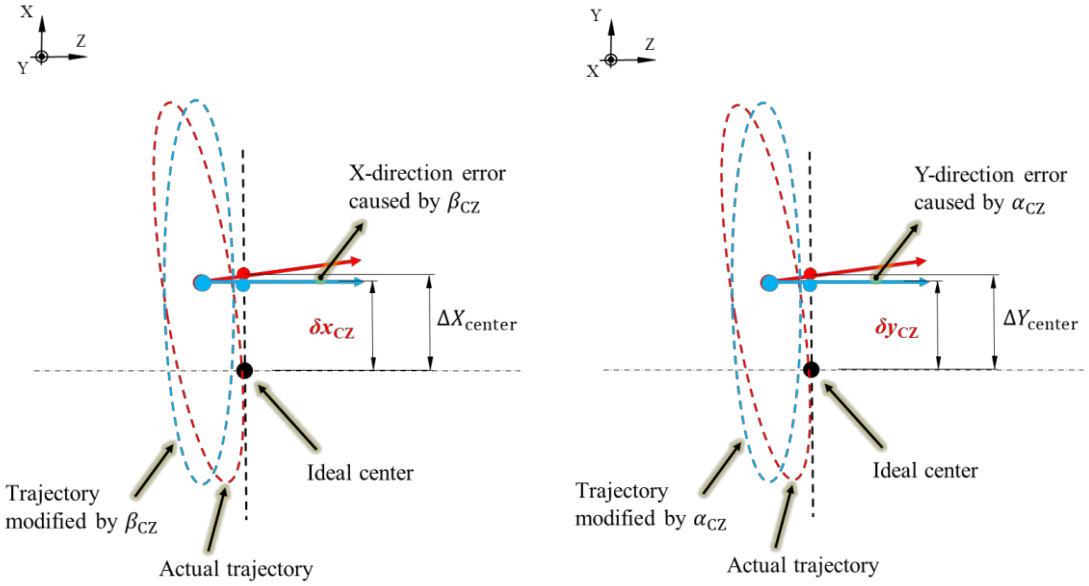

(a) Influence of δx_{CZ} in X-Z plane (b) Influence of δy_{CZ} in Y-Z plane

Figure 5.16 Calculation method of two positional deviations (δx_{CZ} and δy_{CZ})

The values of δx_{CZ} and δy_{CZ} are calculated by Eq. (5.7). The parameter Z_C in Eq. (5.7) is shown in Figs. 5.14 and 5.15, which is the distance between the center of reference sphere and the surface of workpiece table. ΔX_{center} and ΔY_{center} are the errors of measured trajectory center in the X and Y directions, respectively.

$$\begin{bmatrix} \delta x_{CZ} \\ \delta y_{CZ} \\ Z_C \end{bmatrix} = \begin{bmatrix} 1 & 0 & 0 \\ 0 & \cos(-\alpha_{CZ}) & -\sin(-\alpha_{CZ}) \\ 0 & \sin(-\alpha_{CZ}) & \cos(-\alpha_{CZ}) \end{bmatrix} \begin{bmatrix} \cos(-\beta_{CZ}) & 0 & \sin(-\beta_{CZ}) \\ 0 & 1 & 0 \\ -\sin(-\beta_{CZ}) & 0 & \cos(-\beta_{CZ}) \end{bmatrix} \begin{bmatrix} \Delta X_{center} \\ \Delta Y_{center} \\ Z_C \end{bmatrix} \tag{5.7}$$

Regarding the geometric deviations of B axis, it is difficult to measure them directly because the touch-trigger probe is fixed on the B axis with geometric deviations. The position of the touch-trigger probe is affected by the geometric deviations of B axis. Thus, the origin of the tool coordinate system is changed with the rotation of B axis. Therefore, although the position of the reference sphere does not change, the coordinate values of the reference sphere measured by the touch-trigger probe are different at the different rotary angles of B axis. The main idea to identify the geometric deviations of B axis is to analyze the influence factors on the different coordinate values measured at different rotary angles of B axis.

Six geometric deviations are associated with B axis, three of them (δx_{BT}, δz_{BT}, α_{BT}) exist between B axis and the spindle and the other three (α_{XB}, β_{XB}, γ_{XB}) exist between B axis and X axis. The influence of these six geometric deviations on the center coordinate of reference sphere in the machine coordinate system is analyzed in the X-Z, X-Y, and Y-Z planes, respectively. They are shown in Figs 5.17, 5.18 and 5.19.

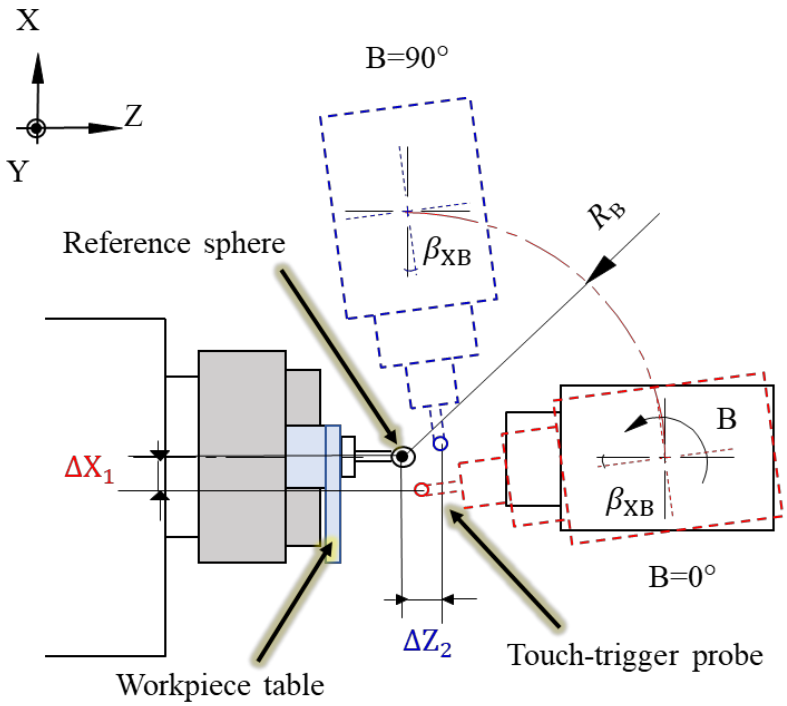

(a) β_{XB}

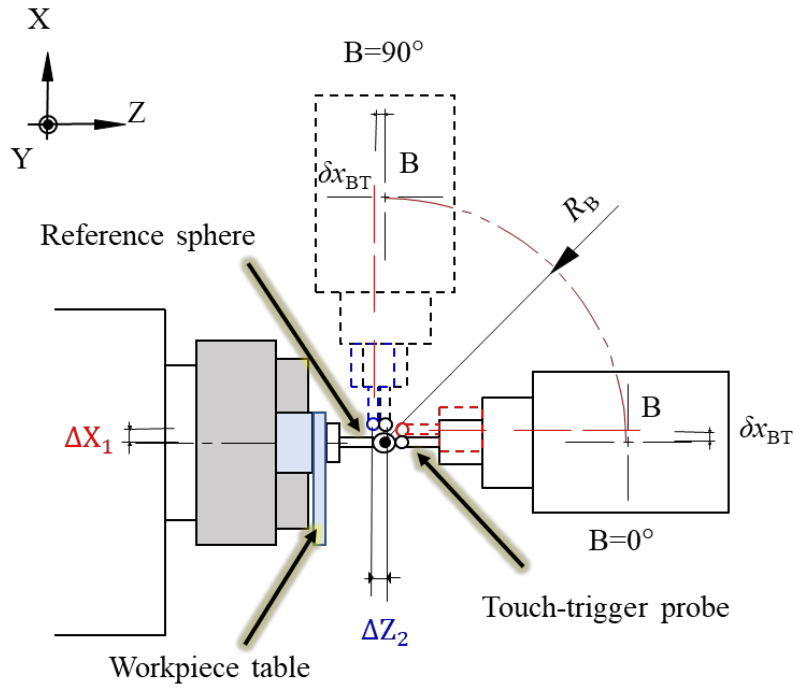

(b) δx_{BT}

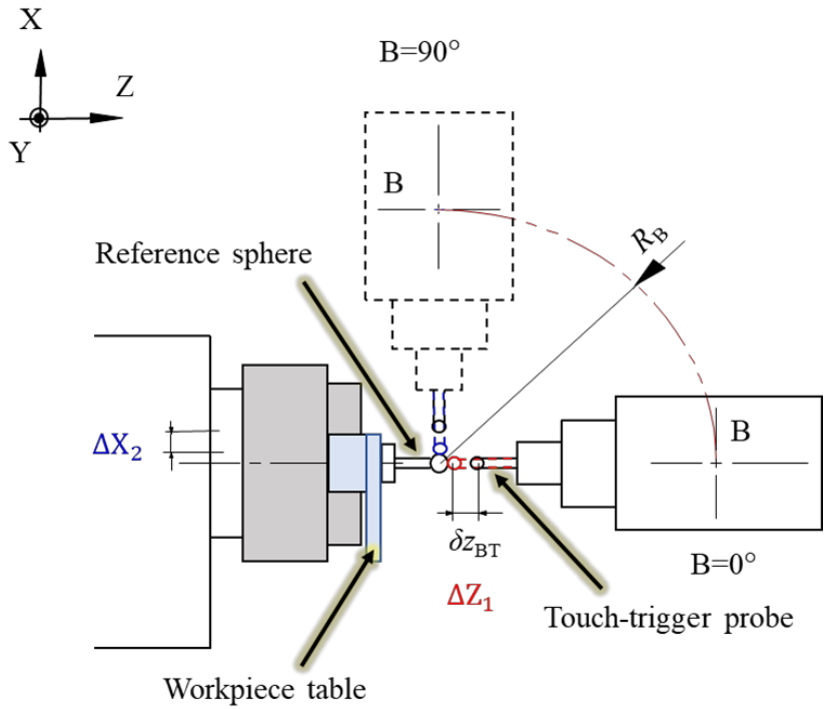

(c) δz_{BT}

Figure 5.17 Influence of geometric deviations on the center coordinate of reference sphere in the X-Z plane

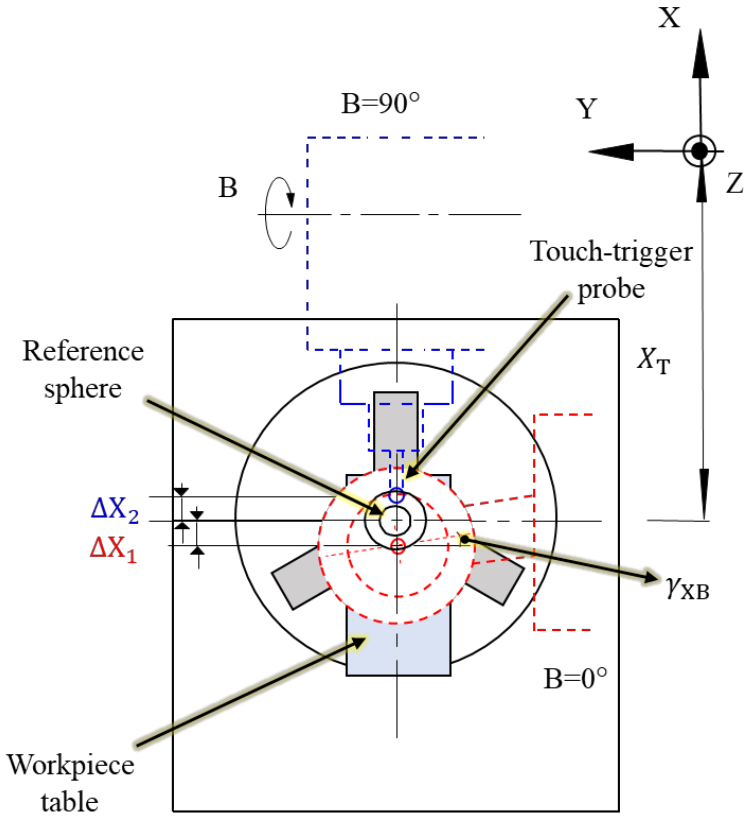

Figure 5.18 Influence of geometric deviation γ_{XB} on the center coordinate of reference sphere in the X-Y plane

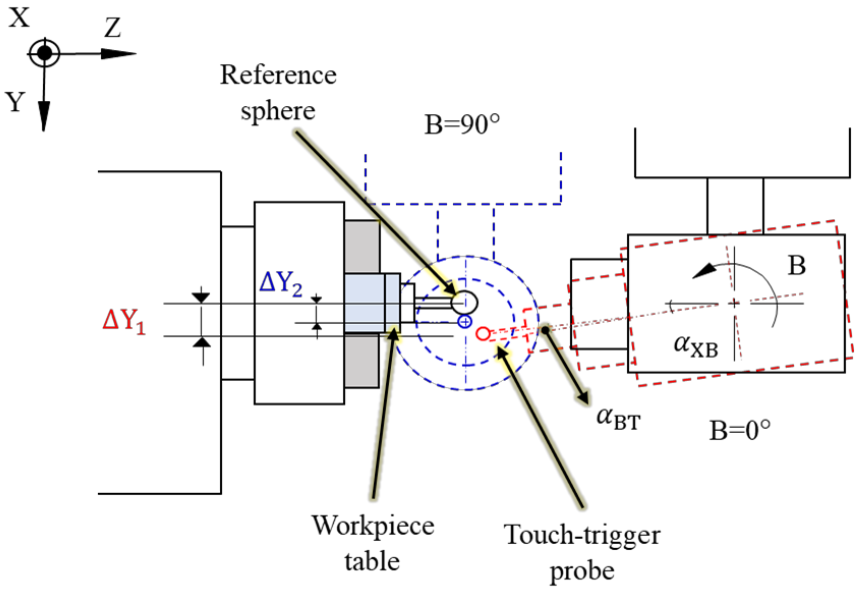

Figure 5.19 Influence of geometric deviations on the center coordinate of reference sphere in the Y-Z plane

In Figs. 5.17, 5.18 and 5.19, the black solid line represents the ideal position of B axis without any geometric deviations. The red dashed line represents the actual position in case of B=0°, and the blue dashed line represents the actual position in case of B=90°. The

suffixes 1 and 2 for X, Y, and Z correspond to the positions at B=0° and B=90°, respectively. R_{B} is the distance of the probe sphere center from the origin of B axis along Z direction. X_{T} is the nominal X position of the reference sphere in the machine coordinate system.

In X-Z plane, as shown in Fig. 5.17, there are three geometric deviations (δx_{BT}, δz_{BT} and β_{XB}) which affect the center error of the reference sphere as follows.

1. As is illustrated in Fig. 5.17(a), when only β_{XB} exists and all the other geometric deviations are zero, the measured positional error $\Delta \mathrm{X}_1$ at B=0° can be expressed as $\Delta \mathrm{X}_1 = R_{\mathrm{B}} \times \beta_{\mathrm{XB}}$. In case of B=90°, it becomes $\Delta \mathrm{Z}_2 = -R_{\mathrm{B}} \times \beta_{\mathrm{XB}}$. Therefore, the influence of angular deviation β_{XB} on the center error of the reference sphere can be expressed by Eq. (5.8).

$$\Delta \mathrm{X}_1 - \Delta \mathrm{Z}_2 = 2R_{\mathrm{B}} \times \beta_{\mathrm{XB}} \tag{5.8}$$

2. As is illustrated in Fig. 5.17(b), when only δx_{BT} exists and all the other geometric deviations are zero, the geometric deviation δx_{BT} causes a center error in X direction in case of B=0° while it causes a center error in Z direction in case of B=90°. Thus, the measured center error of the reference sphere can be expressed by Eq. (5.9).

$$\Delta \mathrm{X}_1 - \Delta \mathrm{Z}_2 = 2\delta x_{\mathrm{BT}} \tag{5.9}$$

As a result,

$$\Delta \mathrm{X}_1 - \Delta \mathrm{Z}_2 = 2R_{\mathrm{B}} \times \beta_{\mathrm{XB}} + 2\delta x_{\mathrm{BT}} \tag{5.10}$$

There are two unknown values, δx_{BT} and β_{XB}, in Eq. (5.10). Two unknown values are not calculated by only one equation. Therefore, according to the measuring procedure described in Section 5.2.3, steps 3 and 4 of B axis measurement are conducted by changing the tool length from R_{B} to R'_{B} and another relationship is obtained as Eq. (5.11).

$$\Delta \mathrm{X}'_1 - \Delta \mathrm{Z}'_2 = 2R'_{\mathrm{B}} \times \beta_{\mathrm{XB}} + 2\delta x_{\mathrm{BT}} \tag{5.11}$$

Combining with Eq. (5.10), two geometric deviations are calculated by the following Eqs. (5.12) and (5.13).

$$\beta_{\mathrm{XB}} = \frac{(\Delta \mathrm{X}'_1 - \Delta \mathrm{Z}'_2) - (\Delta \mathrm{X}_1 - \Delta \mathrm{Z}_2)}{2(R'_{\mathrm{B}} - R_{\mathrm{B}})} \tag{5.12}$$

$$\delta x_{\mathrm{BT}} = \frac{R'_{\mathrm{B}}(\Delta \mathrm{X}_1 - \Delta \mathrm{Z}_2) - R_{\mathrm{B}}(\Delta \mathrm{X}'_1 - \Delta \mathrm{Z}'_2)}{2(R'_{\mathrm{B}} - R_{\mathrm{B}})} \tag{5.13}$$

3. As is illustrated in Fig. 5.17(c), when only δz_{BT} exists and all the other geometric deviations are zero, the geometric deviation δz_{BT} causes a center error in Z direction in case of B=0° while it causes a center error in X direction in case of B=90°. Thus, the measured center error of the reference sphere can be expressed by Eq. (5.14).

$$\Delta \mathrm{Z}_1 + \Delta \mathrm{X}_2 = 2\delta z_{\mathrm{BT}} \tag{5.14}$$

Therefore,

$$\delta z_{\mathrm{BT}} = \frac{\Delta \mathrm{Z}_1 + \Delta \mathrm{X}_2}{2} \tag{5.15}$$

In X-Y plane, as shown in Fig. 5.18, one geometric deviation (γ_{XB}) affects the center

error of the reference sphere in X direction as follows. It can be expressed by Eq. (5.16).

$$\Delta X_2 - \Delta X_1 = X_T \times \gamma_{XB} \tag{5.16}$$

Therefore,

$$\gamma_{XB} = \frac{\Delta X_2 - \Delta X_1}{X_T} \tag{5.17}$$

In Y-Z plane, as shown in Fig. 5.19, two geometric deviations (α_{XB} and α_{BT}) affect the center error of the reference sphere in Y direction. Since the spindle axis is not controlled for angular positioning, the angular deviation α_{BT} related to the milling spindle is not reflected in the actual position of the touch-trigger probe sphere. Therefore, the influence of α_{BT} on the center error of the reference sphere can't be measured. In this case, the center error of the reference sphere in Y direction is caused by α_{XB} and it can be expressed by Eq. (5.18).

$$\Delta Y_1 - \Delta Y_2 = R_B \times \alpha_{XB} \tag{5.18}$$

Therefore,

$$\alpha_{XB} = \frac{\Delta Y_1 - \Delta Y_2}{R_B} \tag{5.19}$$

5.3 Identified results and discussion

5.3.1 Experimental results

The above measuring procedure and calculation method using a touch-trigger probe is applied to a multi-tasking machine tool, INTEGREX i-200, whose parameters are described in Section 4.3.1. To identify the geometric deviations of C axis, the distance between the center line of C axis and the center of the reference sphere is set as $R_C = 100\ mm$. The distance from the workpiece table surface to the center of the reference sphere is $Z_C = 64.838\ mm$.

During B axis measurement, two styli are used to change the tool length, the theoretical length of the short one is 50 mm and the other long one is 100 mm. Thus, the tool length is $R_B = 382.950\ mm$ and $R'_B = 433.062\ mm$. Feed speed is set to 100 mm/min in the circular motion.

The measurement path, shown in Fig. 5.11, is used to measure the actual positions of reference sphere when C axis rotates to 0°, 90°, 180°, and 270° positions. The actual positions of reference sphere are also measured by using two different length styluses of the touch-trigger probe when B axis rotates to 0° and 90° positions. The actual center coordinates of the reference sphere at different positions are calculated from the previously measured points by a MATLAB program. They are summarized in Table 5.2. In order to reduce the measuring error, the average value is used to identify the geometric deviations in the following section.

Table 5.2 Actual center coordinates of the reference sphere

	Center coordinate of reference sphere (Rotation angle)	1st (mm)	2nd (mm)	Average (mm)
Measurements for C axis	X_1 (0°)	-389.9998	-390.0007	-390.00025
	Y_1 (0°)	0.0006	0.0009	0.00075
	Z_1 (0°)	-471.9977	-471.9973	-471.9975
	X_2 (90°)	-489.7417	-489.7417	-489.7417
	Y_2 (90°)	99.7007	99.7011	99.7009
	Z_2 (90°)	-472.0087	-472.0088	-472.00875
	X_3 (180°)	-589.4389	-589.4389	-589.4389
	Y_3 (180°)	-0.0392	-0.0388	-0.039
	Z_3 (180°)	-472.0268	-472.0271	-472.02695
	X_4 (270°)	-489.7001	-489.7001	-489.7001
	Y_4 (270°)	-99.738	-99.738	-99.738
	Z_4 (270°)	-472.013	-472.013	-472.013
Measurements for B axis at R_B	X_1 (0°)	-490	-490.0106	-490.0053
	Y_1 (0°)	0	-0.0008	-0.0004
	Z_1 (0°)	-471.9958	-471.992	-471.9939
	X_2 (90°)	-493.2167	-493.2266	-493.2217
	Y_2 (90°)	0.0343	0.0344	0.03435
	Z_2 (90°)	-468.8545	-468.8513	-468.8529
Measurements for B axis at R'_B	X'_1 (0°)	-490.0001	-489.9983	-489.9992
	Y'_1 (0°)	0.0003	0.0014	0.00085
	Z'_1 (0°)	-471.9935	-471.9924	-471.993
	X'_2 (90°)	-493.2248	-493.2213	-493.2231
	Y'_2 (90°)	0.0466	0.0483	0.04745
	Z'_2 (90°)	-468.8452	-468.8432	-468.8442

5.3.2 Identified geometric deviations

Two angular deviations of C axis (α_{CZ}, β_{CZ}) are calculated by substituting the average values of the center coordinate of the reference sphere into Eqs. (5.5) - (5.6). Then, two positional deviations of C axis (δx_{CZ}, δy_{CZ}) are calculated by substituting the errors of measured trajectory center (ΔX_{center}, ΔY_{center}) into Eq. (5.7). The identified results are shown in Table 5.3.

To identify the geometric deviations of B axis, the errors of the reference sphere center

positions at every measuring condition are calculated firstly. Then, by substituting the errors into Eqs. (5.12), (5.13), (5.15), (5.17), and (5.19), results of the geometric deviations are identified in Table 5.3. Viewing from Eqs. (5.10) and (5.16), three geometric deviations (β_{XB}, δx_{BT}, and γ_{XB}) affect the error ΔX_1 in the X direction. But the influence of γ_{XB} on the error is constant for two measuring conditions of R_B and R'_B. Therefore, it can be excluded by subtracting between $\Delta X'_1$ and ΔX_1 during the calculation of β_{XB} and δx_{BT}. To simplify the solution, β_{XB} and δx_{BT} is firstly calculated before γ_{XB}.

Table 5.3 Identified geometric deviations of rotary axes

Geometric deviation	Identified value	Geometric deviation	Identified value
δx_{CZ}(μm)	80.64	β_{XB}(arcsecond)	-19.04
δy_{CZ}(μm)	-36.68	γ_{XB}(arcsecond)	5.46
α_{CZ}(arcsecond)	-3.7	δx_{BT}(μm)	-1335
β_{CZ}(arcsecond)	-26.28	δz_{BT}(μm)	-1804
α_{XB}(arcsecond)	-20.76	α_{BT}(arcsecond)	Not be identified

From the results in Table 5.3, it can be said that δx_{BT} and δz_{BT} are not identified correctly. Figure 5.20 explains the reason. Under the simultaneous three axis motions, the measured point that the spindle actually moves to is located at the head of spindle nose. Then, the previously measured tool length is accumulated to the actual position of the spindle nose to calculate the central coordinate value of the touch-trigger probe sphere. Thus, the result of δz_{BT} is affected by the measuring error of the tool length. And the value of δx_{BT} is not reflected correctly in the coordinate value of the touch-trigger probe sphere because the origin of B axis is difficult to be determined in the experiment.

In addition, as shown in Fig. 5.21, the value of α_{BT} is not reflected in the actual position of the touch-trigger probe sphere because the spindle is not controlled for angular positioning. Therefore, the geometric deviations related to the milling spindle are not identified through the proposed measuring procedure.

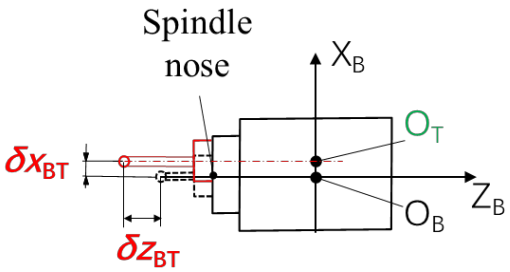

Figure 5.20 Explanation of the incorrect identifications of δx_{BT} and δz_{BT}

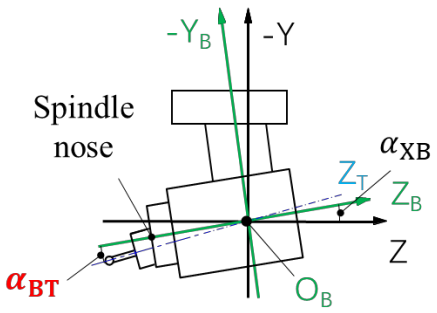

Figure 5.21 Explanation of the impossible identification of α_{BT}

From the identified results, it is also to be noted that angular geometric deviations have the smaller contribution to the total deviations in contrast to the positional geometric deviations. Therefore, a sufficiently small relative positional error between the workpiece and the spindle can obviously decreases the machining error caused by the geometric deviations inherent to the multi-tasking machine tool.

5.3.3 Comparison with the identified values of ball bar

The values of geometric deviations identified by a touch-trigger probe and those identified by a ball bar in Chapter 4 are summarized, as shown in Table 5.4.

It is noted that there is great difference about the values of positional deviations from using these two measuring instruments. With regard to the ball bar measurement, since the relative displacement of the spindle side ball and the workpiece side ball is measured, (δx_{CZ} -δx_{BT}) is considered as one unknown parameter. The value of (δx_{CZ} -δx_{BT}) can be calculated although the values of δx_{CZ} and δx_{BT} can't be identified respectively. However, as to the touch-trigger probe measurement, δx_{CZ} is identified in case of C axis rotation, which is irrelevant to B axis. But δx_{BT} is not identified correctly because it is not reflected correctly in the coordinate value of the touch-trigger probe sphere during the experiment. Therefore, it is meaningless to compare the identified values of δx_{CZ} and (δx_{CZ} -δx_{BT}).

Regarding the positional geometric deviation δy_{CZ}, it is found that the difference obtained from these two measuring instruments is about 10 micrometers. The reason is that dynamics error has included in the identified value of the continuous measurement by ball bar. Therefore, the identified value measured by ball bar is larger than that from the touch-trigger probe.

In addition, with regard to the positional deviation δz_{BT}, it is not identified correctly by both of these two measuring instruments because it is strongly affected by the measuring error of the tool length.

Table 5.4 Comparison between identified values of geometric deviations using a touch-trigger probe and using a ball bar

Geometric deviation	By a touch-trigger probe	By a ball bar
δx_{CZ}(μm)	80.64	(δx_{CZ} -δx_{BT}): 53.13
δy_{CZ}(μm)	-36.68	-45.63
α_{CZ}(arcsecond)	-3.7	1.10
β_{CZ}(arcsecond)	-26.28	-25.16
α_{XB}(arcsecond)	-20.76	-20.89
β_{XB}(arcsecond)	-19.04	-24.11
γ_{XB}(arcsecond)	5.46	5.63
δx_{BT}(μm)	-1335 (Not be identified)	(δx_{CZ} -δx_{BT}): 53.13
δz_{BT}(μm)	-1804 (Not be identified)	Not be identified
α_{BT}(arcsecond)	Not be identified	9.63 (Not be compensated)

As to the angular deviations obtained from these two measuring instruments, identified values are almost the same exclude the geometric deviation α_{BT}. α_{BT} can be identified with the ball bar measurement according to the simulation results. However, it is not compensated by the compensation method descripted in Chapter 3 because the milling spindle is not controlled for angular positioning. As to the touch-trigger probe measurement, α_{BT} can't be identified since it can't be reflected in the actual position of the touch-trigger probe sphere. Therefore, the remaining six geometric deviations except for δx_{CZ}, δx_{BT}, δz_{BT}, and α_{BT} are compared in the following Fig. 5.22.

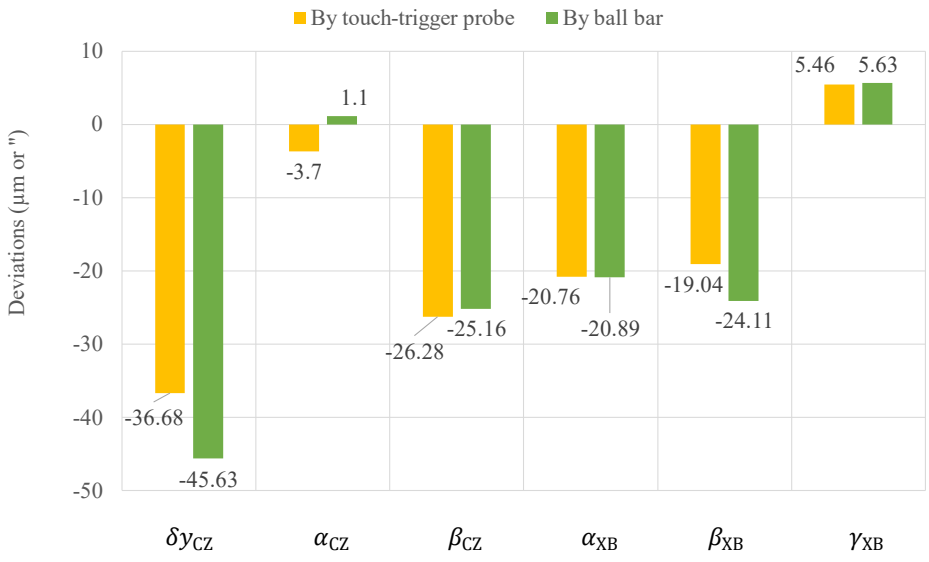

Figure 5.22 Comparison of the identified values by two measuring instruments

From Fig. 5.22, it can be found that the difference of the identified values for angular deviations from two measuring instruments is not over 5.1 arcseconds. It is due to the thermal deformation error of the machine tool or the measuring error of the operator. It is concluded that the angular geometric deviations related to the rotary B and C axes for a multi-tasking machine tool can be correctly identified either by the ball bar or by the touch-trigger probe. The identification and compensation methods by a ball bar described in Chapter 4 are effective to identify the angular geometric deviations related to the rotary B and C axes except for the geometric deviations of milling spindle.

5.4 Conclusion

In this chapter, a touch-trigger probe is used to identify the geometric deviations related to two rotary axes of a multi-tasking machine tool. A measuring procedure is devised, and the calculation method is derived based on the character of the respective rotations of B and C axes. The proposed measuring procedure and calculation method are conducted in INTEGREX i-200. The identified values of geometric deviations are compared and analyzed with the results identified by a ball bar described in Chapter 4. Conclusions are summarized as follows.

1. A simple measuring procedure by a touch-trigger probe for identifying the geometric deviations is designed according to the analysis of the influence of the geometric deviations on the measurements for the respective rotations of B and C axes.
2. The geometric deviations of INTEGREX i-200 are identified by the proposed measuring procedure. From the identified results, it is found that the geometric deviations related to the milling spindle (α_{BT}, δx_{BT}, and δz_{BT}) are not identified correctly. The number of geometric deviations identified by a touch-trigger probe is limited and fewer than that identified by a ball bar.
3. Compared with the identified values from the ball bar measurement, the difference of the angular deviations is not over 5.5 arcseconds except for α_{BT}. Therefore, the angular geometric deviations related to the rotary B and C axes of a multi-tasking machine tool can be correctly identified by using the identification method of ball bar described in Chapter 4.
4. It is verified that measuring procedure by ball bar of Chapter 4 is effective to identify the geometric deviations of multi-tasking machine tool.

Chapter 6 Conclusions

6.1 Achieved results in this study

With the rapid evolution of industrialization and automation, multi-tasking machine tools have been extensively utilized in machining components with complex geometric structures and sculptured surfaces, such as an impeller, a turbine blade, etc. The main advantage of the multi-tasking machine tool is to gather around almost all of the manufacturing processes in it to reduce human, material resources, and the number of independent machines for each manufacturing process and improve the production efficiency. To perform multiple processing such as turning, drilling, thread cutting, and pendulum, the multi-tasking machine tool is equipped with a rotary spindle based on a lathe to allow the spindle to tilt relative to the workpiece at various angles. However, with the increase of the rotary degrees of freedom, the increased mechanical structure may cause additional errors to the machine tool. Therefore, calibration of the rotary axes is needed to improve the accuracy of the multi-tasking machine tool.

The geometric deviation is the major error source that accounts for most of the errors of multi-tasking machine tools. A measuring procedure and an evaluation method to identify and compensate the geometric deviation has not been clarified especially for the geometric deviations related to the rotary axis. Therefore, this study aims to find an effective identification and compensation method for the geometric deviations related to the rotary axis to improve positioning accuracy of tool center point. Based on the identification method for the geometric deviations of a five-axis machining center researched by Mr. Tone et al., the identification and compensation methods for the geometric deviations inherent to a multi-tasking machine tool are proposed. And their effectiveness is verified on a common multi-tasking machine tool measured by a ball bar.

The results of this study are summarized as follows.

In Chapter 2, to identify the geometric deviations which exist in a multi-tasking machine tool, the trajectories of simultaneous three-axis motions are investigated. The mathematical model is established, and the simulation is conducted both in the cylindrical coordinate system and in the Cartesian coordinate system, respectively. Conclusions are summarized as follows.

1. According to the structural configuration of a multi-tasking machine tool with a

swivel spindle head in a horizontal position, the geometric deviations which will cause the position error of tool center point are clarified.

2. The simulation both in the cylindrical coordinate system and in the Cartesian coordinate system is conducted based on the established mathematical model to the targeted machine tool.

3. From the simulation results, it is confirmed that in order to eliminate the influence of the mounting errors of the W-side ball on the eccentricities of the circular trajectories, measurements for the B axis should be performed in Cartesian coordinate system and those for the C axis should be performed in cylindrical coordinate system. It is the first time to measure the geometric deviations related to a swivel spindle in Cartesian coordinate system.

4. Through the relationship between the geometric deviations and the eccentricities of the measured trajectories, it is found that the circular trajectories of the B axis X direction, B axis Y direction, C axis radial direction and C axis axial direction are adequate to identify the geometric deviations by designing an appropriate measuring procedure.

In Chapter 3, to compensate the geometric deviations which exist in a multi-tasking machine tool, the current algorithms and compensation methods for five-axis machining centers are investigated firstly. Then, a simple compensation method without any iteration is established based on the idea of screw method. Conclusions are summarized as follows.

1. Based on the analysis of the compensation methods for five-axis machining centers, the idea of screw method is used to model kinematics of the targeted multi-tasking machine tool.

2. The forward and inverse kinematics are analyzed in detail for the targeted machine tool. According to the topological structure, the formulae for the compensation are derived and they can be used to modify the NC code for compensating the influence of the geometric deviations on the position of tool center point.

In Chapter 4, a measuring procedure for identifying geometric deviations is investigated. The B axis measurements in the Cartesian coordinate system and the C axis measurements in the cylindrical coordinate system are conducted in a multi-tasking machine tool by a ball bar. An experiment modifying the NC code is also conducted to compensate the influence of the geometric deviations on TCP. Conclusions are summarized as follows.

1. A measuring procedure by a ball bar for identifying the geometric deviations is designed according to the analysis of the influence factors for each trajectory. Four measuring patterns are conducted to identify eight geometric deviations which are inherent to a multi-tasking machine tool.

2. The trajectories after the compensation by modifying the NC code are also

measured and compared with those before the compensation.

3. From the experimental results, the geometric deviations about two rotary axes (B and C axes) could be compensated effectively. However, the geometric deviations of the spindle (α_{BT}, δx_{BT}, and δz_{BT}) could not be compensated by this method.

4. After modifying the NC code, the corresponding values of angular geometric deviations are not over 2.2 arcseconds except for α_{BT} and positional geometric deviations are not over 2.4 micrometers. Therefore, it is confirmed that the position error of TCP is reduced significantly after the compensation.

In Chapter 5, a touch-trigger probe is used to identify the geometric deviations related to two rotary axes of a multi-tasking machine tool. A measuring procedure is devised, and the calculation method is derived based on the character of the respective rotations of B and C axes. The proposed measuring procedure and calculation method are conducted in INTEGREX i-200. The identified values of geometric deviations are compared and analyzed with the results identified by a ball bar described in Chapter 4. Conclusions are summarized as follows.

1. A simple measuring procedure by a touch-trigger probe for identifying the geometric deviations is designed according to the analysis of the influence of the geometric deviations on the measurements for the respective rotations of B and C axes.

2. The geometric deviations of INTEGREX i-200 are identified by the proposed measuring procedure. From the identified results, it is found that the geometric deviations related to the spindle (α_{BT}, δx_{BT}, and δz_{BT}) are not identified correctly. The number of geometric deviations identified by a touch-trigger probe is limited and fewer than that identified by a ball bar.

3. Compared with the identified values from the ball bar measurement, the difference of the angular deviations is not over 5.5 arcseconds except for α_{BT}. Therefore, the angular geometric deviations related to the rotary B and C axes of a multi-tasking machine tool can be correctly identified by using the identification method of ball bar described in Chapter 4.

4. It is verified that measuring procedure by ball bar of Chapter 4 is effective to identify the geometric deviations of multi-tasking machine tool.

6.2 Future prospects

Even though this research makes some original contributions to identify and compensate the geometric deviations of rotary axis in the multi-tasking machine tool and to significantly reduce the position error of tool center point, there are still several problems need to be solved.

1. Application of the identified values in the industry.

A machining test can be designed to compensate the identified inherent geometric deviations to evaluate the positioning accuracy by comparing the machined results before and after compensation. It is worth to be researched in the future to apply the identified values in the industry.

2. Verification by comparing with other methods

The patent of Okuma has provided a method by a touch-trigger probe to identify the geometric deviations of a multi-tasking machine tool. The proposed method in this thesis can be compared with the patent method by identifying the same machine tool to verify the identified results.

3. Identification and compensation methods for the geometric deviations related to spindle.

In Chapter 4, it is found that the geometric deviations of the spindle (α_{BT}, δx_{BT}, and δz_{BT}) could not be identified and compensated by analyzing the eccentricity of the trajectory measured by ball bar. The reason is considered that the positional deviations (δx_{BT} and δz_{BT}) are greatly affected by the error of the tool length and the setting error of the ball bar. The angular deviation α_{BT} can not be compensated by modifying NC code because the spindle axis is not controlled for angular positioning. Therefore, to realize high precision positioning of the tool center point, it is necessary to make clear the identification and compensation methods for the geometric deviations related to spindle in the future.

4. Verification of identification and compensation methods of ball bar by a multi-tasking machine tool with a swivel spindle head in a vertical position.

In this study, the identification and compensation methods of ball bar are only used in INTEGREX i-200, a multi-tasking machine tool with a swivel spindle head in a horizontal position. Another type of multi-tasking machine tool with a swivel spindle head in a vertical position is more common in the manufacturing and industry. Therefore, it is necessary to verify the identification and compensation methods of ball bar on a multi-tasking machine tool with a swivel spindle head in a vertical position to verify the effectiveness of these methods and expand the scope of application.

References

[1] JIS B 0105 : 2012 工作機械 - 名称に関する用語，財団法人　日本規格協会.

[2] 稲崎一郎，工作機械の形状創成理論 －その基礎と応用－，株式会社 養賢堂 (1997).

[3] 鈴木信貴，モジュール型産業におけるインテグリティーの獲得－日本工作機械産業の事例－，赤門マネジメント・レビュー, 9 巻 9 号 (2010), pp. 635-662.

[4] G. Sun, G. He, D. Zhang, Y. Sang, X. Zhang, B. Ding, Effects of geometrical errors of guideways on the repeatability of positioning of linear axes of machine tools, International Journal of Advanced Manufacturing Technology, Vol. 98, Issues 1-4 (2018), pp. 2319–2333.

[5] ISO 230-1. Test code for machine tools - Part 1: Geometric accuracy of machines operating under no-load or quasi-static conditions, (2012).

[6] ISO 230-2. Test code for machine tools - Part 2: Determination of accuracy and repeatability of positioning of numerically controlled axes, (2014).

[7] ISO 230-4. Test code for machine tools - Part 4: Circular tests for numerically controlled machine tools, (2005).

[8] H. Shen, J. Fu, Y. He, X. Yao, On-line asynchronous compensation methods for static/quasi-static error implemented on CNC machine tools, International Journal of Machine Tools and Manufacture, Vol. 60, (2012), pp. 14–26.

[9] R. Ramesh, M.A. Mannan, A.N. Poo, Error compensation in machine tools — a review Part I: geometric, cutting-force induced and fixture- dependent errors, International Journal of Machine Tools and Manufacture, Vol. 40, Issue 9 (2000), pp. 1235–1256.

[10] G. Florussen, Accuracy analysis of multi-axis machines by 3D length measurements, Dissertation of Eindhoven University of Technology, (2002).

[11] J. Ni, CNC machine accuracy enhancement through real - time error compensation, Journal of Manufacturing Science and Engineering, Vol. 119, Issue 4B (1997), pp. 717-725.

[12] ISO 10791-6. Test conditions for machining centres - Part 6: Accuracy of speeds and interpolations, (2014).

[13] E. Gomez-Acedo, A. Olarra, J. Orive, L.N. Lopez de la Calle, Methodology for the design of a thermal distortion compensation for large machine tools based in state-space representation with Kalman filter, International Journal of Machine Tools and Manufacture, Vol. 75, (2013), pp. 100–108.

[14] W.G. Weekers, P.H.J. Schellekens, Compensation for dynamic errors of coordinate measuring machines, Measurement, Vol. 20, Issue 3 (1997), pp. 197–209.

[15] G. Urbikain, D. Olvera, L.N. López de Lacalle, A. Beranoagirre, A. Elías-Zuñiga, Prediction methods and experimental techniques for chatter avoidance in turning systems: a review, Applied Sciences, Vol. 9, Issue 21 (2019), 10.3390/app9214718.

[16] D. Olvera, L.N.L. de Lacalle, F.I. Compeán, A. Fz-Valdivielso, A. Lamikiz, F.J. Campa, Analysis of the tool tip radial stiffness of turn-milling centers, International Journal of Advanced Manufacturing Technology, Vol. 60, Issues 9-12 (2012), pp. 883–891.

[17] F. Theuws, Enhancement of machine tool accuracy: theory and implementation, Dissertation of Eindhoven University of Technology, (1991).

[18] S. Ibaraki, W. Knapp, Indirect measurement of volumetric accuracy for three-axis and five-axis machine tools: a review, International Journal of Automation Technology, Vol. 6, No. 2 (2012), pp. 110–124.

[19] H. Schwenke, W. Knapp, H. Haitjema, A. Weckenmann, R. Schmitt, F. Delbressine, Geometric error measurement and compensation of machines—An update, CIRP Annals, Vol. 57, Issue 2 (2008), pp. 660–675.

[20] A.W. Khan, C. Wuyi, Systematic Geometric error modeling for workspace volumetric calibration of a 5-axis turbine blade grinding machine, Chinese Journal of Aeronautics, Vol. 23, Issue 5 (2010), pp. 604–615.

[21] A.C. Okafor, Y.M. Ertekin, Derivation of machine tool error models and error compensation procedure for three axes vertical machining center using rigid body kinematics, International Journal of Machine Tools and Manufacture, Vol. 40, Issue 8 (2000), pp. 1199–1213.

[22] H. Schwenke, R. Schmitt, P. Jatzkowski, C. Warmann, On-the-fly calibration of linear and rotary axes of machine tools and CMMs using a tracking interferometer, CIRP Annals, Vol. 58, Issue 1 (2009), pp. 477–480.

[23] B. Iñigo, A. Ibabe, G. Aguirre, H. Urreta, L.N. López de Lacalle, Analysis of laser tracker-based volumetric error mapping strategies for large machine tools, Metals, Vol. 9, Issue 7 (2019), 10.3390/met9070757.

[24] S.H.H. Zargarbashi, J.R.R. Mayer, Assessment of machine tool trunnion axis motion error, using magnetic double ball bar, International Journal of Machine Tools and Manufacture, Vol. 46, Issue 14 (2006), pp. 1823–1834.

[25] S. Esmaeili, J.R.R. Mayer, An integrated geometric and hysteretic error model of a three axis machine tool and its identification with a 3D telescoping ball-bar, Journal of Manufacturing and Materials Processing, Vol. 4, Issue 1 (2020), 10.3390/jmmp4010024.

[26] J.R.R. Mayer, Five-axis machine tool calibration by probing a scale enriched reconfigurable uncalibrated master balls artefact, CIRP Annals, Vol. 61, Issue 1 (2012), pp. 515–518.

[27] W.T. Lei, I.M. Paung, C.-C. Yu, Total ballbar dynamic tests for five-axis CNC machine

tools, International Journal of Machine Tools and Manufacture, Vol. 49, Issue 6 (2009), pp. 488–499.

[28] W.T. Lei, M.P. Sung, W.L. Liu, Y.C. Chuang, Double ballbar test for the rotary axes of five-axis CNC machine tools, International Journal of Machine Tools and Manufacture, Vol. 47, Issue 2 (2007), pp. 273–285.

[29] K.-I. Lee, S.-H. Yang, Measurement and verification of position-independent geometric errors of a five-axis machine tool using a double ball-bar, International Journal of Machine Tools and Manufacture, Vol. 70, (2013), pp. 45–52.

[30] K.-I. Lee, D.-M. Lee, S.-H. Yang, Parametric modeling and estimation of geometric errors for a rotary axis using double ball-bar, International Journal of Advanced Manufacturing Technology, Vol. 62, Issues 5-8 (2012), pp. 741–750.

[31] K.-I. Lee, D.-H. Shin, S.-H. Yang, Parallelism error measurement for the spindle axis of machine tools by two circular tests with different tool lengths, International Journal of Advanced Manufacturing Technology, Vol. 88, Issues 9-12 (2017), pp. 2883–2887.

[32] M. Tsutsumi, A. Saito, Identification and compensation of systematic deviations particular to 5-axis machining centers, International Journal of Machine Tools and Manufacture, Vol. 43, Issue 8 (2003), pp. 771–780.

[33] M. Tsutsumi, A. Saito, Identification of angular and positional deviations inherent to 5-axis machining centers with a tilting-rotary table by simultaneous four-axis control movements, International Journal of Machine Tools and Manufacture, Vol. 44, Issues 12-13 (2004), pp. 1333–1342.

[34] M. Tsutsumi, S. Tone, N. Kato, R. Sato, Enhancement of geometric accuracy of five-axis machining centers based on identification and compensation of geometric deviations, International Journal of Machine Tools and Manufacture, Vol. 68, (2013), pp. 11–20.

[35] Tsutsumi M., Miyama N., Tone S., Saito A., Cui C., Dassanayake, K.M.M., Correction of squareness of translational axes for identification of geometric deviations inherent to five-axis machining centres with a tilting-rotary table, Transactions of the Japan Society of Mechanical Engineers Series C, Vol. 79, Issue 799 (2013), pp. 759–774. (In Japanese)

[36] K.M.M. Dassanayake, M. Tsutsumi, A. Saito, A strategy for identifying static deviations in universal spindle head type multi-axis machining centers, International Journal of Machine Tools and Manufacture, Vol. 46, Issue 10 (2006), pp. 1097–1106.

[37] Y. Zhang, J. Yang, K. Zhang, Geometric error measurement and compensation for the rotary table of five-axis machine tool with double ballbar, International Journal of Advanced Manufacturing Technology, Vol. 65, Issues 1-4 (2013), pp. 275–281.

[38] A.W. Khan, W. Chen, A methodology for error characterization and quantification in rotary joints of multi-axis machine tools, International Journal of Advanced

Manufacturing Technology, Vol. 51, (2010), pp. 1009–1022.

[39] S. Xiang, J. Yang, Y. Zhang, Using a double ball bar to identify position-independent geometric errors on the rotary axes of five-axis machine tools, International Journal of Advanced Manufacturing Technology, Vol. 70, Issues 9-12 (2014), pp. 2071–2082.

[40] J. Chen, S. Lin, B. He, Geometric error measurement and identification for rotary table of multi-axis machine tool using double ballbar, International Journal of Machine Tools and Manufacture, Vol. 77, (2014), pp. 47–55.

[41] S. Ibaraki, M. Sawada, A. Matsubara, T. Matsushita, Machining tests to identify kinematic errors on five-axis machine tools, Precision Engineering, Vol. 34, Issue 3 (2010), pp. 387–398.

[42] M.S. Uddin, S. Ibaraki, A. Matsubara, T. Matsushita, Prediction and compensation of machining geometric errors of five-axis machining centers with kinematic errors, Precision Engineering, Vol. 33, Issue 2 (2009), pp. 194–201.

[43] S. Ibaraki, I. Yoshida, A five-axis machining error simulator for rotary-axis geometric errors using commercial machining simulation software, International Journal of Automation Technology, Vol. 11, No. 2 (2017), pp. 179–187.

[44] S. Ibaraki, Y. Nagai, H. Otsubo, Y. Sakai, S. Morimoto, Y. Miyazaki, R-test analysis software for error calibration of five-axis machine tools – application to a five-axis machine tool with two rotary axes on the tool side –, International Journal of Automation Technology, Vol. 9, No. 4 (2015), pp. 387–395.

[45] C. Hong, S. Ibaraki, Observation of thermal influence on error motions of rotary axes on a five-axis machine tool by static R-test, International Journal of Automation Technology, Vol. 6, No. 2 (2012), pp. 196–204.

[46] C. Hong, S. Ibaraki, C. Oyama, Graphical presentation of error motions of rotary axes on a five-axis machine tool by static R-test with separating the influence of squareness errors of linear axes, International Journal of Machine Tools and Manufacture, Vol. 59, (2012), pp. 24–33.

[47] S. Ibaraki, C. Oyama, H. Otsubo, Construction of an error map of rotary axes on a five-axis machining center by static R-test, International Journal of Machine Tools and Manufacture, Vol. 51, Issue 3 (2011), pp. 190–200.

[48] S. Ibaraki, Y. Ota, Error calibration for five-axis machine tools by on-the-machine measurement using a touch-trigger probe, International Journal of Automation Technology, Vol. 8, No. 1 (2014), pp. 20–27.

[49] J. Li, F. Xie, X.-J. Liu, Z. Dong, Z. Song, W. Li, A geometric error identification method for the swiveling axes of five-axis machine tools by static R-test, International Journal of Advanced Manufacturing Technology, Vol. 89, Issues 9-12 (2017), pp. 3393–3405.

[50] R. Ramesh, M.A. Mannan, A.N. Poo, Error compensation in machine tools — a review

Part II: thermal errors, International Journal of Machine Tools and Manufacture, Vol. 40, Issue 9 (2000), pp. 1257–1284.

[51] S. Xiang, Y. Altintas, Modeling and compensation of volumetric errors for five-axis machine tools, International Journal of Machine Tools and Manufacture, Vol. 101, (2016), pp. 65–78.

[52] S. Xiang, M. Deng, H. Li, Z. Du, J. Yang, Volumetric error compensation model for five-axis machine tools considering effects of rotation tool center point, International Journal of Advanced Manufacturing Technology, Vol. 102, Issues 5-8 (2019), pp. 4371–4382.

[53] J. Li, B. Mei, C. Shuai, X. Liu, D. Liu, A volumetric positioning error compensation method for five-axis machine tools, International Journal of Advanced Manufacturing Technology, Vol. 103, (2019), pp. 3979–3989.

[54] C. CUI, K. HIGASHIYAMA, M. Tsutsumi, M. Dassanayake, A method for identifying geometric deviations inherent to multi-tasking turning centers, Transactions of the Japan Society of Mechanical Engineers Series C, Vol. 75, Issue 750 (2009), pp. 228–235. (In Japanese)

[55] ISO 13041-5. Test conditions for numerically controlled turning machines and turning centres - Part 5: Accuracy of speeds and interpolations, (2015).

[56] Díaz-Tena, E.; Ugalde, U.; López de Lacalle, L.N.; De La Iglesia, A.; Calleja, A.; Campa, F.J. Propagation of assembly errors in multitasking machines by the homogenous matrix method, International Journal of Advanced Manufacturing Technology, Vol. 68, Issues 1-4 (2013), pp. 149–164.

[57] A.W. Khan, W. Chen, A methodology for systematic geometric error compensation in five-axis machine tools, International Journal of Advanced Manufacturing Technology, Vol. 53, Issue 5 (2011), pp. 615–628.

[58] W.T. Lei, Y.Y. Hsu, Accuracy enhancement of five-axis CNC machines through real-time error compensation, International Journal of Machine Tools and Manufacture, Vol. 43, Issue 9 (2003), pp. 871–877.

[59] Y.Y. Hsu, S.S. Wang, A new compensation method for geometry errors of five-axis machine tools, International Journal of Machine Tools and Manufacture, Vol. 47, Issue 2 (2007), pp. 352–360.

[60] F.Y. Peng, J.Y. Ma, W. Wang, X.Y. Duan, P.P. Sun, R. Yan, Total differential methods based universal post processing algorithm considering geometric error for multi-axis NC machine tool, International Journal of Machine Tools and Manufacture, Vol. 70, (2013), pp. 53–62.

[61] J. Yang, Y. Altintas, Generalized kinematics of five-axis serial machines with non-singular tool path generation, International Journal of Machine Tools and Manufacture,

Vol. 75, (2013), pp. 119–132.

[62] Hoffman F. Ramirez, Oscar F. Avilés, Mauricio F. Mauledoux, Forward kinematic modeling by screw theory of a 3 DOF exoskeleton for human upper limb, ARPN Journal of Engineering and Applied Sciences, Vol. 12, No. 20 (2017), pp. 5677–5681.

[63] W. Tian, W. Gao, D. Zhang, T. Huang, A general approach for error modeling of machine tools, International Journal of Machine Tools and Manufacture, Vol. 79, (2014), pp. 17–23.

[64] J. Yang, J.R.R. Mayer, Y. Altintas, A position independent geometric errors identification and correction method for five-axis serial machines based on screw theory, International Journal of Machine Tools and Manufacture, Vol. 95, (2015), pp. 52–66.

[65] S. Zhu, G. Ding, S. Qin, J. Lei, L. Zhuang, K. Yan, Integrated geometric error modeling, identification and compensation of CNC machine tools, International Journal of Machine Tools and Manufacture, Vol. 52, Issue 1 (2012), pp. 24–29.

[66] N. Zimmermann, S. Ibaraki, Self-calibration of rotary axis and linear axes error motions by an automated on-machine probing test cycle, International Journal of Advanced Manufacturing Technology, Vol. 107, Issue 1 (2020), pp. 2107–2120.

Achievements

Journal Papers

1. Y. Yao, K. Nishizawa, N. Kato, M. Tsutsumi, and K. Nakamoto, Identification method of geometric deviations for multi-tasking machine tools considering the squareness of translational axes, Applied Sciences, Vol. 10, Issue 5 (2020), 10.3390/app10051811. (Chapter 2)
2. Y. Yao, Y. Itabashi, M. Tsutsumi, and K. Nakamoto, Position error reduction of tool center point in multi-tasking machine tools through compensating influence of geometric deviations identified by ball bar measurements, Precision Engineering, Vol. 72, (2021), pp. 745-755. (Chapter 4)

International Proceedings

1. Y. Yao, K. Nishizawa, N. Kato, M. Tsutsumi, K. Nakamoto, Identification method of geometric deviations for multi-tasking machine tools with a swivel tool spindle head in vertical position, Proceedings of the 8th International Conference of Asian Society for Precision Engineering and Nanotechnology, (2019), USB B37. (Chapter 2)
2. Y. Yao, Y. Itabashi, K. Nishizawa, M. Tsutsumi, K. Nakamoto, Proposal of identification and compensation method of geometric deviations for multi-tasking machine tools to improve motion accuracy, Proceedings of the International Symposium on Precision Engineering and Sustainable Manufacturing, (2020), P-061. (Chapter 3)
3. Y. Yao, Y. Itabashi, M. Tsutsumi, K. Nakamoto, A simple measuring procedure to identify geometric deviations of multi-tasking machine tools by a touch-trigger probe, Proceedings of the 10th International Conference on Leading Edge Manufacturing in 21st Century, (2021), USB 075. (Chapter 5)

Acknowledgement

This study is conducted at the Department of Mechanical Systems Engineering, Tokyo University of Agriculture and Technology from October 2017 to March 2022. I would like to express my sincere gratitude to my supervisor, Associate Professor K. Nakamoto for his continuous guidance, helpful suggestions, and hearty encouragement throughout my study. Although he is very busy, he is able to actively communicate with students and give a lot of suggestion and guidance on my research. As a result, I can complete my study smoothly.

It is my great honor to have four reviewers: Professor Y. Tagawa, Professor W. Natsu, Professor H. Sasahara, and Associate Professor T. Maeda. Professors spare their valuable time guiding my dissertation and giving helpful comments, so that I will find more depth in this study.

In particular, I would like to express my grateful appreciation to Professor M. Tsutsumi, the professor emeritus of Tokyo University of Agriculture and Technology, for presenting various important references and consulting on the experimental results. I would like to express my deepest gratitude for pointing out the problems and improved methods of the ball bar experiments and the touch-trigger probe experiments so that I can carry out the experiments successfully.

I am very grateful to Mr. Y. Itabashi, a 1st year master graduate student, and Mr. K. Nishizawa and Mr. M. Kogo, graduated students of the Nakamoto Laboratory. Since the research contents are similar, I have received a lot of consultation about the research. In addition, due to my shortcomings in Japanese, I have received much help in the operation of my experiments.

I would like to express my appreciation to Professor H. Sasahara, Associate Professor K. Nakamoto, everyone in the Sadahara Laboratory, and everyone in the Nakamoto Laboratory. I have received many sharp suggestions from them at graduate seminars, which helped me proceed with my research smoothly.

In addition, I would also like to thank Mr. M. Xu and Miss X. Chen, Chinese students in the Nakamoto Laboratory. I have got their great encouragement and help in my job hunting and my daily life.

I would also like to thank Dr. Y. Inoue and Dr. M. Kumanotani, graduated doctoral students of the Nakamoto Laboratory, for their strong support in the confirmation of the report materials on my mid-term defense and the international conference. I am very grateful for sparing their time in revising my report when their research activities were busy.

With the support of many people, I have led a fulfilling laboratory life over the past four and a half years. I will be a member of the Japanese society in April. I will remember

this valuable experience in the university and use it in my future life.

Finally, I would like to express my heartfelt appreciation to my parents and family to complete my research work. Thanks to their understanding and support.